FEASIBILITY OF TAPERED ROLLER BEARINGS FOR MAIN-SHAFT ENGINE APPLICATIONS

SKF Industries, Incorporated

PREPARED FOR
Army Air Mobility Research and Development Laboratory

August 1973

DISCLAIMERS

The findings in this report are not to be construed as an official Department of the Army position unless so designated by other authorized documents.

When Government drawings, specifications, or other data are used for any purpose other than in connection with a definitely related Government procurement operation, the United States Government thereby incurs no responsibility nor any obligation whatsoever; and the fact that the Government may have formulated, furnished, or in any way supplied the said drawings, specifications, or other data is not to be regarded by implication or otherwise as in any manner licensing the holder or any other person or corporation, or conveying any rights or permission, to manufacture, use, or sell any patented invention that may in any way be related thereto.

Trade names cited in this report do not constitute an official endorsement or approval of the use of such commercial hardware or software.

DISPOSITION INSTRUCTIONS

Destroy this report when no longer needed. Do not return it to the originator.

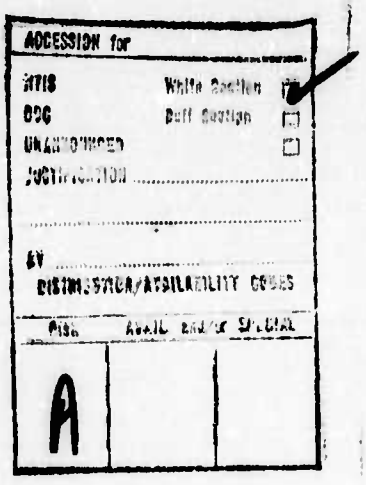

Unclassified
Security Classification

DOCUMENT CONTROL DATA - R & D

(Security classification of title, body of abstract and indexing annotation must be entered when the overall report is classified)

1. ORIGINATING ACTIVITY (Corporate author)	2a. REPORT SECURITY CLASSIFICATION
SKF Industries, Incorporated 1100 First Avenue King of Prussia, Pennsylvania	Unclassified 2b. GROUP

3. REPORT TITLE

FEASIBILITY OF TAPERED ROLLER BEARINGS FOR MAIN-SHAFT ENGINE APPLICATIONS

4. DESCRIPTIVE NOTES (Type of report and inclusive dates)

Final Technical Report

5. AUTHOR(S) (First name, middle initial, last name)

Thomas F. Conners
Frank R. Morrison

6. REPORT DATE	7a. TOTAL NO. OF PAGES	7b. NO. OF REFS
August 1973	173	7

8a. CONTRACT OR GRANT NO.	9a. ORIGINATOR'S REPORT NUMBER(S)
DAAJ02-70-C-0047 b. PROJECT NO. 1F162203A119 c. d.	USAAMRDL Technical Report 73-46 9b. OTHER REPORT NO(S) (Any other numbers that may be assigned this report) SKF Industries Report AL73T009

10. DISTRIBUTION STATEMENT

Approved for public release; distribution unlimited.

11. SUPPLEMENTARY NOTES	12. SPONSORING MILITARY ACTIVITY
	Eustis Directorate U. S. Army Air Mobility R&D Laboratory Fort Eustis, Virginia

13. ABSTRACT

A survey of 2- to 10-pounds/second-airflow aircraft gas turbine manufacturers indicated an increase in shaft speed in projected applications. A shaft speed increase results in an increase in the load-carrying requirement, and contact stresses due to centrifugal forces on the rolling elements, in the main-shaft bearings. One approach to reducing the contact stresses in the thrust-loaded bearing is to increase the contact area between the rolling elements and races by using tapered roller bearings in place of angular-contact ball bearings. An analytical study of tapered roller bearings is discussed, and the results of an analysis are given in which the principal design parameters were varied to optimize the design for high speed. This analysis included the standard inner ring flange design and a novel outer ring flange design. The results of tests performed with three different tapered roller bearing designs (commercial, aircraft-quality inner ring flange, outer ring flange) are presented. Tests were successfully conducted up to 2.4 million DN and 2.13 million DN on the outer ring flange and inner ring flange designs respectively. Thus, the feasibility of both bearing designs as candidates for very-high-speed gas turbine main-shaft support applications was established.

DD FORM 1 NOV 68 1473 REPLACES DD FORM 1473, 1 JAN 64, WHICH IS OBSOLETE FOR ARMY USE.

Unclassified
Security Classification

14. KEY WORDS	LINK A		LINK B		LINK C	
	ROLE	WT	ROLE	WT	ROLE	WT
Gas Turbine Support Bearings						
Tapered Roller Bearings						
High-Speed Bearings						
Main-Shaft Bearings						

8485-73

DEPARTMENT OF THE ARMY
U. S. ARMY AIR MOBILITY RESEARCH & DEVELOPMENT LABORATORY
EUSTIS DIRECTORATE
FORT EUSTIS, VIRGINIA 23604

The work described herein was conducted by SKF Industries, Inc., under U. S. Army Contract DAAJ02-70-C-0047. The work was performed under the technical management of Mr. David B. Cale of the Technology Applications Division of this Directorate.

The objective of this contractual effort was to determine the feasibility of using tapered roller bearings as main-shaft support bearings in high-speed gas turbine engines.

Two different tapered roller bearing designs were successfully tested at speeds in excess of 2 million DN (product of shaft speed in rpm and bearing bore in millimeters). This is by far the highest DN value for tapered roller bearings reported to date.

Appropriate technical personnel of this Directorate have reviewed this report and concur with the conclusions and recommendations contained herein.

Project 1F162203A119
Contract DAAJ02-70-C-0047
USAAMRDL Technical Report 73-46
August 1973

FEASIBILITY OF TAPERED ROLLER BEARINGS FOR MAIN-SHAFT ENGINE APPLICATIONS

Final Report

SKF Industries, Inc. Report AL73T009

By

T. F. Conners
F. R. Morrison

Prepared by

SKF Industries, Inc.
King of Prussia, Pennsylvania

for

EUSTIS DIRECTORATE
U.S. ARMY AIR MOBILITY RESEARCH AND DEVELOPMENT LABORATORY
FORT EUSTIS, VIRGINIA

iib.

SUMMARY

The purpose of this program was to complete the necessary engineering design study and analysis leading to the establishment of a tapered roller bearing design for high-speed operation. This design was then subjected to experimental developmental study to establish its feasibility for application as a gas turbine engine main-shaft support bearing. This program was conducted in three phases as follows:

In Phase I, a survey was made of engine manufacturers to identify the present and projected application requirements for bearings which would be used in 2-10 pounds/second-airflow gas turbine engines. Design concepts were established for high-speed tapered roller bearings, and a comprehensive analytical study was completed to optimize bearing designs which could meet the application requirements.

In Phase II, the candidate bearing designs were evaluated in a series of functional tests conducted at constant load under a step-speed procedure to a maximum speed of 46,000 rpm (1.1×10^6 DN)*. This testing confirmed the basic feasibility of very-high-speed tapered roller bearings and demonstrated that the design changes incorporated did improve the high-speed operating characteristics of these bearings as compared to those of the standard commercial design.

The tests also indicated that speed capabilities in excess of the original target speed of 1.5 million DN could be easily obtained with tapered roller bearings. Thus, the goals of the program were altered to include the development of a bearing with speed capabilities in the 2 to 3 million DN range. A test facility was concurrently developed to provide test capability in the speed range.

In addition, the Phase I analytical effort indicated that the standard inner-ring-flange tapered roller bearing design might be subject to a maximum speed limitation resulting from the lift-off of the rollers from the inner ring roller path due to centrifugal force. This "declutching" might result in an unstable dynamic condition which could not be tolerated, or the resultant excessive flange loads might precipitate

*Product of shaft speed in rpm and the bearing bore in mm.

early flange failures. If either event occurred, a viable 3 million DN bearing could not be achieved using the inner-ring-flanged bearing design.

Phase III was then added to continue high-speed development of the original inner ring flanged design, to create a novel bearing design with the flange on the outer ring, and to test this concept. Tests were successfully conducted up to 2.4 million DN on the outer ring flanged design and 2.13 million DN on the inner ring flanged design, by far the highest DN values for tapered roller bearings reported to date. These results established the feasibility of both bearing designs as candidates for very-high-speed gas turbine main-shaft support applications, and revealed that inner ring flanged and outer ring flanged tapers each had advantages and disadvantages. The former declutches at very high speed under fixed axial load, and rotor instabilities can result. Of the two designs, however, it can carry the higher axial load for a given speed. The outer ring flanged design does not declutch and was capable of operating to rig speed limits in the tests conducted, but specific flange loads are higher for a given external load than for the inner ring flange.
The choice among the two designs depends thus on the rotor design and application parameters. An attractive choice for a typical turbine rotor imposing predominant thrust load in one direction but subject to occasional reverse thrust is a combination of one inner ring and one outer ring flanged taper.

FOREWORD

This report represents the results of a study conducted by SKF Industries, Inc., for the Eustis Directorate, U.S. Army Air Mobility Research and Development Laboratory, Fort Eustis, Virginia, under Contract DAAJ02-70-C-0047, Project 1F162203A119. This report encompasses the development and evaluation effort conducted from May 25, 1970, to November 25, 1972.

Eustis Directorate technical direction was provided by Mr. David Cale, Technology Applications Division.

The principal investigators for the program were T. F. Conners, Scientist, Mechanical Test Section, who was the project leader; Mr. F. R. Morrison, Section Supervisor, Mechanical Test Section; Dr. C. G. Hingley, Section Supervisor, Configuration Section; Mr. H. M. Martinie, Senior Researcher, Configuration Section; and J. Y. Liu, Scientist, Physics Section. Additional significant contributions were made by Messrs. L. B. Sibley, Manager, Research Department; R. A. Nash, Research Scientist, Mechanical Processing Section; W. L. Rhoads, Section Supervisor, Test Equipment Section; and H. Esten, Research Scientist, Test Equipment Section.

TABLE OF CONTENTS

TABLE OF CONTENTS (CONTINUED)

LIST OF ILLUSTRATIONS

LIST OF ILLUSTRATIONS (CONTINUED)

LIST OF ILLUSTRATIONS (CONTINUED)

LIST OF ILLUSTRATIONS (CONTINUED)

LIST OF TABLES

LIST OF TABLES

LIST OF SYMBOLS AND TERMS

DN	Product of shaft speed in rpm and bearing bore in millimeters
Outer Ring Roller Path Angle	Angle the outer ring roller path makes with the axis of the bearing
Inner Ring Roller Path Angle	Angle the inner ring roller path makes with the axis of the bearing
Roller Included Angle	Included angle formed by the roller OD in a diametral plane
Roller/Flange Contact Angle	Angle formed by the roller/flange contact force relative to the axis of the bearing
Roller End Radius	Radius of roller sphered end expressed in terms of inches or % bearing apex radius
F_a F_a' etc	Externally applied axial load
F_c	Centrifugal force acting on a rolling element
Q_o	Contact load on the outer race roller path
Q_i	Contact load on the inner race roller path
Q_{fo}	Contact load on the outer ring flange
Q_{fi}	Contact load on the inner ring flange
Z	Number of rolling elements
α_o	Roller path angle, outer ring
α_i	Roller path angle, inner ring

I. INTRODUCTION

A. STATEMENT OF THE PROBLEM

Currently, a typical small, 2- to 10-lb/sec airflow, gas turbine engine main-shaft support system consists of a thrust-carrying bearing unit and one or more radial bearings. The typical thrust bearing is a split inner ring angular contact ball bearing. Engine designers attempt to minimize the standard operating thrust loads through balancing of the power turbine and compressor loads, but a considerable thrust load exists at some points in the cycle. This can be large enough to require the stacking of thrust bearings, i.e., the use of multiple bearings, an obviously undesirable feature due to difficulties in providing adequate lubrication and load sharing. Such tandem thrust bearing designs are often used on larger turbine engine mainshafts and on helicopter transmission pinion shafts.

Engine main-shaft bearing problems are already a major contributor to Army gas turbine engine part failures, although it is realized that many factors other than just the bearings themselves are responsible. Advancements in weapons systems continually place more stringent demands on power plants and will continue to require performance increases in future systems.

Recent technological advances have made it possible to develop gas-turbine power plants which can supply these increases in performance. New turbine blade materials have been identified which can withstand higher centrifugal stresses at higher temperatures than conventional materials and systems to provide compressor bleed air cooling of the turbine blades have been developed. This makes it possible for the turbine to withstand higher peripheral speeds and allows designers to take advantage of the engine efficiencies gained from higher shaft rotational speeds. Concurrently considerations of shaft stress and vibration criticals dictate the use of larger diameter shafts at these higher rotational speeds. These factors all result in a drastic increase in the required peripheral speeds of the highly loaded thrust bearings in gas turbine power plants, with no reduction in anticipated main-shaft thrust bearing loads or in extended bearing life requirements. As a result of the increased speed, gas turbine engine bearings will operate at speeds where the centrifugal force of the rolling elements is a significant addition to total bearing load.

B. METHOD OF APPROACH

In order to reduce the load-carrying requirement of these bearings, attempts are now under way to produce low-density or hollow rolling elements as a means of limiting centrifugal forces. These efforts are promising but are by no means the only approach to an ultrahigh-speed rolling bearing with longer life and/or higher load capacity.

It has long been recognized that line contacts can have a substantially increased load carrying capability over that of even a closely conforming ball-to-race contact. This then indicates the desirability of having a line contact bearing for the main thrust position in a gas turbine engine. A tapered roller bearing can conceivably be used, and with it, a significantly greater load-carrying capacity can be developed as compared to a similarly sized ball bearing. However, these bearings have a reputation as a low-speed bearing and have not, to this point in time, been developed so as to be suitable for critical high-speed applications. It is now considered that bearing technology can provide analytical and manufacturing techniques to counter that low-speed image. Recent advances in cage design, roller end/flange interface design, and lubrication techniques to insure an elastohydrodynamic oil film at the flange contact have made it feasible to consider tapered roller bearings for the main-shaft application. Thus, it was considered desirable to develop such a high-speed bearing and demonstrate its feasibility.

II. TEST FACILITY

A high-speed, high-temperature bearing test machine was used for all testing conducted under this contract. A detailed discussion of the design and operation of this test rig is given below. The original configuration included a mechanical drive train, and attempts were made to increase the speed of this system to meet the demands of this test program. When that proved to be impractical, an air turbine drive was incorporated to provide the high-speed capability. The basic layout and all of the modifications completed on this test system are discussed in the following paragraphs.

A. TEST RIG - MECHANICAL DRIVE

A layout sketch of the basic test head is shown in Figure 1. The tester mounts two bearings-the test bearing and a 7205 angular contact ball bearing - on the same shaft. The test bearing is mounted in a movable housing through which load is applied, called a load plug, and the 7205 ball bearing is mounted on the drive end to act as a slave bearing. The axial load is applied by a deadweight and lever arm system which thrust loads the bearings against each other. The drive input is from a 50-h.p. variable-speed, electric motor, acting through a high-speed gearbox and a quill coupling to the test shaft. A shear pin in the quill coupling protects the system from damage due to excessive torque buildup in any component.

The bearings tested in this program were lubricated with a MIL-L-23699 specification oil supplied from an external 15-gallon sump. Oil scavenging was performed by two pumps, connected to the inboard and outboard drain lines of a bearing respectively.

The oil was delivered through three jets to the inboard (open) side of the inner ring flanged bearings and also through the hollow shaft to the inner ring undercut (roller large end/ flange interface) by means of radial holes drilled through the shaft and from the bearing bore to the flange undercut.

When outer ring flanged bearings were run, the oil was jetted into the outboard (open) side of the bearing. No inner ring under-race lubricating oil was supplied in the absence of an inner ring flange.

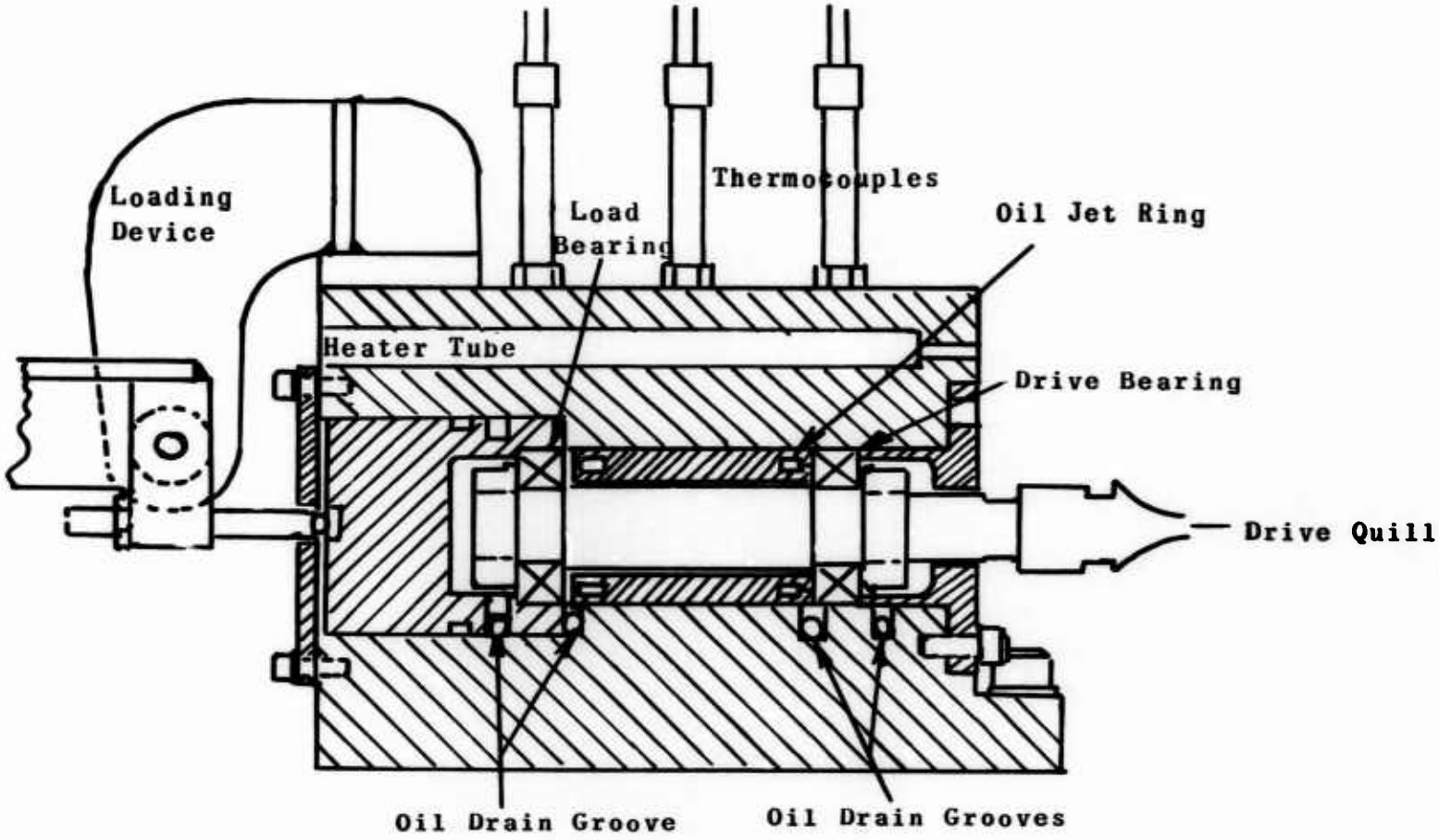

Figure 1. Schematic of High-Speed, High-Temperature Test Rig Mechanically Driven.

The maximum speed obtained with this arrangement was 46,000 rpm.

B. TEST RIG - AIR-DRIVEN TURBINE

The test rig was modified to provide speed capability in excess of the 46,000 rpm by the installation of an air-driven turbine on an extension of the bearing shaft (Figure 2). The air was supplied by a 750-cfm, 150-psig air compressor through heaters provided to eliminate the formation of ice at the nozzles and to increase the specific volume of the air, thereby providing greater power output of the turbine.

The air turbine was provided with safety devices to safeguard personnel and test equipment in the event of mechanical malfunctions within the rig. In the event of the loss of oil line pressure, the air supply is automatically vented to the atmosphere, bypassing the turbine assembly. Additionally, if the air supply pressure drops below a preset level, the heaters in the air line are automatically shut off.

Concurrently the load system was redesigned to apply the test load through a direct-acting spring system. Although spring systems are generally less accurate than deadweight loads, it had been found that at the higher speeds, the test machine developed shaft vibrations which were related to the natural frequency of the deadweight system and the constant nature of the applied load. The use of spring loading provided less vibrating mass and a positive load/displacement gradient under the axial motions characteristic of the disturbances, and thus provided a stabilizing influence. In this manner, it was possible to obtain test speeds in excess of the first shaft critical, which was in the vicinity of 63,000 rpm.

To minimize the vibration of high speeds, the shaft assembly was balanced to 0.001 oz-in. for each test setup.

The lubricant injection system was varied to accommodate the cooling demands imposed on the system by the high speeds attained. Although the inboard-side oil supply, combined with under-race cooling oil, had been sufficient to lubricate and cool the inner ring flanged bearings at the low speeds, this method did not provide the quantities or placement of

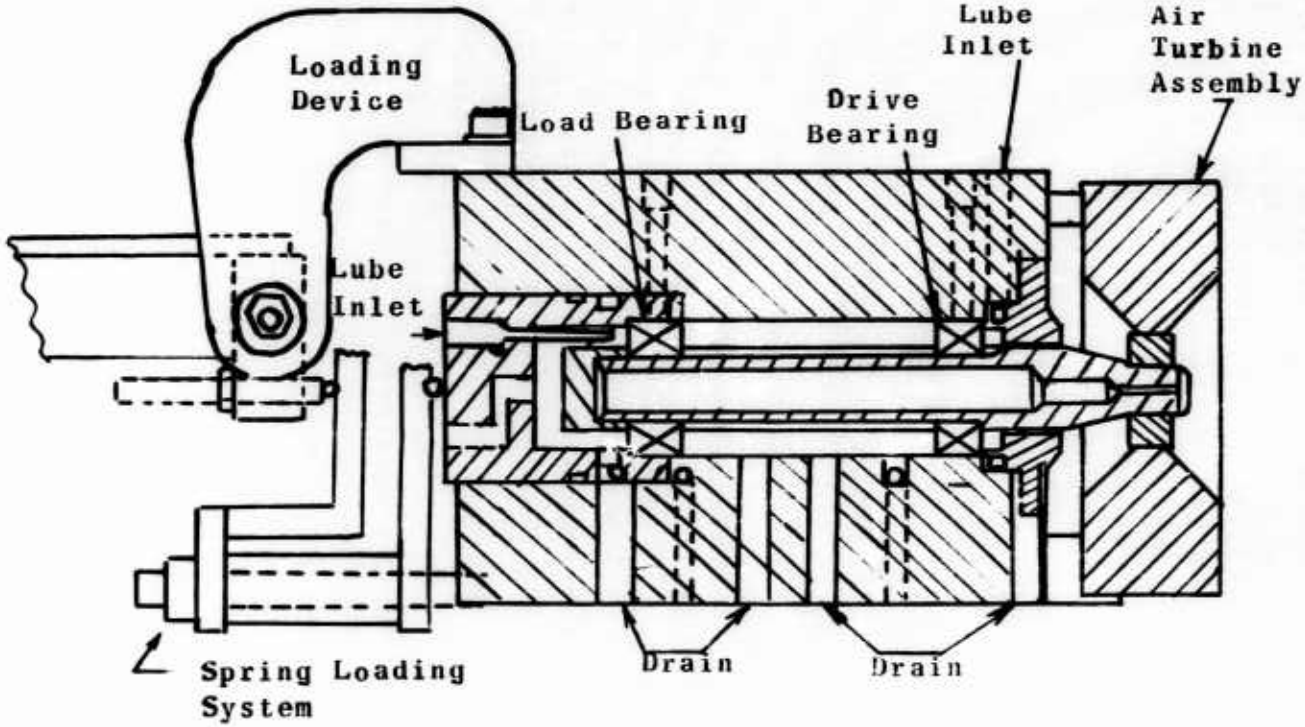

Figure 2. Schematic of High-Speed Tester, Air Turbine Driven.

oil necessary for the effective cooling of the flange area (Sketch 1). An outboard oil delivery system which complemented the natural pumping action of the tapered roller bearing was therefore used to lubricate both design bearing tests at high speeds in addition to the inboard supply jets (Sketch 2).

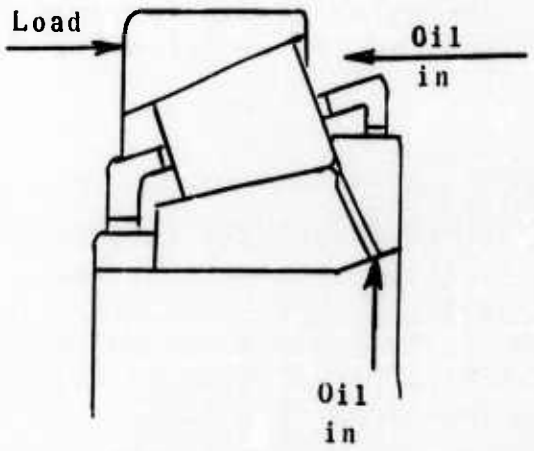

Sketch 1

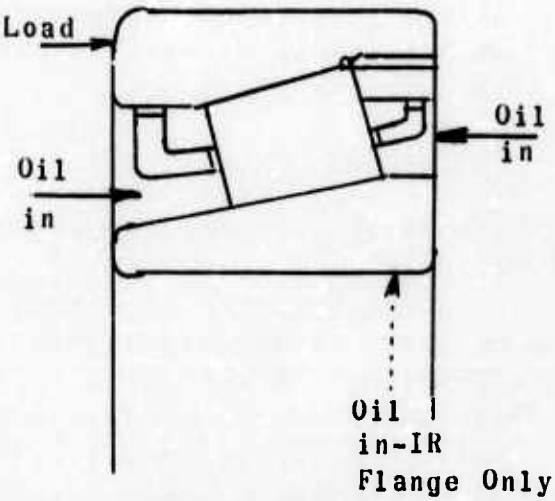

Sketch 2

The oil scavenging system remained the same in all cases. Scavenge pumps drew the oil from drain holes provided inboard and outboard of each bearing and returned it to the sump, with the oil passing through a heat exchanger in order to maintain temperature stability of the oil supply.

III. TEST BEARINGS

The major objective of this program was to develop the design for a tapered roller bearing capable of operating in critical high-speed, thrust-loaded applications, such as gas turbine engines, and which has advantages over those bearings now being used. The approach taken was to establish the critical design parameters of such a bearing analytically, to experimentally develop and evaluate design improvements, and then to compile an optimized design. In the course of completing this effort, four variations of inner ring flanged bearings were utilized, and a novel outer ring flanged design bearing was developed. The major design features of each of these variations are discussed in the following paragraphs.

A. COMMERCIAL BEARINGS

The first group of tapered roller bearings used in this program were standard class 4 bearings obtained through commercial sources and made by Timken Company and by Tyson Division of SKF Industries, Inc. The major external design dimensions of this bearing, which is illustrated in Figure 3, are an 11° inner ring angle, a 15° outer ring angle, and rollers of 0.244 inch large end diameter and a crown diameter of 250 inches. These bearings are manufactured from case carburized material, have flanges on both ends of the inner ring, and are fitted with a pressed steel roller riding cage. Only the large-end flange carries roller load.

Samples of the measurements taken on critical bearing dimensions are given in Table 1.

B. MODIFIED COMMERCIAL BEARINGS

The second group of bearings used in the program was comprised of commercial bearings which were modified as illustrated in Figure 4. Six 0.062-inch-diameter holes were drilled through the inner ring from a taper added at the large end bore corner, into the undercut at the junction of the race and load-carrying flange, to allow oil to be supplied directly into the critical roller end/flanged contact area. A machined steel, silver-plated cage was manufactured and balanced to typical (3 gm-cm) aircraft design standards. This cage was designed to be inner ring

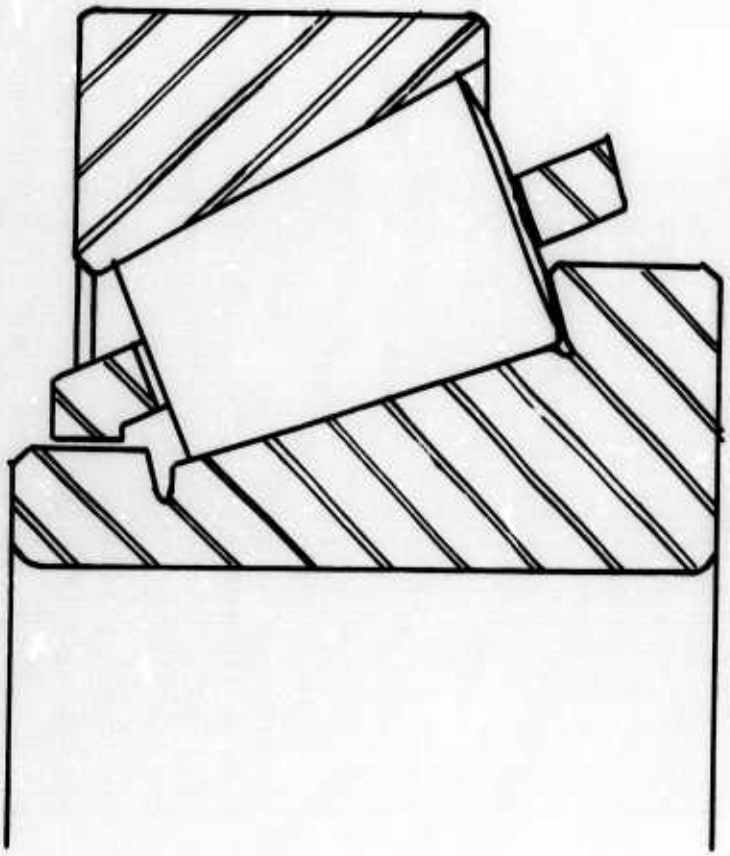

Figure 3. Commercial Tapered Roller Bearing.

TABLE I. NOMINAL* INTERNAL GEOMETRY DIMENSIONS - TAPERED ROLLER BEARINGS

	Inner Ring		Rollers			Outer Ring				
	Roller Path Angle	Flange Angle	Angle	Large End Diam. (in.)	Sphered End Radius (in.)	Roller Path Angle	Flange Angle	Cage Type	Ring Steel	Bearing No. Series
PHASE II - INNER RING FLANGED DESIGN										
Commercial Bearings Timken	11°0'42.7"	11°48'25"	3°57'14.5"	0.244	3.504	29°55'81"	None	Pressed Steel	Carburized	
Tyson	11°0'0"	11°32'42"	4°0'0"	0.244	3.496	30°0'0"	None	Pressed Steel	Carburized	
Modified Commercial Grade	11°0'0"	11°32'42"	4°0'0"	0.244	3.320	30°0'0"	None	Machined Silver Plated 4340 Steel	Carburized	093100
Aircraft Toleranced, Standard Design	11°0'0"	11°32'42"	4°0'0"	0.244	2.630	30°0'0"	None	Machined Silver Plated 4340 Steel	52100	093200
Experimental Bearings	11°43'20"	11°43'20"	3°16'40"	0.200	2.450	30°0'0"	None	Machined Silver Plated 4340 Steel	52100	093300
PHASE III-OUTER RING FLANGED DESIGN										
Outer Ring Flanged Brgs.	11°43'20"	None	3°16'40"	0.200	2.450	30°0'0"	90°0'0"	Machined Silver Plated 4340 Steel	52100	094100

*Values for Timken Commercial Bearings are Measured Values.

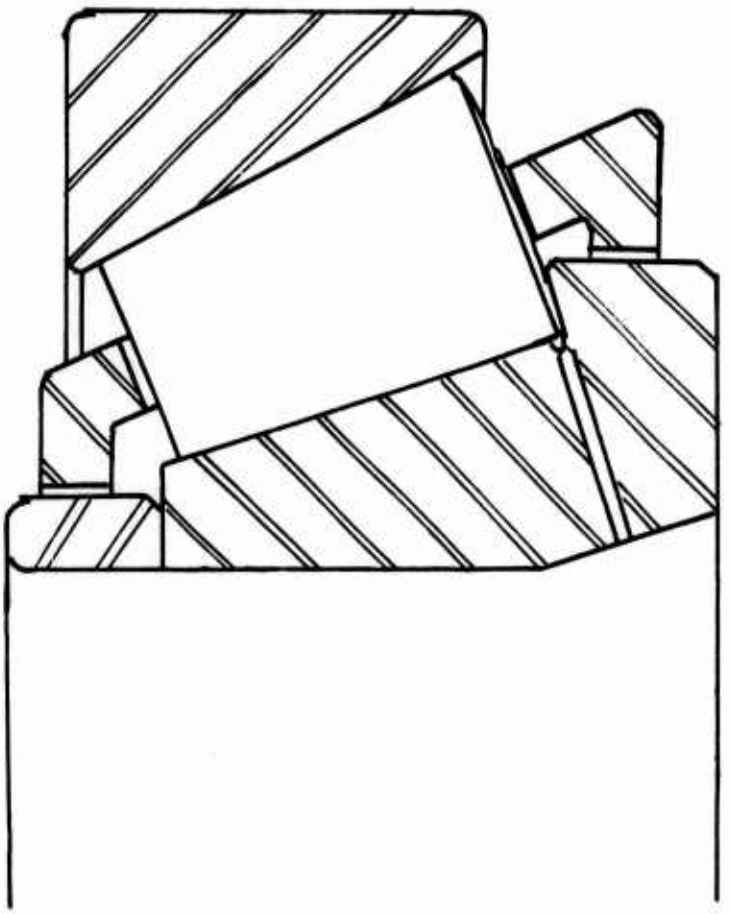

Roller End Radius 3.320"
Roller -.244" x .364"
Cup Angle 30° (included)

Figure 4. Modified Commercial Bearing Design.

land-riding, in lieu of roller riding, which is also a typical aircraft design feature. To allow the assembly of the bearing with the new cage, the flange normally present on the small end of the inner ring taper in the standard design was removed and a separable shoulder ring was added to pilot the small end of the cage.

Since standard components were utilized, this bearing had the same nominal dimensions as the previous bearings, i.e., an inner ring roller path angle of 11°, an outer ring roller path angle of 15°, and a roller included angle of 4°. Nominal dimensions of these bearings are also shown in Table I.

C. AIRCRAFT TOLERANCED, STANDARD DESIGN BEARINGS

The third group tested consisted of bearings having rings manufactured to the commercial standard design, but using aircraft tolerances, fitted with standard rollers which were slightly modified. The standard rollers were reground on the large end to have a sphere radius equal to 75% of the distance to the inner ring apex, in lieu of the 95% normally used, in order to provide a more closely controlled roller/flange contact.

The rings were manufactured from through-hardened 52100 steel to grade 00 tolerances and were identical in design to the rings of the previous group except that the small end cage land-riding shoulder was integral with the bearing, three 0.0625 inch-diameter holes were provided through the inner ring instead of six, and the flange angle was slightly modified to match the altered roller sphere end radius.

Once again, a ground, 4340 steel, silver-plated and balanced inner ring land-riding cage was used. This bearing design is illustrated in Figure 5. Nominal internal geometry features are listed in Table I.

D. EXPERIMENTAL BEARINGS

The fourth group of bearings utilized in this program were completely manufactured of 52100 steel to an inner ring flange design developed under this program. This design was evolved

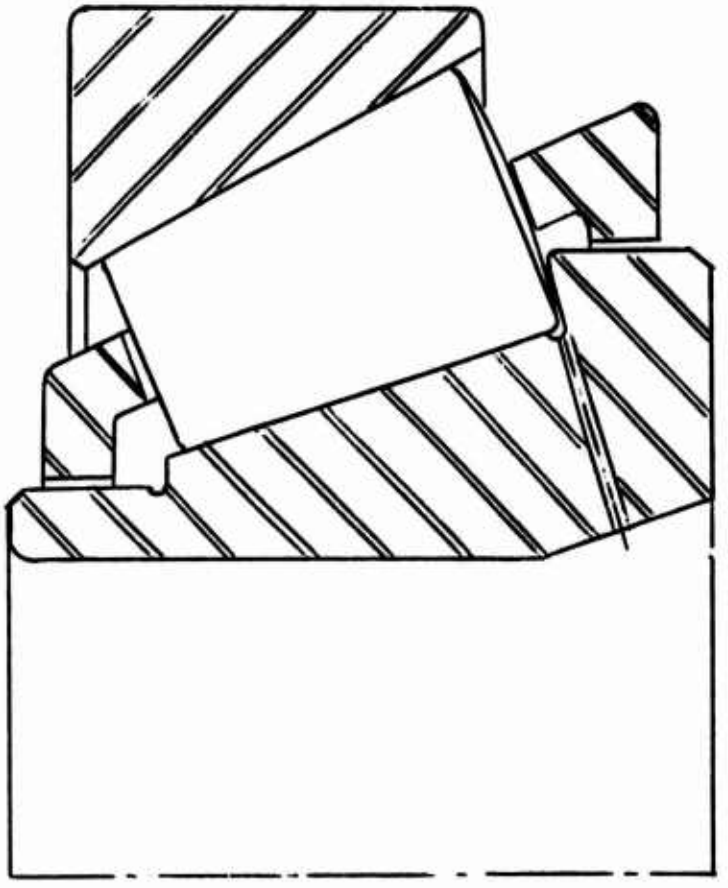

Roller End Radius 2.630"
Roller -.244" x .364"
Cup Angle 30° (Included)

Figure 5. Aircraft Toleranced, Standard Bearing Design Configuration.

from the results of the analytical work conducted in Phase 1 of this program and the results of testing the previous three groups of bearings. The complex interplay of the various geometric parameters of a tapered roller bearing design requires that the final product contain an optimized combination based on computer calculation, design engineering judgment, and manufacturing capability. The basic concept followed in the development of this bearing considered (1) the use of rollers of reduced diameter relative to those of the commercial bearing of a similar envelope dimension to reduce the magnitude of the roller centrifugal forces, and (2) the use of a reduced included roller angle relative to that of the commercial bearing to reduce the flange loading.

These bearings were also manufactured to aircraft tolerance levels, and utilized most of the improved design features of the previous bearings. The rollers had a large-end diameter of 0.200 inch and an included angle of 3° 16' 40", and the sphere end radius was again reduced, this time to 70% of the apex distance. The number of holes through the inner ring was returned to six, and a cage of the same successful design as that of the two previous groups was used. This design is illustrated in Figure 6, and nominal dimensions are given in Table I.

E. OUTER RING FLANGED BEARINGS

The analytical work that had been conducted illustrated that with increasing shaft speeds, the load carried by the inner ring would gradually be transferred from the race surface to the flange surface. This phenomenon is illustrated in the force diagram contained in Figure 7. At a critical speed, related to the magnitude of the applied load, the force at the race contact tends to go to zero and the entire load is carried by the flange. Although this declutching does not necessarily prevent bearing operation, it does have the undesirable feature of supporting all of the applied load on the critical sliding contact at the flange, which is limited in area. Also, questions arise as to the dynamic stability of a bearing operating in this regime, as well as the ability of a bearing to withstand the increases in heat generation and roller wear which would be encountered.

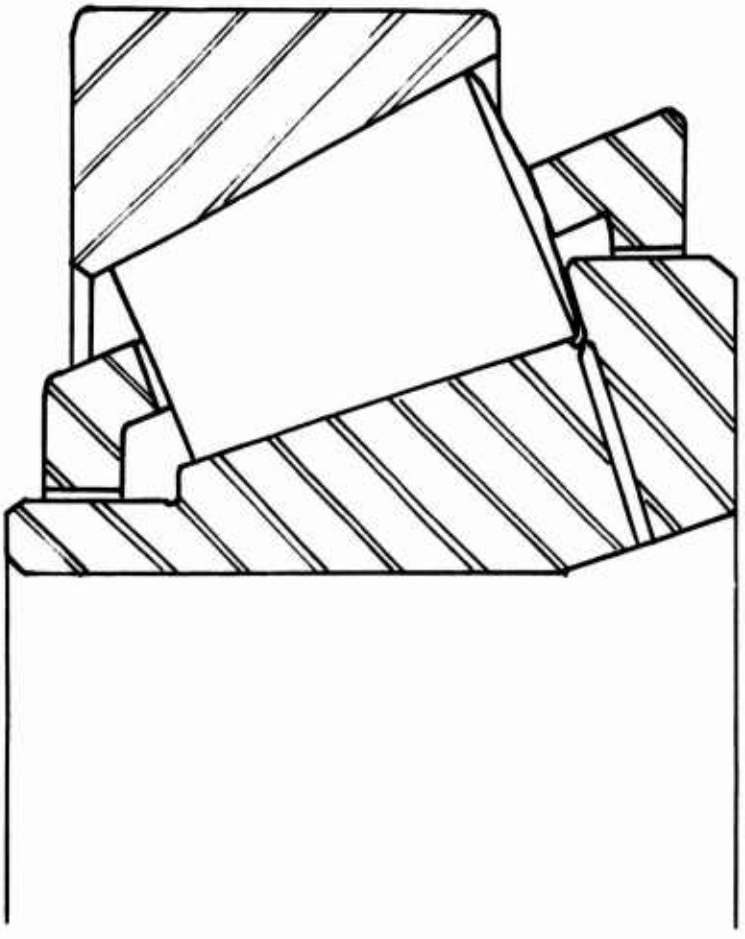

Roller End Radius 2.150"
Roller .200" x .364"
Cup Angle 30° (Included)

Figure 6. Experimental Bearing - Computer-Assisted Design.

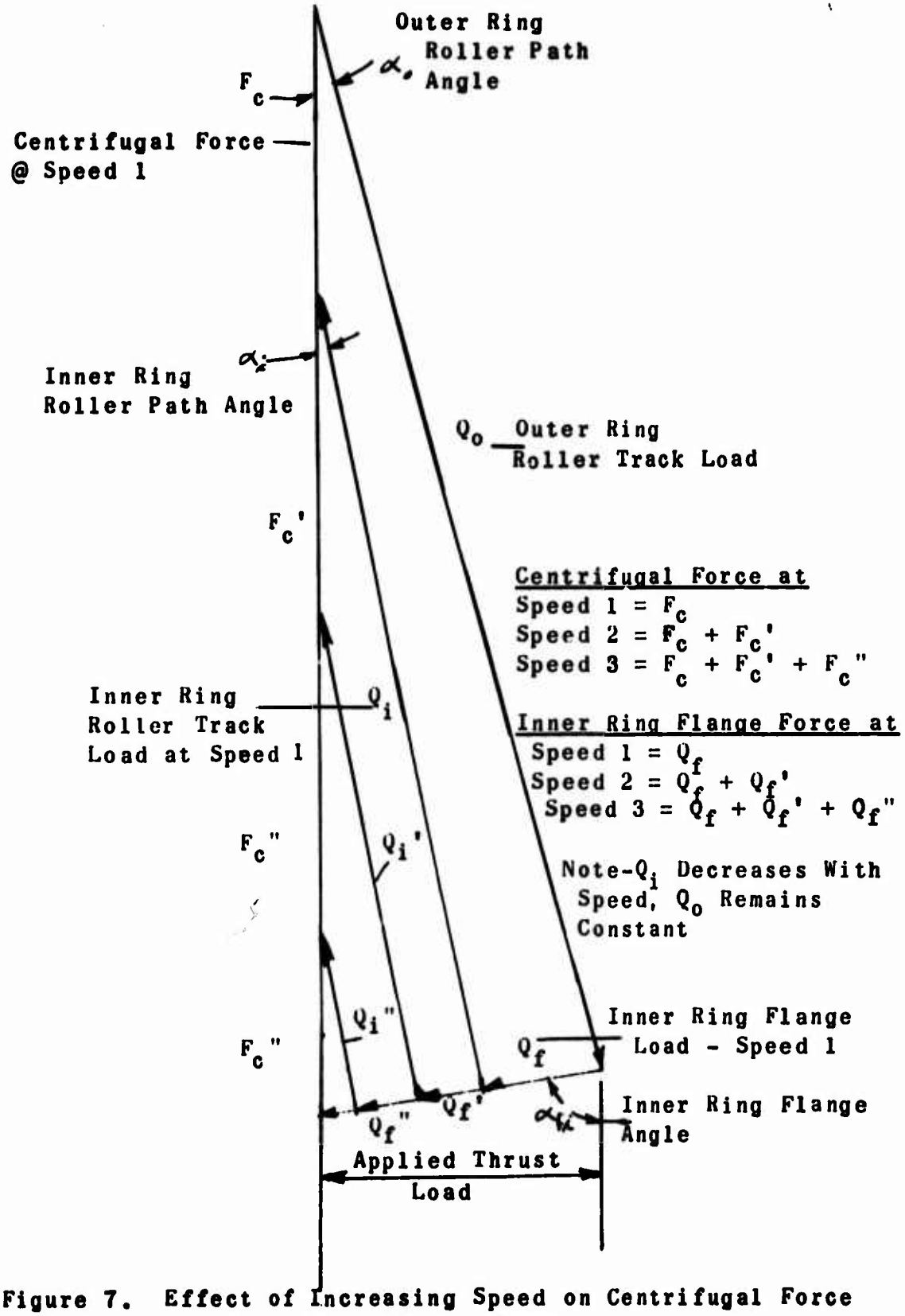

Figure 7. Effect of Increasing Speed on Centrifugal Force and Inner Ring Flange Force.

Rotor systems and bearing mounting configurations can no doubt be evolved to operate in the declutched condition, if not to prevent declutching altogether. However, it seemed more desirable at the present stage of development to investigate the design of a bearing in which declutching does not occur. Such a configuration results if the flange is transferred from the inner ring to the outer ring. Figure 8 shows the force diagram for this design and illustrates the effects of increasing speed. It is obvious that declutching will not occur in this configuration, but the flange and contact loading is increased rather drastically as a result.

Thus, fifth bearing design was made and a group of bearings manufactured for experimental evaluation at high speeds. This design configuration is illustrated in Figure 9. The rings of these bearings were manufactured of 52100 steel. An outer ring land-riding, machined and ground, silver-plated steel cage was manufactured. This design utilized the same reduced-diameter rollers as the experimental inner ring flanged design. The nominal dimensions of this design are given in Table I.

It did not appear to be necessary to provide radial holes through the inner ring for lubrication purposes in the absence of an inner ring flange. However, the placement of the flange on the outer ring did seem to create a pocket where oil could be trapped by the centrifugal effects on the oil due to bearing rotation. If so trapped, the oil would be heated by churning and cooler oil would be prevented access to the critical flange area, which might result in inadequate cooling and lubrication. Therefore, in an attempt to provide a path to insure oil drainage, six axial holes, 1/16 inch in diameter, were put in the flange face to the flange undercut.

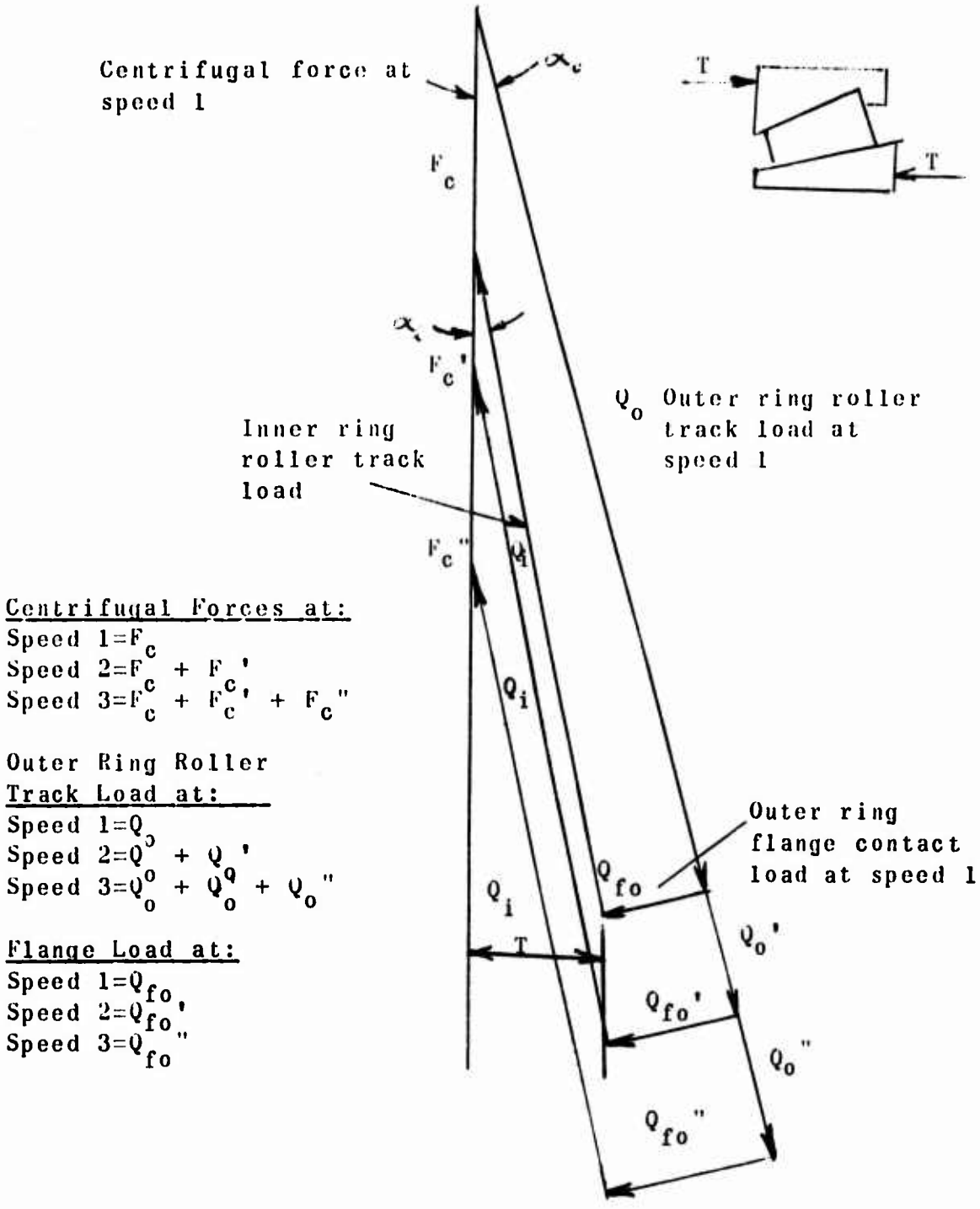

Note: Q_i remains constant with speed

Figure 8. Effect of Outer Ring Flange on Force Diagram.

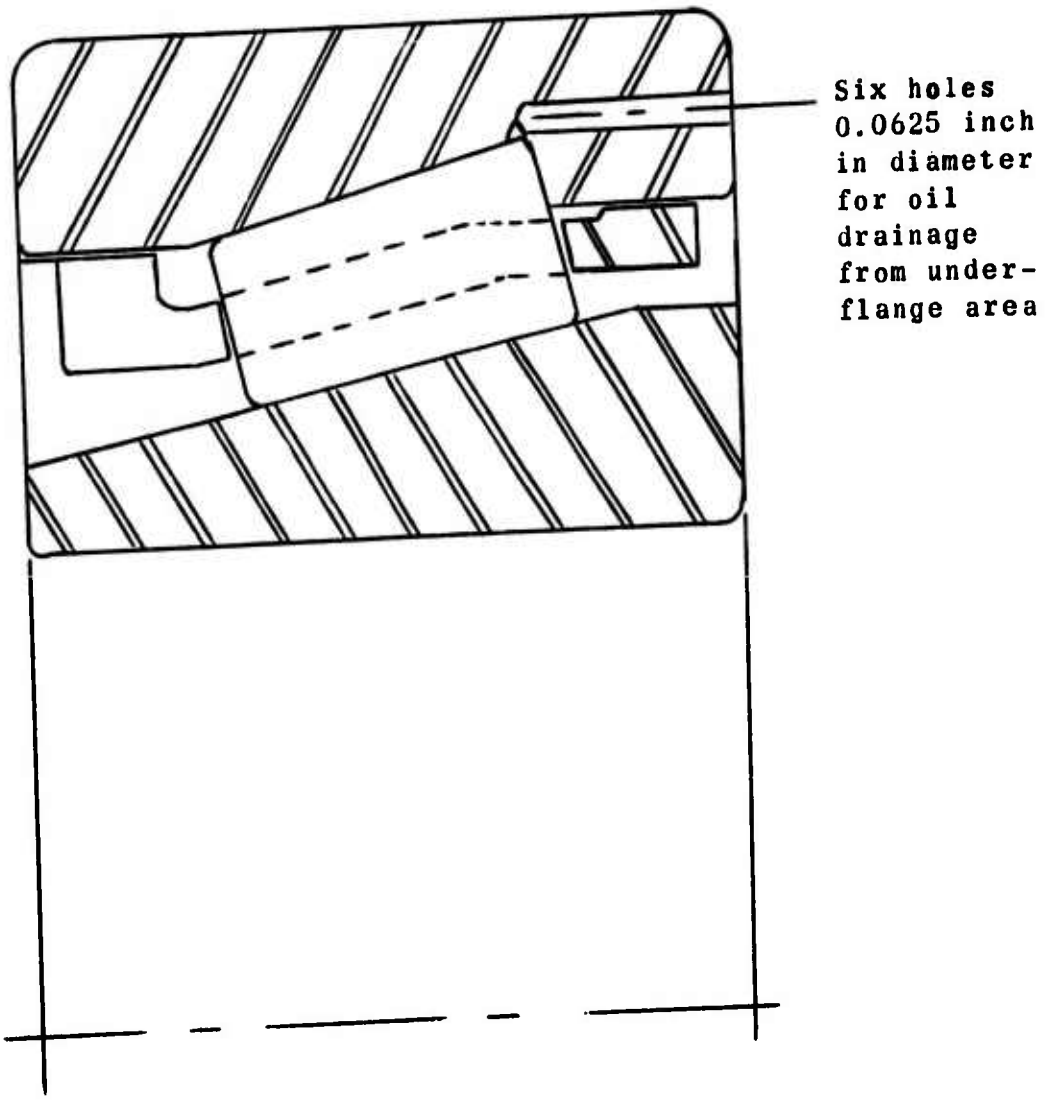

Figure 9. Modified Tapered Roller Bearing Design With Outer Ring Flange.

IV. METHODS OF INVESTIGATION

A. PHASE I

Phase I of this program was comprised of three distinct activities. This first of these was a survey of the major manufacturers of gas turbine engines in the 2-10 lb/sec airflow range to determine the requirements for bearing systems to be used in existing engines, and the planned or foreseen requirements of advanced engines. Coincidentally, detailed analytical studies were made to define the design concepts necessary for the development of a high-speed tapered roller bearing and their applicability to the requirements established through the survey. The third part of this phase then comprised the selection of actual bearing designs for manufacture and test.

1. Survey of Major Small Gas Turbine Engine Manufacturers

The goal of the survey of major manufacturers of small gas turbine engines was to establish the range of main-shaft bearing operating condition, i.e., rotational speeds, temperature, loads and oil flow rates, in existing and advanced 2-10 lb/sec airflow gas turbine engines. The results of the survey were used to establish performance criteria that would have to be met or exceeded by the proposed tapered roller bearing configurations. These results were then used as inputs for the computer-aided bearing design analyses which followed.

This survey was conducted during July and August 1970, and the following manufacturers were contacted:

1. AVCO, Lycoming Division, Stratford, Conn.
2. General Electric Co., West Lynn, Mass.
3. Allison Division of General Motors Corporation, Indianapolis, Indiana
4. Pratt and Whitney Aircraft, West Palm Beach, Florida

2. Analytical Program for Bearing Design Parameters

Analytical design studies were undertaken to establish the

necessary design criteria, in conjunction with experimental analysis, for high-speed tapered roller bearings. The variables included in the study are:

a. Cup angle - The angle which the outer ring race makes with the axis of the bearing (α_o).

b. Cone angle - The angle which the inner ring race makes with the axis of the bearing (α_i).

c. Roller included angle.

d. Roller/flange contact angle (α_f) - This angle, which is a function of flange angle and sphere end radius, is the angle which the roller/flange contact force makes with the axis of the bearing.

Optimization of the design parameters leads to many conflicting trends, requiring practical compromises. These factors were analyzed in detail and compromises were reached and evaluated prior to the establishment of the final test bearing design.

3. Selection of Tapered Roller Bearing Designs for Test

A digital computer program was written and used to conduct parametric studies of the effect of operating and design parameters on heat generation, roller contact loads and stresses, centrifugal forces, and bearing life as key performance characteristics of tapered roller bearings of the single flanged design.

A careful review of the data resulting from the program execution, past experience with tapered roller bearings, the established application requirements, and the results of the preliminary tests allowed the establishment of final design values for the numerous bearing variables.

B. PHASE II

The second phase of this program consisted of the functional testing for step-speed performance characteristics and extended testing of two of the bearings at maximum operating speed. All tests were initiated in the mechanically driven

tester, described in Section IIA, and the test sequence was completed on the turbine-powered rig described in Section iib, when it became clear that the operational capability of the bearing far exceeded the speed capability of the mechanically driven tester. The following procedures were followed in the tests.

1. The critical parameters of each test bearing were measured and the data recorded. Those dimensions considered to be critical were (1) the flange angle, (2) the roller path diameter and the roller included angles, (3) the cross-roller-path profile geometry, and (4) the concentricity of the inner ring roller path to the bore. The high point of the inner ring eccentricity was located and marked on the shoulder of the ring so that the bearings could be mounted on the shaft with these high points diametrically opposed to the shaft high points, minimizing shaft runout. The rollers for each bearing were selected for uniformity of outer diameter, with the maximum allowable diameter variation in each set being 20×10^{-6} inches. The rollers were manufactured to an angle tolerance defined by the maximum permissible diameter variation, end to end, of 0.000050 inch. The cages used in each bearing were balanced to 0.014 ounch-inch.

2. For those tests conducted at high speed, i.e., in the air turbine rig, the total rotating assembly shown in Figure 10, was balanced to within 0.001 ounce-inch. This was conducted by rotating the assembly on the test bearings in a calibrated balancing machine and adjusting the mass distribution until it was acceptable.

3. Those bearings tested in the mechanically driven rig were assembled with the test bearing located in the load plug and the support ball bearing located at the drive end (Figure 1). The 460-pound axial load was applied, and the drive quill was connected to the drive end of the shaft from the high-speed gearbox. It was adjusted to have a maximum runout of $\leq$ 0.001 inch.

The functional tests were started by bringing the test assembly to 4000 rpm and allowing the bearings to run in at that speed for approximately 8 hours. During this period, oil temperature was maintained at approximately 100°F with a

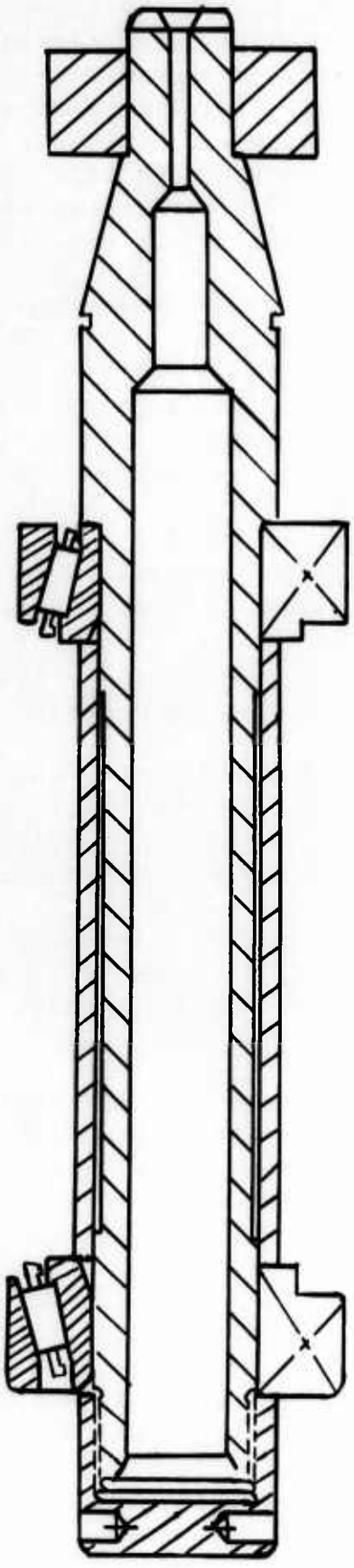

Figure 10. Test Shaft Assembly as Balanced.

flow of 0.6-0.7 gpm to provide an outer ring operating temperature of 130°F. After that period, the speed was increased in increments of approximately 4000 rpm, with 2-hour intervals being allowed between speed changes for system thermal stabilization. This was continued to a maximum speed of 46,000 rpm, and this speed was maintained for 20 hours. Testing was terminated at the end of this period, and the test bearing was removed for inspection.

All test bearing temperatures were monitored during the test sequence, along with the oil-in and oil-out. Oil pressures to both bearings were also monitored and recorded. Vibration sensitive switches monitored the vibration level of the bearings and provided automatic machine shutdown in the event of bearing failure through spalling.

4. After the testing of the first two outer ring flanged bearings, the procedure was modified to conduct all subsequent outer ring flanged tests under a reduced load of 240 pounds to provide roller path contact forces at 50,000 rpm similar to those of the inner ring flanged design. All other procedures remained as previously described.

5. Tests conducted on the air-turbine-powered test rig were conducted under essentially identical conditions as described in 3 above. However, it was necessary to discontinue the use of a support ball bearing in favor of the mounting of two opposed tapered roller bearings on the test shaft in order to achieve a dynamically stiffer shaft and to increase the (relatively) low shaft critical speed resulting from the use of a "soft" ball bearing along with the stiffer tapered roller bearing.

The shaft was assembled in the test housing and the lubrication system activated. The axial load was applied through two springs mounted on the load end of the test housing (Figure 2). The drive air (heated to 350°F to avoid nozzle icing) was turned on and the test conducted in a step-speed sequence. The bearing slow-speed run-in period was reduced to approximately 4 hours, after which the speed was increased in steps of 5,000-10,000 rpm until the maximum possible speed was attained. For outer ring flanged design bearings, the maximum speed was 95,000 rpm. The inner ring flange design bearings reached the declutched mode at a speed of approximately 85,000 rpm at the test load imposed and was not run faster due to the resulting rotor instability.

V. RESULTS

A. PHASE I

1. Survey of Major Small Gas Turbine Engine Manufacturers

Each of the four manufacturers surveyed was in the process of building and developing an advanced prototype (demonstrator) engine in the 2-10 lb/sec airflow range. The specific conditions under which the main-shaft bearings would be required to operate for each engine and the performance expected were reviewed. These findings are tabulated in Table II. The manufacturers were also asked to speculate on future design trends for small gas turbine engines, especially with regard to main-shaft speeds and diameters. The general out-look of each manufacturer on the problem of main-shaft bearings was summarized into key points, which are also given in Table II and are described more fully below.

All four manufacturers, at the time of the survey, were designing engines with specified DN values for the main-shaft bearing of 1.6 to 2.0 x 10^6, which is within range of current technology. However, trends suggest that bearings capable of 2.5 x 10^6 DN will be required in the next few years and 3.0 x 10^6 DN in the foreseeable future. These higher speeds are desired without having to suffer penalties or tradeoffs in bearing life, load-carrying ability, and reliability.

The limiting factor at the present time which governs the maximum design speed of turbine engines lies with the turbine tips. Owing to the limitations of present materials, turbine tip peripheral speed is not expected to increase drastically within the next 10 years. Lycoming estimates a 10-20% increase during this period. However, this is not to say that shaft speed, and hence bearing speeds, will not increase significantly. Builders are currently planning simplified (low-cost) engines with more-compact dimensions having smaller OD's and shorter lengths which will produce power levels comparable to existing, larger engines. By reducing the diameter of the turbine wheels, higher shaft speeds are possible without exceeding the peripheral speed limitation of the turbine tips. Correspondingly, the use of smaller diameter main shafts (and bearings) is not anticipated owing to considerations of shaft rigidity and critical vibrations,

TABLE II. SUMMARY OF ENGINE MANUFACTURERS' SURVEY

	Lycoming	General Electric (W. Lynn)
Engine	AGT 1500 10 lb/sec Airflow 1500 Horsepower	GE 12 9.5 lb/sec Airflow 1500 Horsepower
Ball Bearing	45 MM Bore M-50 Steel	45-50 MM Bore M-50 Steel
Speed	42,500 rpm	45,000 rpm
Bearing DN Value	1.9 Million	2.0 Million
Load	1000 lb Radial, 500 lb Thrust	500 lb Thrust
Calc. AFBMA L_{10}	1000 hr	$\measuredangle$1000 hr
Lubricant	23699	23699
Oil-In	200°-250°F	200°-250°F
Oil-Out	350°-400°F	300°-350°F (Possibly)
Brg. Temp. (Outer Ring)	-	350°F
Oil Flow Rate	-	-
Outlook	(1) Maximum turbine tip speed to increase 10-20% in next 10 years. (2) 3 million DN bearings will suffice for next 10 years. (3) Would like to have 10 times the load-carrying ability: Thrust compensating devices could be simplified and TBO extended. (4) Could go to higher temperatures using advanced synthetic lubricants. (5) Radial load due to shaft unbalance is an important consideration.	(1) Maximum turbine tip speed will not increase much in next few years. (2) Bearings in smaller engines (to 2 lb/sec) may run 2.5-3 million DN. (3) Interest in mist lubrication as a means of engine simplification and weight reduction. (4) Anticipate higher temperatures.

TABLE II - Continued

	Allison		PWA Florida	
Engine	250 T		ST 9	-
	2.5 lb/sec Airflow		8-9 lb/sec	3.5 lb/sec
	400 Horsepower (Series 2)		1500 Horsepower	450 Horsepower
Ball Bearing	30 mm Bore, M-50 Steel		40-55 MM, M-50 Steel	30 mm Bore
Speed	53,000 rpm		-	65,000 rpm
Brg. DN Value	1.6 Million		2 Million	2 Million
Load	200 lb Thrust		-	300 lb Thrust
Calc. AFBMA L_{10}	-		2000 hr	-
Lubrication	23699 and 7808		23699	23699
Oil-In	225°F		250°F	-
Oil-Out	-		-	-
Brg. Temp. (Outer Ring)	200°F-250°F		-	-
Oil Flow	0.25 GPM (Jetted)		-	-
Outlook	(1) Engine speed may go to 70,000 rpm (2.1 million DN bearing).		(1) 2.5 Million DN in a few years, 3.0 Million DN in foreseeable future.	
	(2) Do not anticipate higher bearing operating temps.		(2) Anticipate highter temperatures along with increased speed.	
	(3) Very interested in using tapered roller bearings in gearboxes.		(3) Advanced smaller engines tending to operate supercritical (pass through shaft criticals).	
	(4) Very high on M-50 steel.		(4) Thrust bearing sees as much radial load as thrust load.	
			(5) Would like to have higher capacity, smaller size bearings.	

although engines are envisioned which operate "supercritical", i.e., pass through shaft vibration criticals during startup, placing added loads on the bearings.

Therefore, the apparent near-future need is for bearings capable of 3 million DN. In the event of any "breakthroughs" in turbine tip technology owing to new materials, designs, etc., a need for 4 million DN (and higher) bearings could materialize.

Three engine manufacturers expected nominal bearing operating temperatures to increase above present levels of 250°-400°F. Higher temperatures up to 600°F are currently possible using CVM M50 steel for bearing components and undoubtedly will be attained as soon as an acceptable, economical lubricant is available. The presently used MIL-L-23699 mixed-ester-based lubricants are generally unsuitable for the higher temperature ranges, so other more advanced synthetic lubricants must be used.

All of the manufacturers were vitally concerned about bearing life, load-carrying ability, and reliability. A key requirement appears to be the obtaining of bearings capable of carrying larger loads than now considered feasible. By allowing bearing thrust loads to increase, the engine thrust-compensating devices could be simplified, resulting in cost and weight savings. Alternately, improvements in bearing life could result in an extension of engine TBO (time between overhaul).

Owing to higher shaft speeds, radial loads resulting from imbalance and maneuvering, as well as from centrifugal ball and roller loads, have increased significantly in recent years. Pratt and Whitney estimates that the thrust bearing (in the late-design engine they used as illustration) sees as much radial load as thrust load, while Lycoming estimates in their case that it sees twice as much radial load as thrust load. Present design practice is to balance off as much of the thrust load, and design out as much of the radial load, as is required to give a calculated bearing life of approximately 1000 hours. During startup, reverse thrust loads are possible and a bearing mounting system designed to support the engine main shaft must be capable of carrying reverse loading.

Additional Findings

Allison and Lycoming expressed interest in the concept of using tapered roller bearings in their gearboxes and tranmissions.

General Electric was interested in the feasibility of using mist lubrication in future low-cost engines as a means of simplification and weight and space savings by eliminating most of the lubrication system components such as pumps, coolers, valves, and return lines.

2. Analytical Evaluation of Bearing Design Parameters

a. Kinematic Relationships of a Tapered Roller Bearing

Prior to the conduct of a computerized design optimization study, a model of the system to be studied was conceived and criteria for the optimization of design parameters were developed. As a basis for the model development, the tapered roller bearing of conventional design schematically represented in Figure 11 was used. A force balance diagram was prepared for a single rolling element for specific operating conditions. Figure 12 presents such a force balance diagram for a single tapered roller operating under an applied thrust load (FA) at a speed sufficient to develop a significant centrifugal force. The weight (as opposed to the mass) of the rolling element can be disregarded, as it is very small in comparison to the other forces discussed.

The following force equilibrium equations can thus be obtained from the force diagram of Figure 12:

$$Q_i \sin\alpha_i + Q_f \sin\alpha_{fi} = Q_o \sin\alpha_o \qquad (1)$$

$$Q_o \cos\alpha_o + Q_f \cos\alpha_{fi} = Q_i \cos\alpha_i + F_c \qquad (2)$$

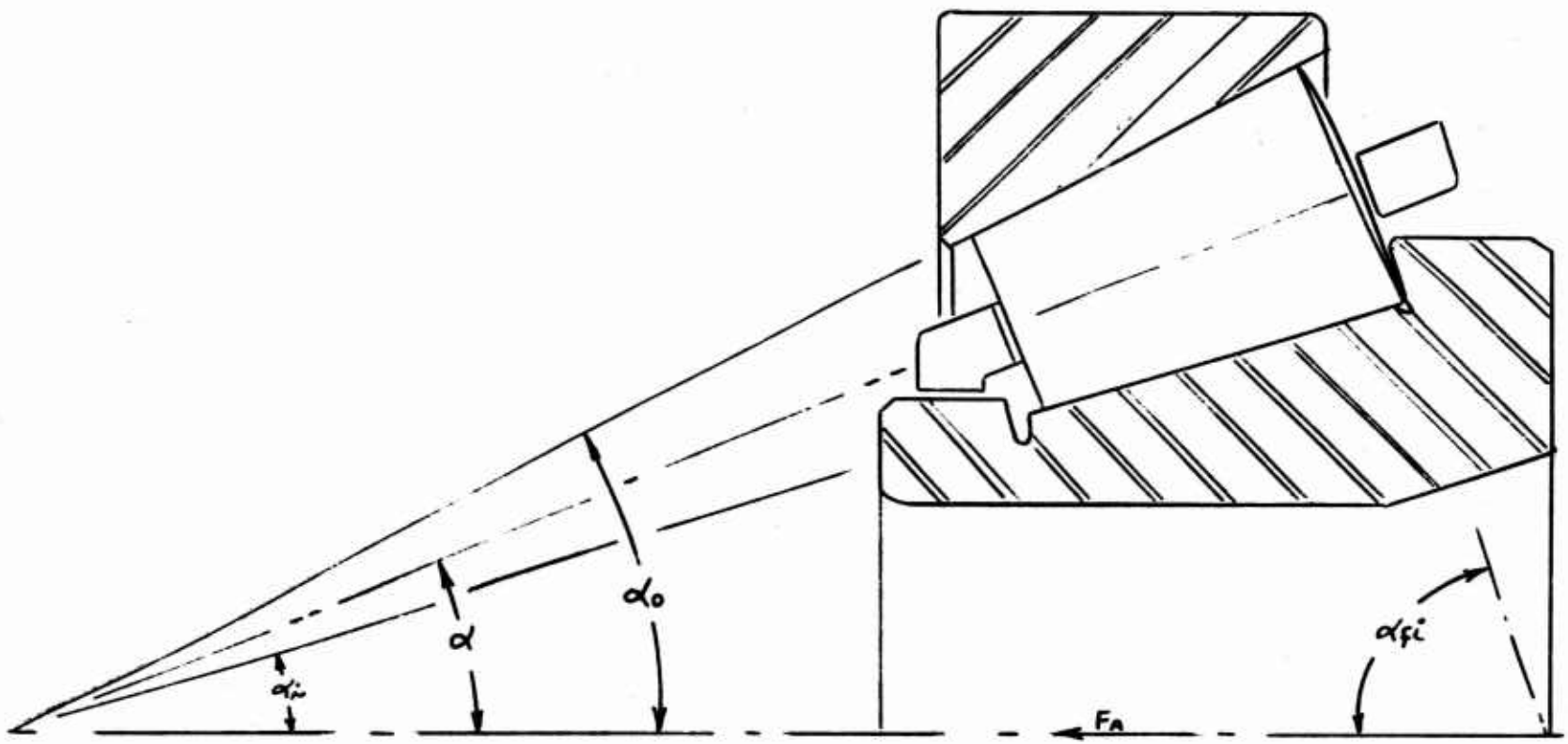

Figure 11. Conventional Tapered Roller Bearing.

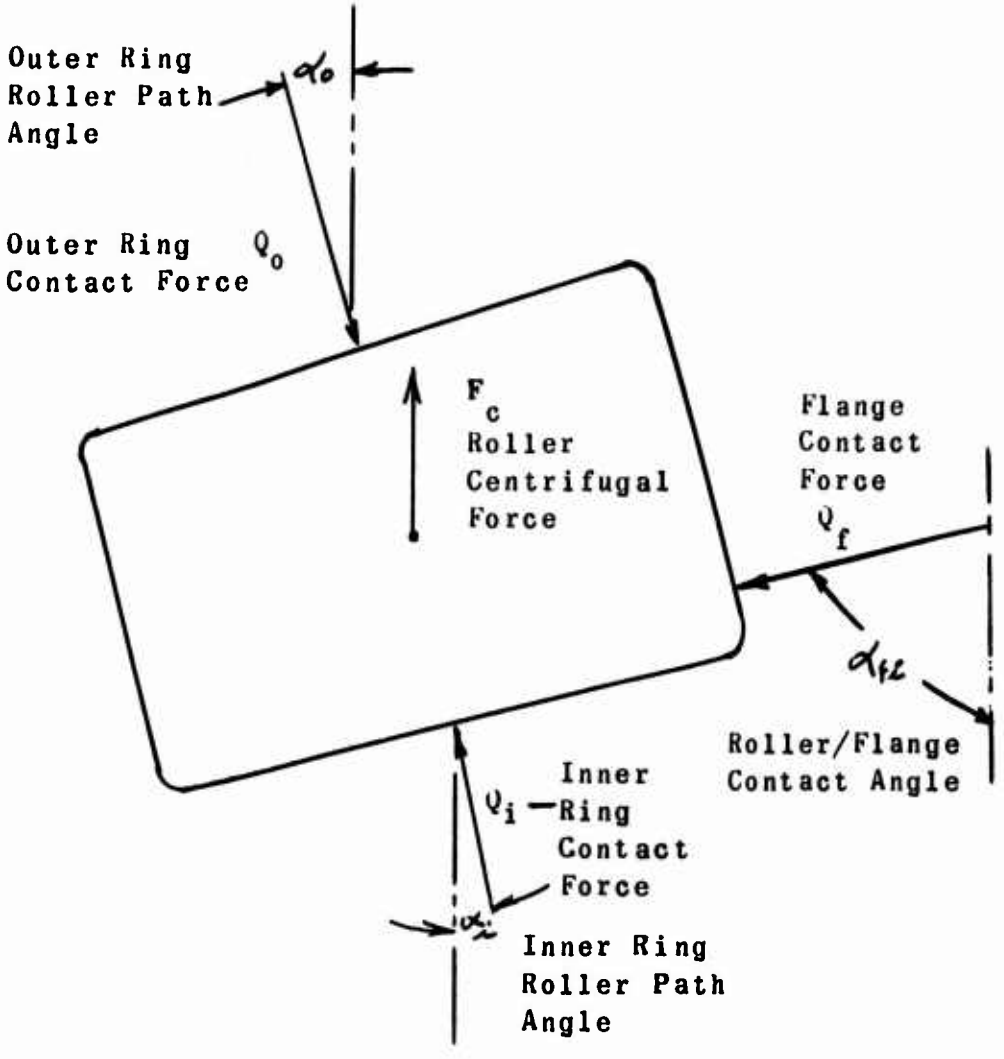

Figure 12. Forces Acting on a Tapered Roller.

where Q_i, Q_o and Q_f are the loads exerted on the roller by the inner ring, outer ring, and flange, respectively, as shown in Figure 12. F_c is the roller centrifugal force, and the angles α are defined in Figure 11.

In a similar fashion, Figure 12 shows the force balance diagram for the cup.

For the condition of pure applied thrust load,

$$Q_o \sin \alpha_o = F_A/Z \tag{3}$$

The substitution of (3) into (1) and (2) and the rearrangement of terms yields

$$Q_i = \left[\frac{F_A}{Z} \sin(\alpha_o + \alpha_{fi}) - F_c \sin\alpha_o \sin\alpha_{fi}\right] \Big/ \sin\alpha_o \sin(\alpha_{fi} + \alpha_i) \tag{4}$$

$$Q_f = \left[Q_i \sin(\alpha_o - \alpha_i) + F_c \sin\alpha_o\right] \Big/ \sin(\alpha_o + \alpha_{fi}) \tag{5}$$

An examination of (4) illustrates that it is possible under high-speed conditions to develop a centrifugal force (Fc) which will overcome the effects of the applied thrust load (Fa/z) and cause the inner ring contact force (Q_i) to go to zero.

This situation, referred to as declutching of the bearing, requires that all of the applied thrust load be reacted at the inner ring through the flange roller end contact. Since this contact is one where sliding occurs, it is desirable to limit the magnitude of the flange contact force. Also, when declutching (the elimination of the inner ring contact force) does occur, all of the roller guidance must be provided by the flange, which could allow excessive roller skew. This could lead to cage wear and to smearing and excessive sliding heat generation at the flange. Therefore, it is desired to avoid declutching. To do so a bearing design should meet the requirements of the following inequality, obtained from equation (4), over the entire range of speeds considered

$$F_c < \frac{F_A \sin(\alpha_o + \alpha_{fi})}{Z \sin\alpha_o \sin\alpha_{fi}} \tag{6}$$

Since Fc is a function of speed, (6) defines the limiting speed for declutching for any inner ring flanged tapered bearing design.

From (3), it can be noted that the outer ring contact force (Q_o) is not a function of the centrifugal force, but only the applied thrust load. This indicates that the centrifugal force is reacted internally in the bearing up to the time that declutching occurs. Once this occurs, the bearing support system must axially confine the bearing, i.e., increase the applied thrust, if the integrity of the bearing system is to be maintained.

An examination of (5) illustrates ways of reducing the flange contact force. This force will be reduced as the outer ring and inner ring angles α_o and α_i approach each other. The obvious limiting case in this approach is a cylindrical roller (These formulas are not applicable in the limit, and it should not be assumed that a cylindrical bearing can carry thrust with no flange load.)

b. Graphical Force Balance Analysis

One of the major goals of the mathematical modeling process was to establish design optimization criteria to be used in the development of bearing designs. Although it is possible to draw conclusions from the formulas developed, the trends thus defined are not intuitively obvious and do not allow the total understanding of the interactions of parameters that is required if a design is to be successfully completed. To obtain further insight into these interactions, a graphical force balance analysis was also completed.

Figure 13 gives the vector force balance diagram for one rolling element of a tapered roller bearing and running at moderate speed. For illustrative purposes, this vector diagram represents a Phase II designed bearing running at 50,000 rpm with a 450 lb thrust load. The magnitudes of the developed

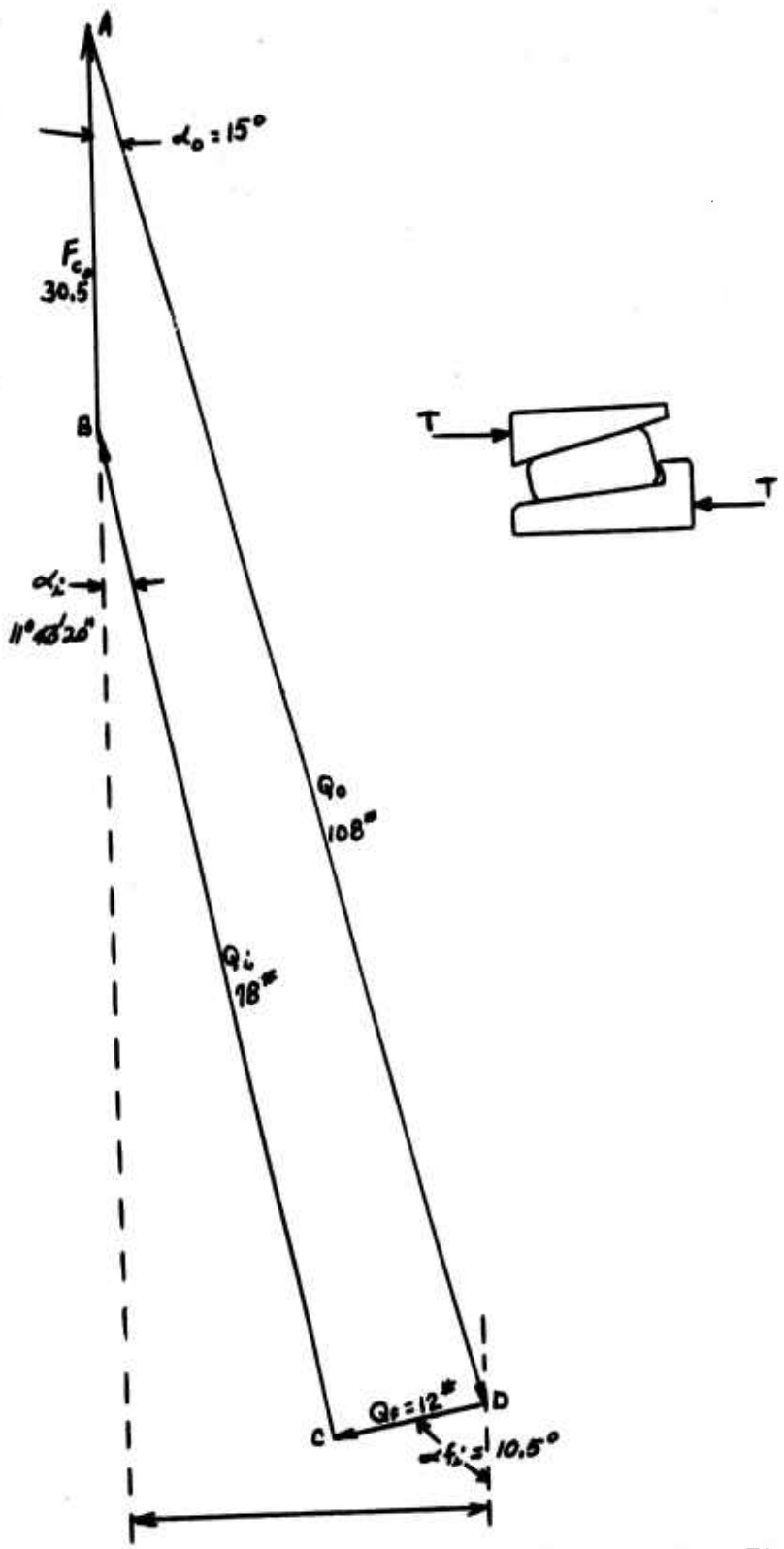

Figure 13. Roller Force Diagram for Inner Ring Flanged Bearing at 50,000 RPM.

loads and angles are given on the drawing.

The declutching phenomenon was illustrated in Figure 7. As the rotational speed of the bearing is increased, the centrifugal force of the roller (Fc) increases to Fc', Fc'', and finally Fc'''. Since the external applied load remains constant, Qo, the outer ring contact force, can not vary and the increase in Fc causes adjustments in the inner ring contact force (Qi) and the flange contact force (Qfi). Increasing Fc produces a decreasing Qi, (e.g., Qi', Qi") and an increasing Qfi (e.g., Qfi', Qfi"). Finally, at the critical speed, Qi goes to zero and Qf is reacting all of the applied thrust load; i.e., declutching has occurred.

The effect of continuing to increase operational speed beyond the declutching point is illustrated in Figure 14. The only way that the increased centrifugal force thus be supported only reactions at the outer ring and flange contacts. This increased reaction can thus be supported if the bearing support system has the capacity to provide an increase in the externally applied thrust load. If such capacity is not available, the bearing will separate under these forces and cease to be effective. Even if the capacity exists, the life of the bearing is detrimentally affected by the increased load at the sliding flange contact and the increased Hertzian stresses in the outer ring which could produce early fatigue failures and/or edge loading, depending upon the magnitude of the forces generated.

At this point, it appears logical to examine the effects of varying some of the basic design parameters. Figure 15 illustrates the effects of varying the outer ring angle (α_o). If the angle is increased, for any given applied thrust load, the inner ring and outer ring contact forces are reduced at the price of increasing the flange contact force. Also, the centrifugal force that can be internally reacted, i.e., the critical speed, is reduced.

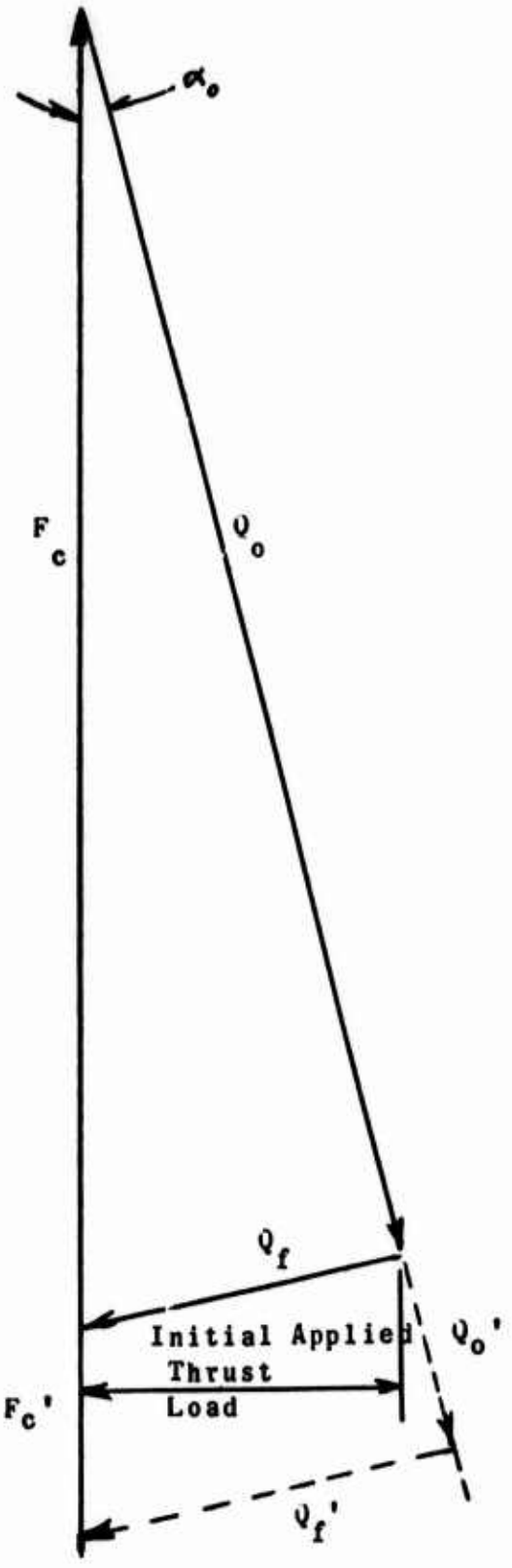

Figure 14. Effect of Increasing Operational Speed Beyond the Point of Declutching.

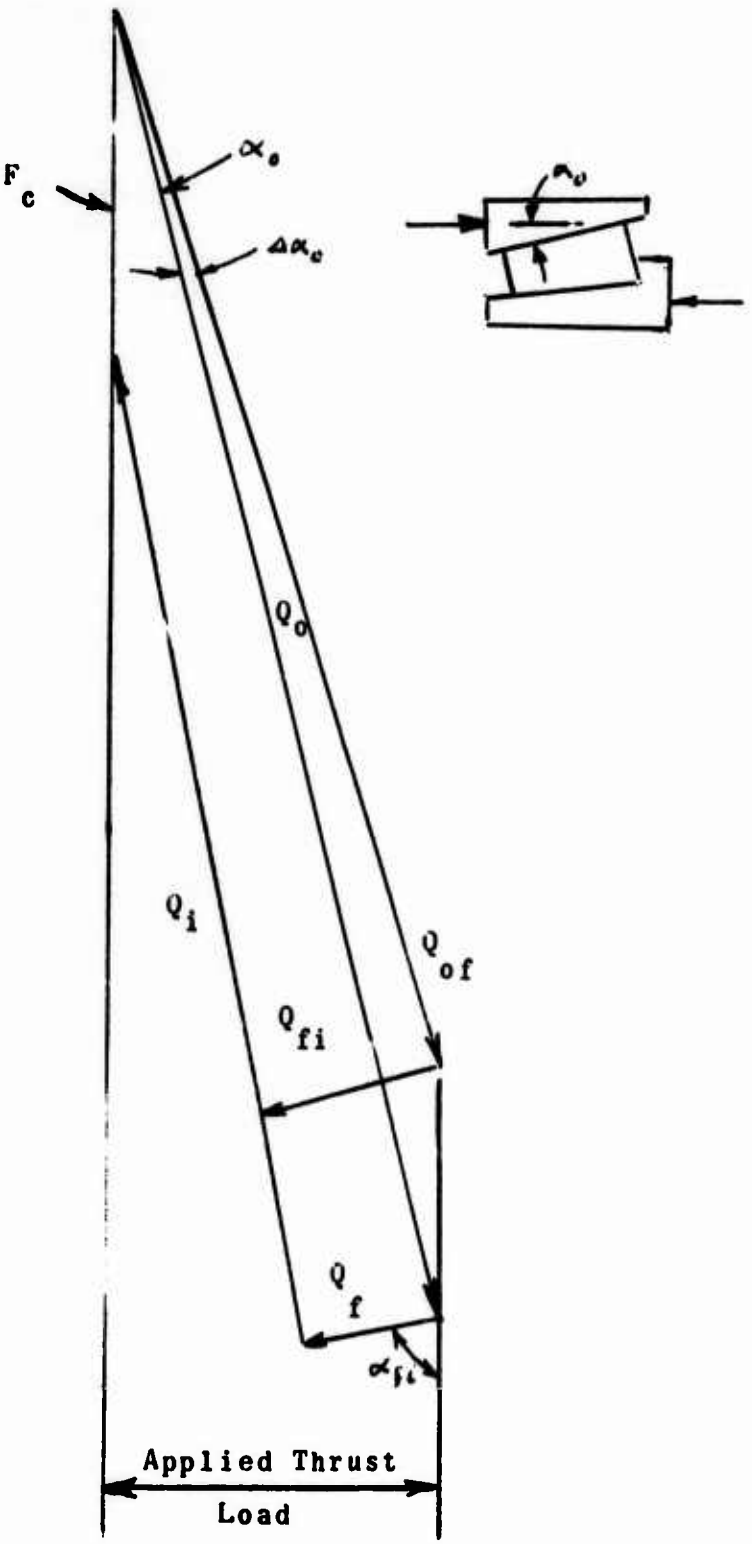

Figure 15. Effect of Varying the Outer Ring Roller Path Angle.

Conversely, if the angle is decreased, the flange force is reduced, while the critical speed and the inner and outer ring contact forces are increased. Since such a change, for a given cone angle, allows less room for a roller, race contact stresses are increased both by the increased loads and the smaller contact area available due to the decreased roller radius. This design compromise must be optimized during design analysis.

Similarly, the cone angle, α_i, must be optimized both as an independent variable and as a factor in the overall force balance of the bearing. Figure 16 shows that an increase in the inner ring roller track angle will provide a decrease in the inner ring flange force and an increase in the roller track contact load. Figure 17 shows that, if both the inner and outer roller track angles are increased the same amount, the controlling angle in the force diagram is the outer roller track angle, α_o. The roller track loads, in this figure, are shown to be reduced substantially with this design change, approximately 29 pounds on the outer roller track and 28 pounds on the inner ring roller track. The corresponding increase in the inner ring flange load is 1.7 pounds/roller.

Two directions of design compromise are possible. Figure 17 illustrates that if the outer ring and inner ring angles are decreased, the minimum angles are limited by the roller path contact forces, which will increase rapidly. (Since the flange/roller force is the major heat generation source, the increasing of the roller path angles is basically undesirable because of the increase in flange load resulting.) The alternate design approach (Figure 18) is to reduce the outer ring angle and increase the inner ring angle to minimize the flange forces, to a point where the bearing fatigue life is not excessively penalized by the resulting increase evident in the roller path contact forces, Q_o and Q_i.

The effect of centrifugal force on an inner ring flanged bearing was shown in Figure 7; this factor reduces the inner roller path contact force and

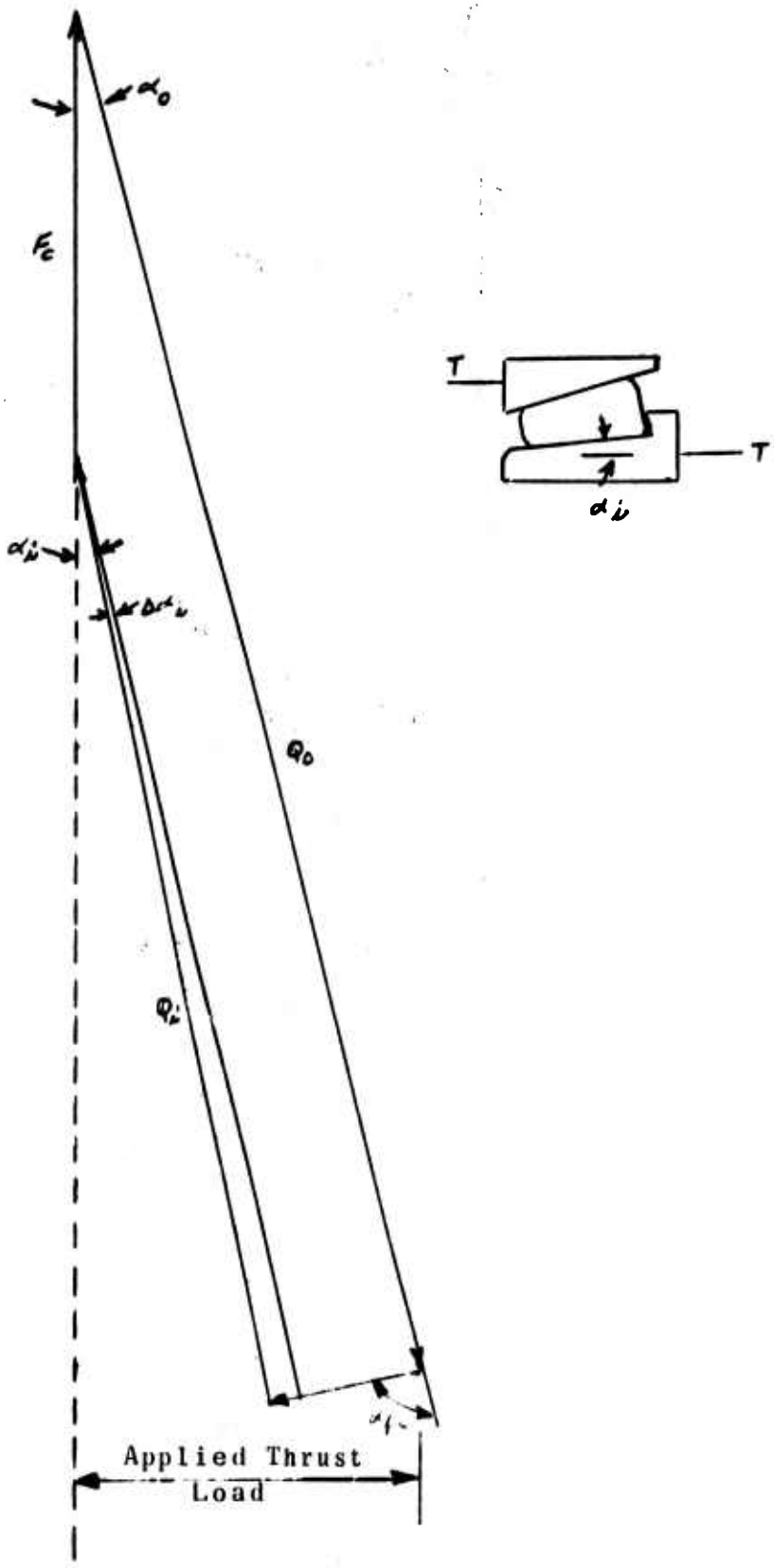

Figure 16. Effect of Varying the Inner Ring Roller Path Angle.

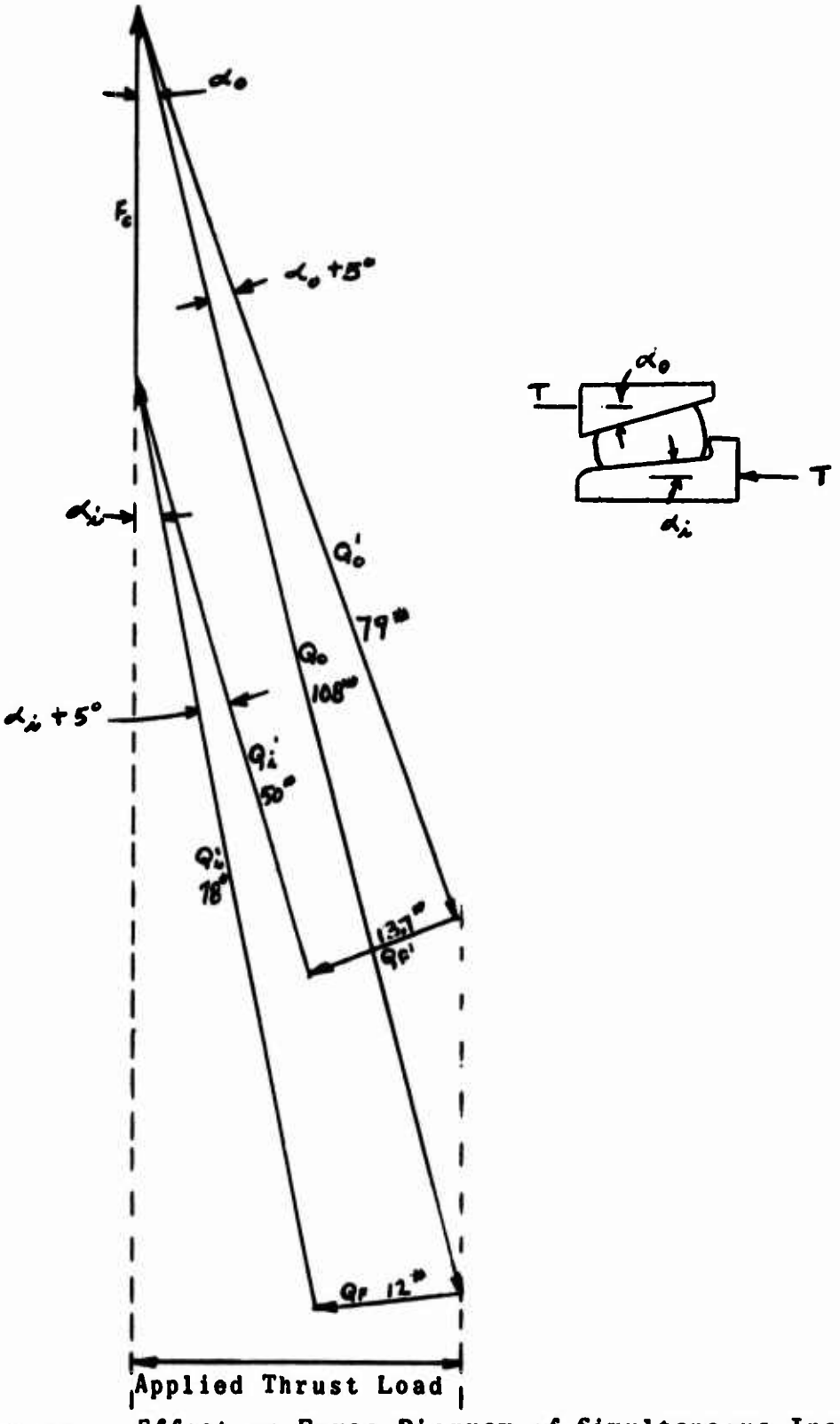

Figure 17. Effect on Force Diagram of Simultaneous Increase in Outer Ring and Ring Roller Path Angles (α_o and α_i).

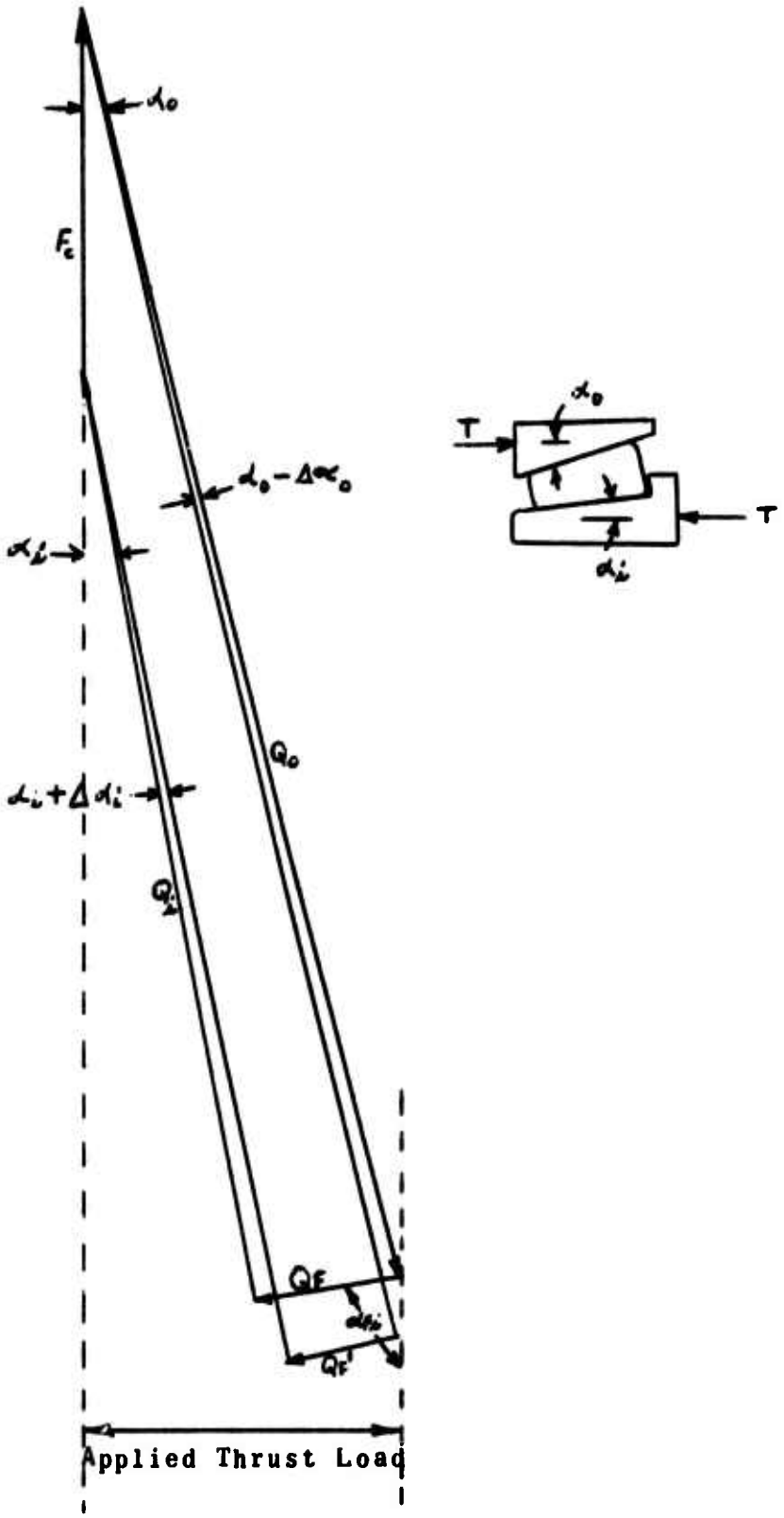

Figure 18. Effect of Simultaneous Change in Inner Ring and Outer Ring Included Angles.

increases the inner ring flange contact force. The ideal design concept, with respect to centrifugal force, is to design the bearing so that the inner and outer roller path angles approach each other (as in Figure 18), resulting in a small roller included angle and a minimum flange force. The small roller included angle also reduces the roller mass and, hence, the centrifugal force, and permits higher speed operation before declutching occurs.

As a means of achieving a high-speed operating regime, without bearing declutching taking place, the use of a preloaded pair of tapered roller bearings can be considered (Figure 19), each having a single functioning flange on the inner ring. The externally applied load, T, smaller than the preload P, on a pair of these bearings results in the force diagram shown. It is immediately clear that declutching will not occur in this mounting configuration even under conditions of reversing thrust when the applied thrust is zero pounds. The force diagram ABCD illustrates the zero externally applied thrust load condition and shows that the preload insures proper bearing operation. It also shows, however, that, for a given speed, the external thrust must always be less than the preload P, or one bearing becomes critical and declutches (force diagrams AEFD and ADG).

As shown in Figure 7, the effect of an increasing centrifugal force will be to decrease the inner ring contact force and increase the flange contact force. In the preloaded bearing pair of Figure 19, under conditions of <u>increased</u> speed (force diagram AHKB), it is shown that a lesser external thrust load compared to force diagram ADCB, representing a slower speed, is sufficient to cause one bearing to declutch.

Thus, in a preloaded tapered roller bearing pair, a relatively high preload and a correspondingly high flange load are required to prevent declutching under the full range of externally applied loads, and

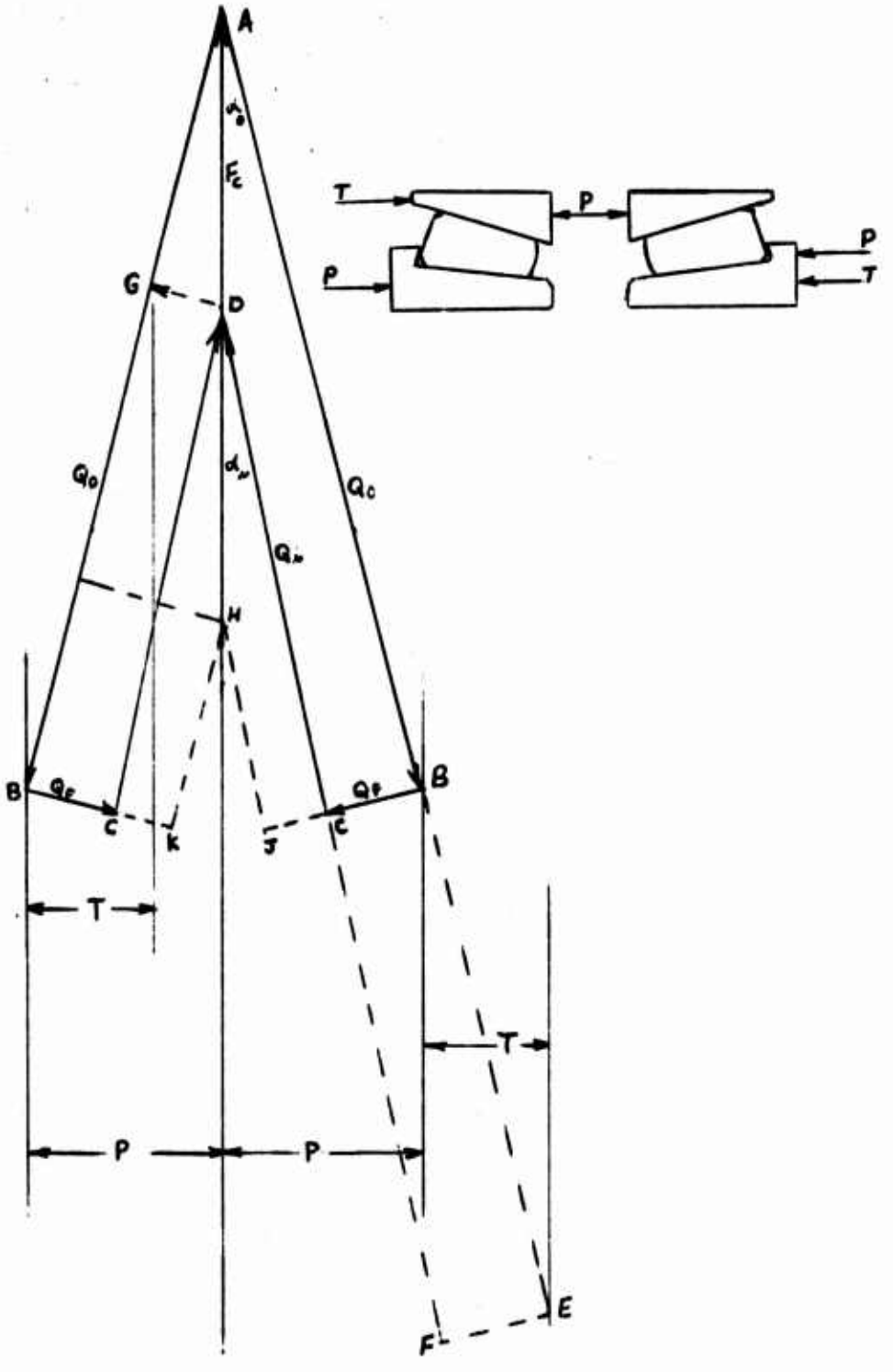

Figure 19. Effect of Preload on a Pair of Tapered Roller Bearings of Conventional Design (See Figure 3).

increasing speeds require increasing preloads.

The recognition of the declutching phenomenon gives rise to consideration of an unconventional tapered roller bearing in which the inner ring is a plain cone and the outer ring is equipped with one functioning flange at the outboard end of the roller (Figures 8 and 9). In this design, all externally applied thrust is transmitted through the inner ring roller track surface and thrust and centrifugal force are carried through the outer roller track and flange. The result is force diagram ABCD shown in Figure 20.

The characteristics of the outer ring flanged bearing shown on Figure 20 are such that the flange force CD is inevitably larger than the inner ring flange force of Figure 13 under the same externally applied thrust load.

In Figure 21 it is seen that the flange force is reduced as the cup and cone angles and/or roller included angle are reduced, as was the case with conventional inner ring flanged bearings shown in Figure 18. The outer ring flanged bearing and the inner ring flanged bearing are compared in Figures 22 and 23; flange forces are comparable in magnitude for these two bearing designs, but the larger force is always on the outer ring flanges for all speed and load conditions up to the condition of speed and load at which the inner ring flanged bearing declutches. The outer ring flanged bearing is still functional at that point and will continue to the flange overload failure point.

The major advantage of the outer ring flanged tapered roller bearing is its lack of the declutching or roller lift-off effect. In the inner ring flanged (conventional design) bearing, Figure 23 shows that at a given speed, the centrifugal force exerted on the roller causes it to declutch, or disengage, from the cone roller track surface. Under this condition, there will be sliding motion

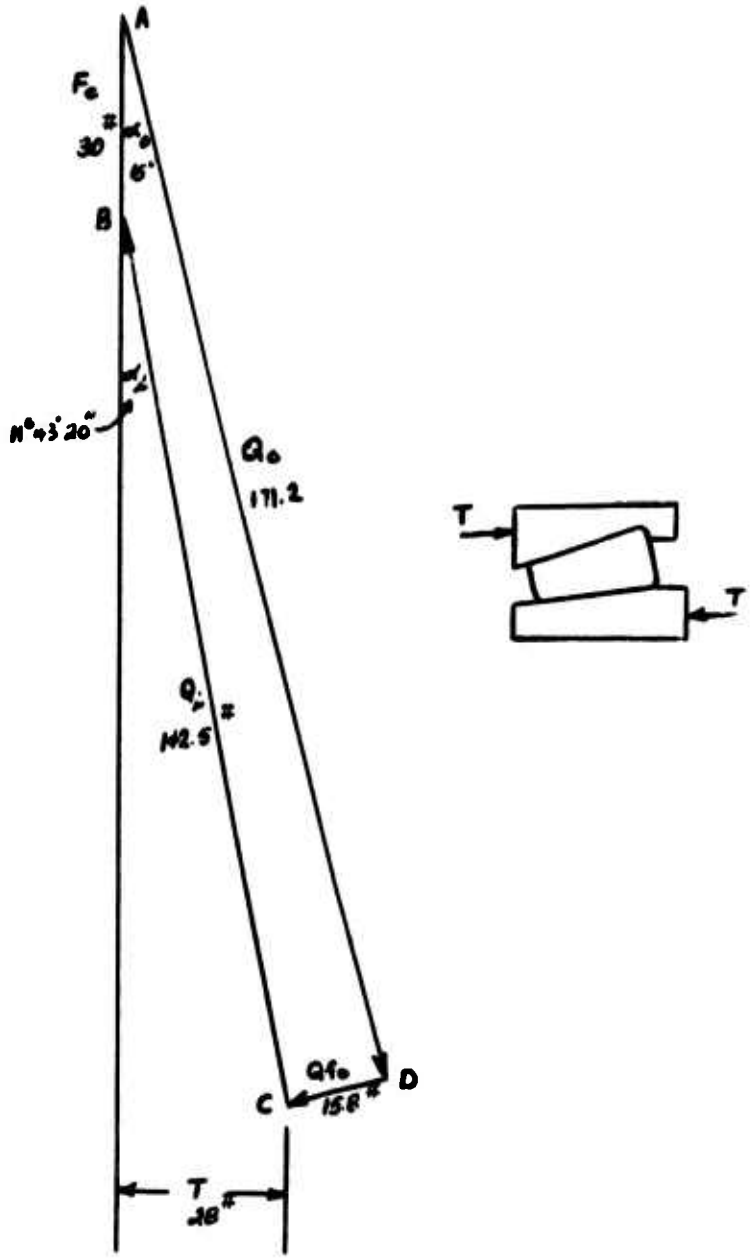

Figure 20. Effect of Outer Ring Flange on Force Diagram.

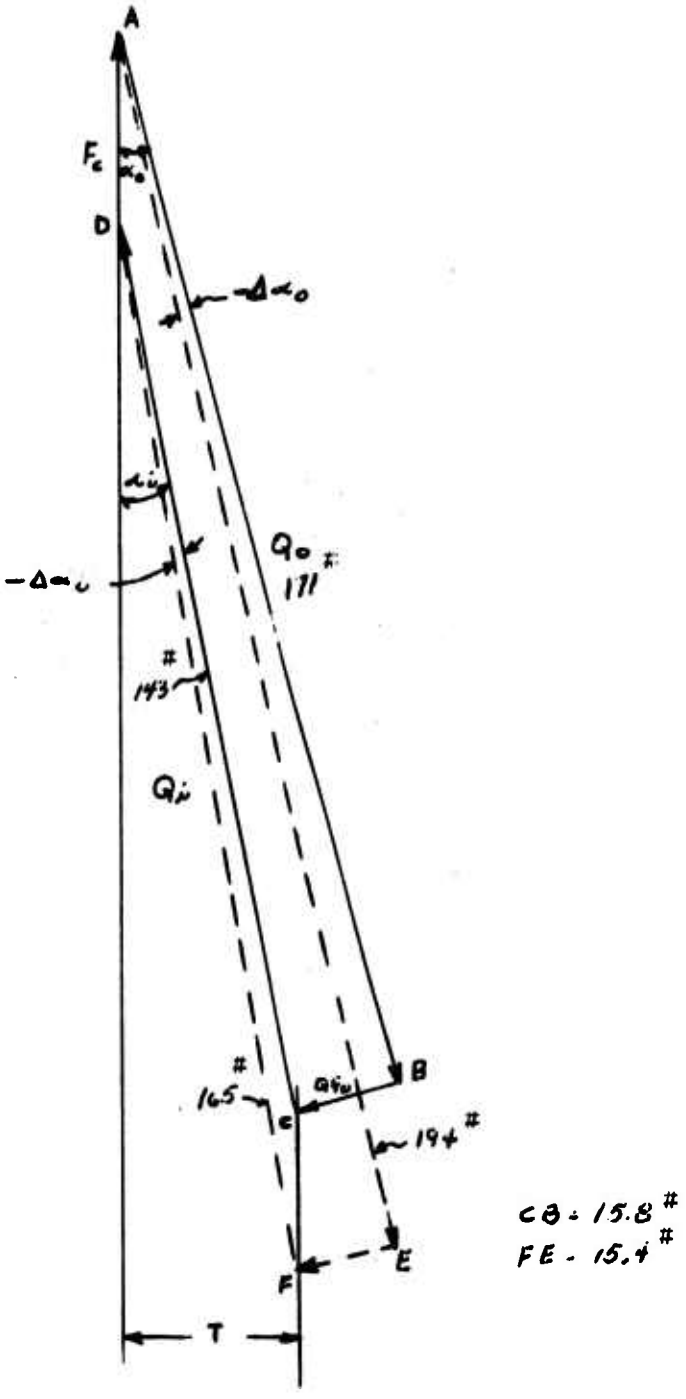

Figure 21. Effect of Change of Roller Path Angles on Outer Ring Flanged Bearing.

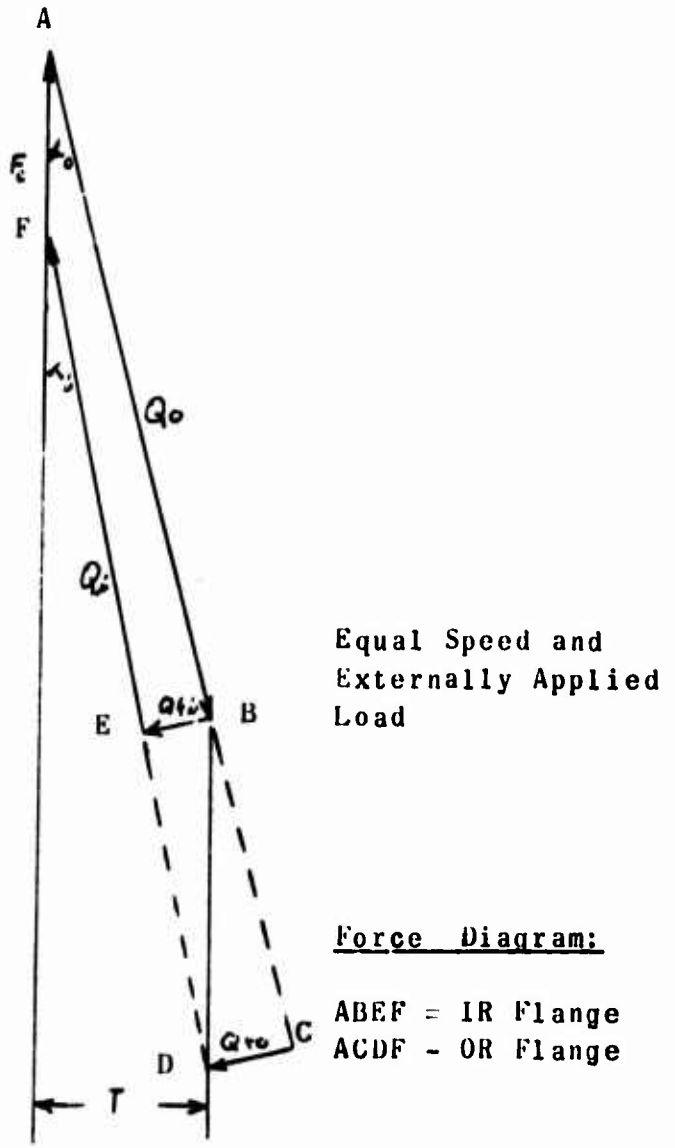

Figure 22. A Comparison of Outer Ring Flanged and Inner Ring Flanged Bearings, Showing Relative Flange Forces.

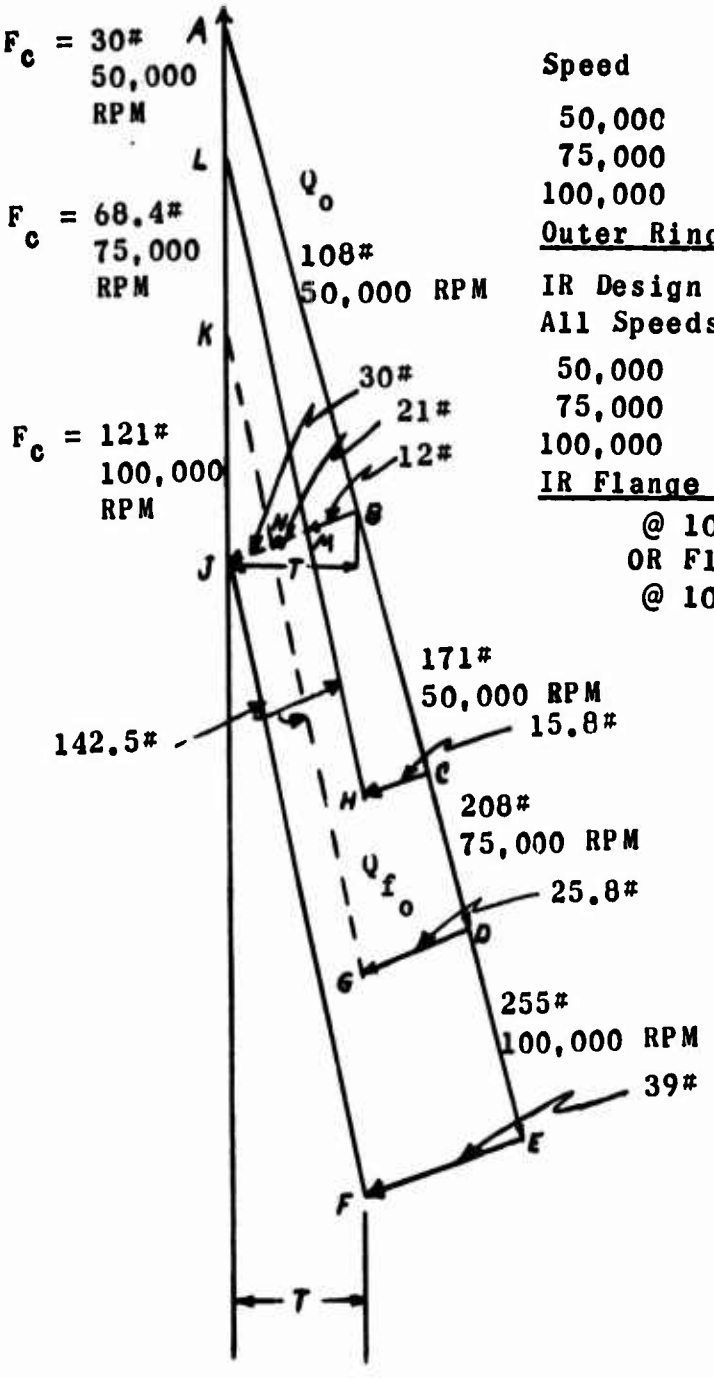

Force Diagram

Speed	IR Flange	OR Flange
50,000	ABML	ACHL
75,000	ABNK	ADGK
100,000	ABJA	AEFJ

Outer Ring Contact Load

IR Design - 460# External Load
All Speeds, 108# Vector AB

50,000	171#	Vector AC
75,000	208#	Vector AD
100,000	255#	Vector AE

IR Flange Force

@ 100,000 RPM = 30#
OR Flange Force = 39#
@ 100,000 RPM

Figure 23. Effect of Increasing Speed on Inner Ring Flanged and Outer Ring Flanged Designs, 460 lb External Load.

between roller and cone surface. In practice, it is unlikely that a "clean" separation between roller and cone occurs at declutching. The very limited amount of axial movement which can be permitted by the other components of the assembly will produce a condition where the lift-off is an intermittent condition. Roller to raceway sliding contact is expected with the intervention of some oil film. Considerable heat generation is expected and skid marking of tracks may arise in this declutched operation. Extensive experiments are needed to determine the limits under which declutched operation can be tolerated.

The penalty which is incurred in the outer ring flange design is evident in Figure 23. The load, and therefore the contact stress, carried by the outer ring roller path (Q_o) and by the outer ring flange (Q_{fo}) increases rapidly with an increase in speed for a given externally applied thrust load. The outer ring line contact can tolerate considerable load without early failure, but there is still a fatigue life penalty from the increased loads. However, destructive sliding and loss of shaft location ability do not take place at high speed.

In applications where reversible thrust is encountered, it is possible to employ a preloaded pair of outer ring flanged bearings, as shown in Figure 24. This figure illustrates that when a small, externally applied thrust load is superimposed on the bearing preload in the forward direction, the bearing inner race load is significantly changed on both bearings. It can be seen also that an externally applied load, T, equal to the preload, P, results in a change in the magnitude of the cone roller path load, to the extent that one bearing carries the entire load and the matching bearing declutches.

It is possible with this configuration to accommodate a reversing thrust load with no loss of axial positioning from the bearing, with the preload insuring proper bearing functioning at the $T = 0$ point in the load transition process.

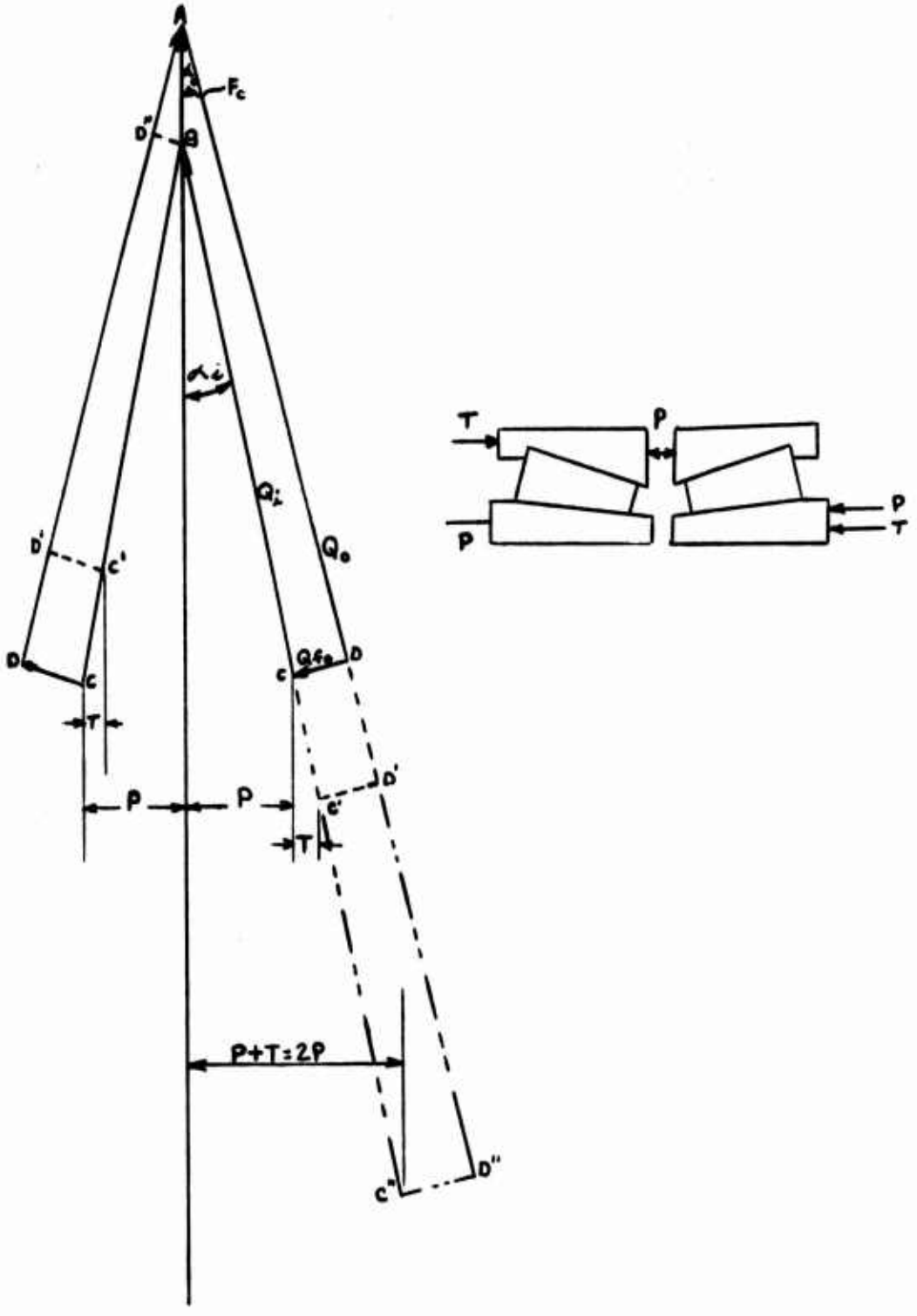

Figure 24. Force Diagram of a Preloaded Pair of Outer Ring Flanged Bearings.

The effect of increasing speed on this pair of preloaded bearings differs from the speed effect on the inner ring flanged preloaded pair in that the applied load required to cause one bearing to declutch remains equal to the preload, whereas it decreases for the inner ring flanged pair (Figure 19).

Another conceptual approach to dual directional thrust capability is shown in Figure 25. This diagram represents a bearing design having one flange on the outer ring and one on the inner ring. Essentially, this concept embodies the preceding bearing pair capabilities and features combined into a single bearing. This design when operating as a conventional inner ring flanged bearing under forward thrust, has a force diagram ADCB, which is shown as it exists for the same level of externally applied thrust as in Figure 20. Under reverse thrust, the inner ring flange functions at the small end of the roller to carry thrust with the outer ring flange. In Figure 25, force diagram AFEDG illustrates the concept of such a tapered roller bearing with reversed thrust. Force AF is carried on the inner ring flange; force EG is the sum of the externally applied thrust and the component of the roller centrifugal force carried by the cup flange.

These results give rise to the concept of a three-flanged tapered roller bearing as shown in Figure 26. At a given rotational speed, represented by the force vector AB, thrust loads are carried by the inner ring flange as shown by vector diagram ABCD. At externally applied loads smaller than T, thrust is carried partly by the inner ring flange and partly by the outer ring flange until, at zero external thrust load, all flange loading would be on the outer ring flange and result from centrifugal force only. Thrust in the reversed direction is represented by vector diagram ABEF and is carried between the small end inner ring flange (AF) and the outer ring flange (EB).

It is also possible to use this inner ring flanged

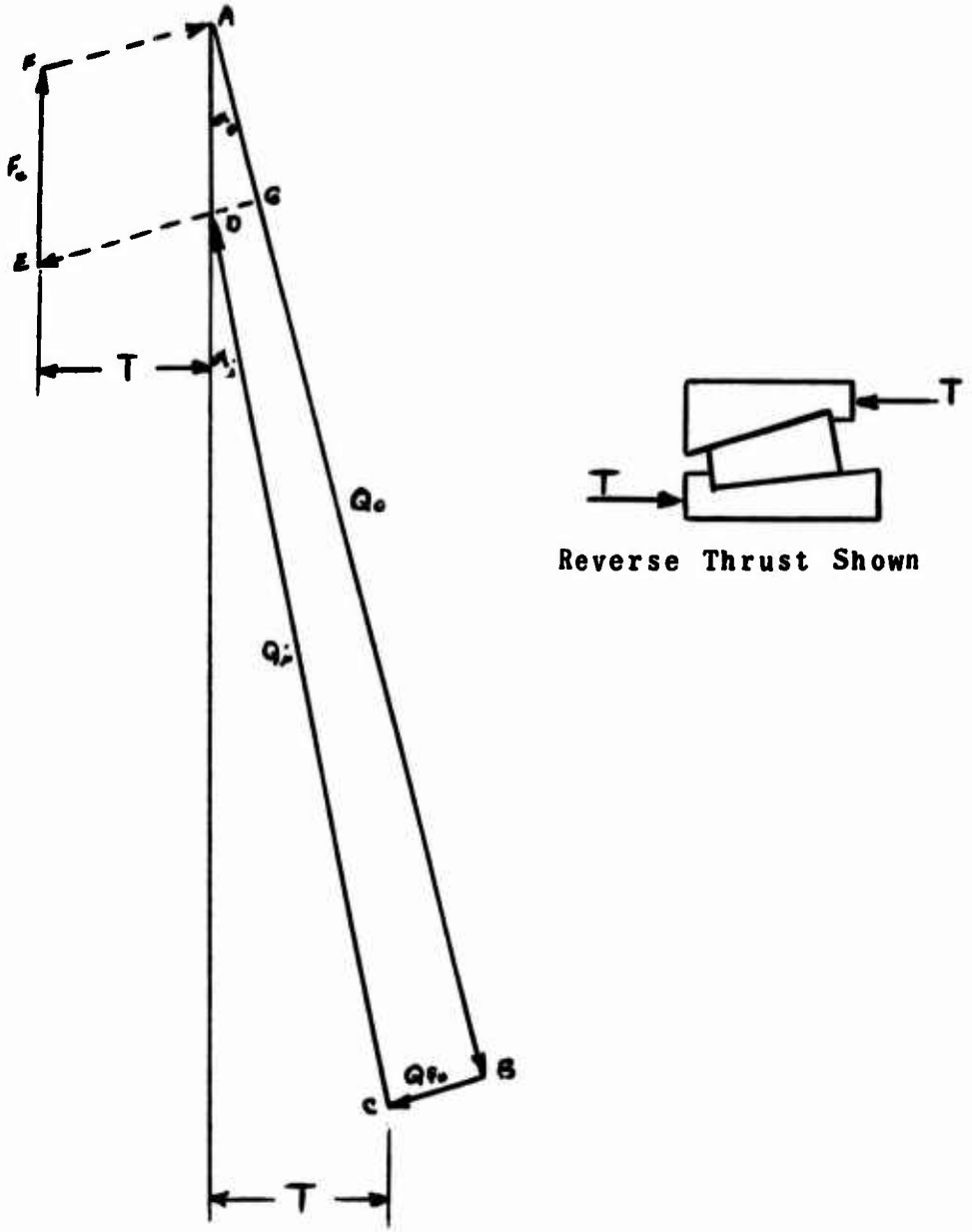

Figure 25. Force Diagram for Reverse Thrust Carried on Small Roller End-Inner Ring Flange Bearing.

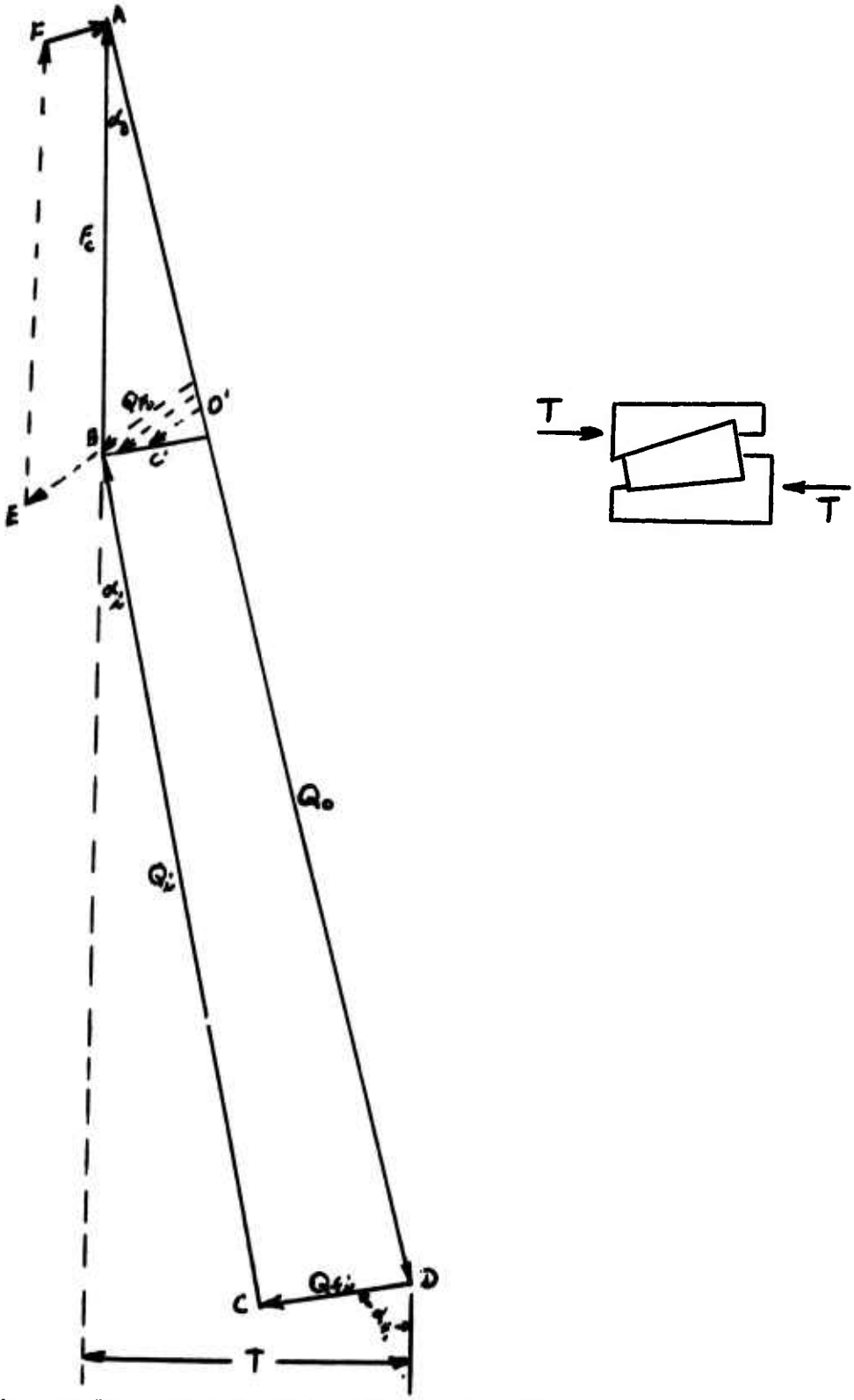

Figure 26. Force Diagram for Three-Flanged Bearing.

and the outer ring flanged bearing in a tandem pair. In this situation, the inner ring flanged bearing, having the greater load-carrying capacity, will carry the normal, steady-state thrust. The outer ring flanged bearing will carry the reversing thrust encountered and will maintain rotor centerline integrity and location under conditions of inner ring flanged bearing declutching. Declutching will occur during periods of decreasing thrust (toward reversing).

3. Selection of Tapered Roller Bearing Designs for Test

The basic angular geometry of a tapered roller bearing is determined by choice of roller diameter (included angle), cone angle, roller end radius and flange angle. The choice of these parameters represents an engineering compromise among several conflicting requirements. One characteristic which differentiates a tapered roller bearing from an angular contact ball bearing is that the inner ring and outer ring contact angles are geometrically fixed and cannot change to suit kinematic conditions, as they do in the ball bearing. The result is that the fixed geometry tapered bearing has a well defined region of performance, in terms of speed and thrust load capability, whose outer boundary is the declutch limit.

In selecting the design parameter, the major competing failure modes must be considered, the primary requirement being that of remaining within the declutch limit at all times. The criteria considered are:

1. Declutching limit
2. Flange (rib) loading
3. Bearing fatigue life
4. Overall bearing power consumption

The primary task in this program has been to select the bearing outer ring angle and roller size which best accomodate the performance target of 100,000 rpm and 450 lb thrust load.

Centrifugal force on the rolling elements is the basic cause of the declutch phenomenon, and consequently the first step in design is to reduce the roller mass by making the roller diameter smaller. The basic reference diameter of the standard (commercial) bearing was 0.244 inch.

Manufacturing limitations, control of roller included angle and flange geometry, roller ℓ/d, and cage configuration and strength all pointed to a minimum diameter of 0.200 in., which was adopted.

The declutch speed limits at 450 lb thrust were computed as a function of cup angle for both standard (0.244 in.) and minimum (0.200 in.) size rollers (Figures 27 and 28 respectively). The figures show that declutching would occur at 100,000 rpm with a 13° outer ring angle bearing equipped with the standard size roller, and in a 15° bearing when using the smaller roller.

The computed declutching points are based on the assumption of conical rolling between the bearing elements. As the bearing inner ring approaches the declutch value, the inner ring contact load becomes very small and some skidding is inevitable. The roller orbit motion will switch from being defined by the conic geometry to bearing epicylic about the rib contact point as the inner ring force approaches zero. This change in roller control leads to an <u>increase</u> in roller orbit speed and a <u>reversal</u> in the direction of slip at the inner ring contact. The computed (rolling) declutch values tend to be on the low side of actuals in the speed increase condition. However, once the declutch phenomenon has occurred, the drive speed must be dropped distinctly below the nominal declutch speed before "reclutching" can occur.

Even acknowledging the effect of skidding, the <u>largest</u> predicted outer ring angle that can be considered for the design is about 15°, for the roller size, speed and load constraints imposed.

The load borne by the inner ring flange is strongly influenced by outer ring angle and speed, as shown in Figure 29, as well as by external thrust load. As would be expected, the flange force becomes equal to the external thrust per roller just prior to reaching the declutch speed. For the design target conditions, the most favorable flange loading occurs at <u>low</u> outer ring angles, and, once more, the largest outer ring angle that can be tolerated is 15°.

The effect of speed on flange force is illustrated more clearly in Figure 30 for a bearing with an outer ring angle of 15°. Flange load increases most rapidly with speed

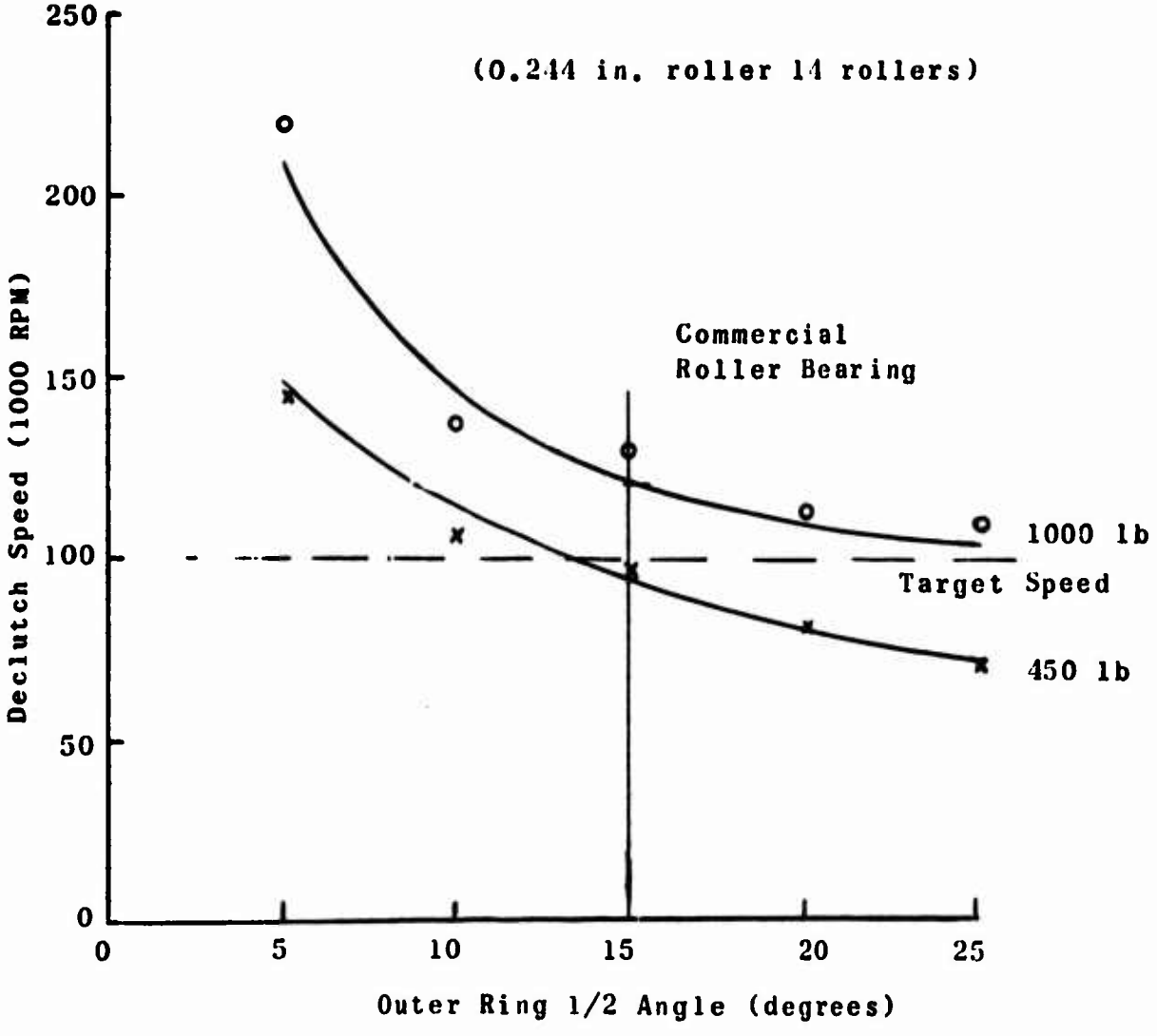

Figure 27. Speed Limits as Affected by Outer Ring Roller Path.

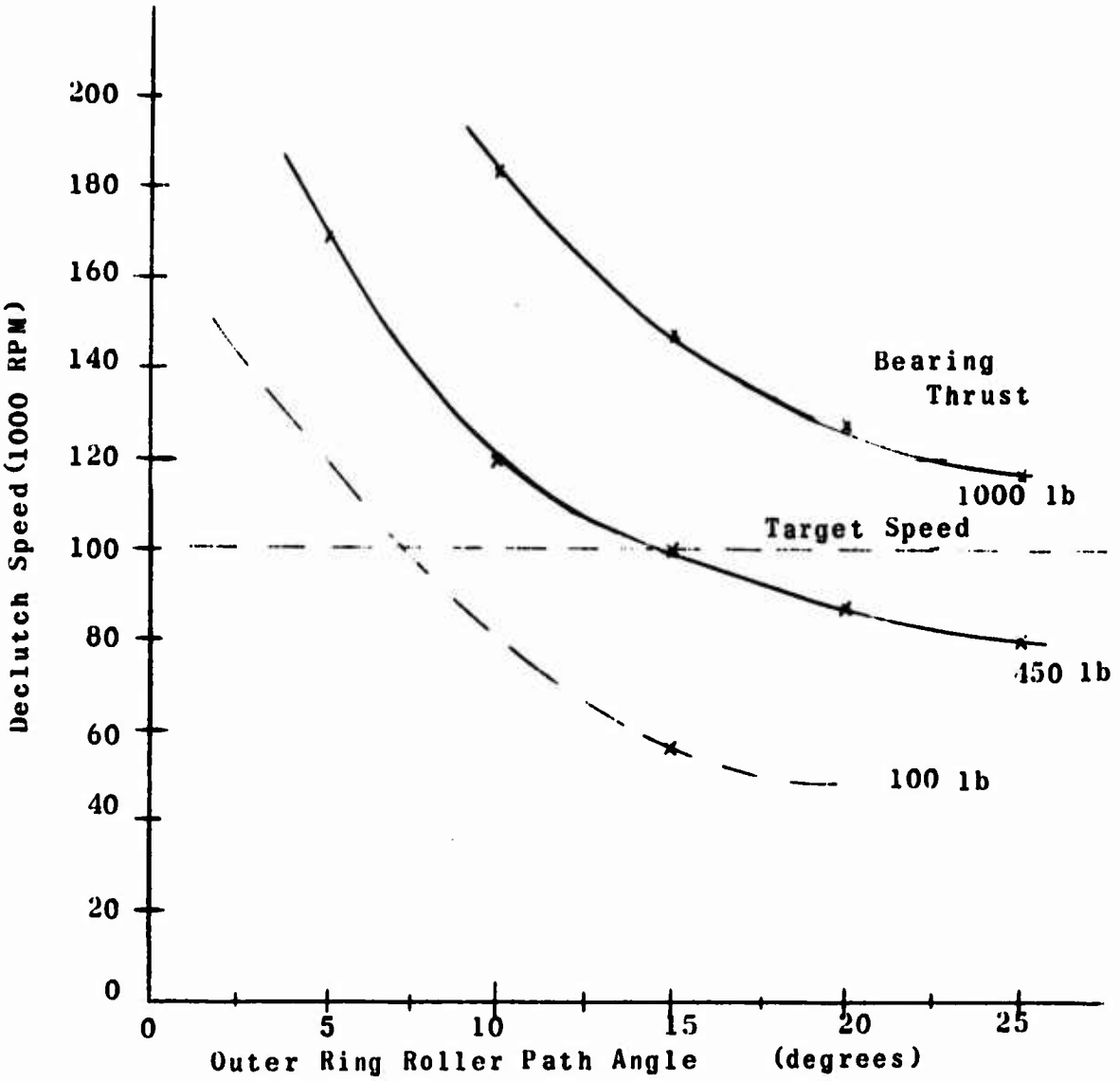

Figure 28. Declutch Speed as Function of Contact Angle and Thrust Load (0.200 In. Roller).

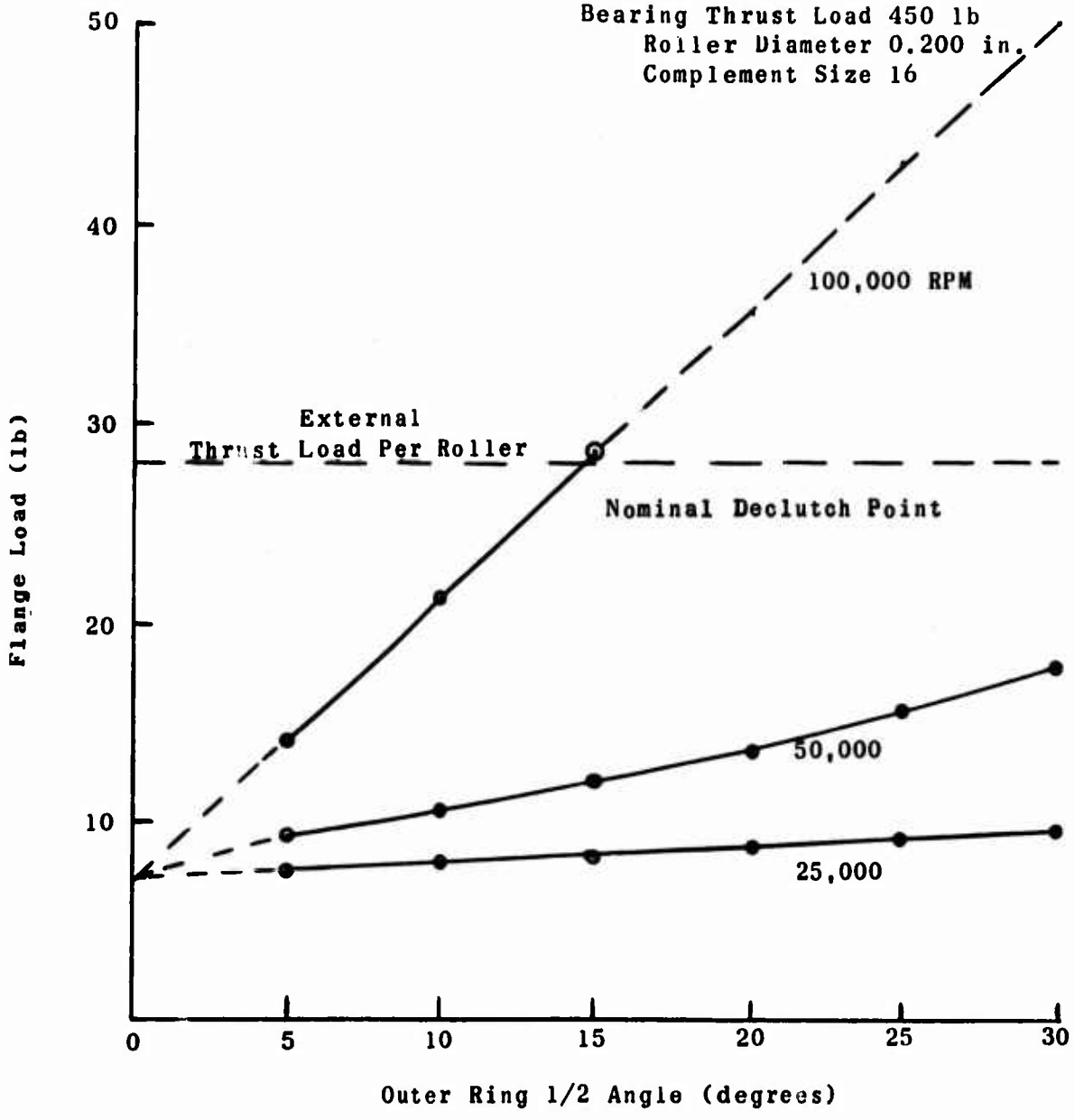

Figure 29. Effect of Outer Ring Angle and Speed on Flange Load.

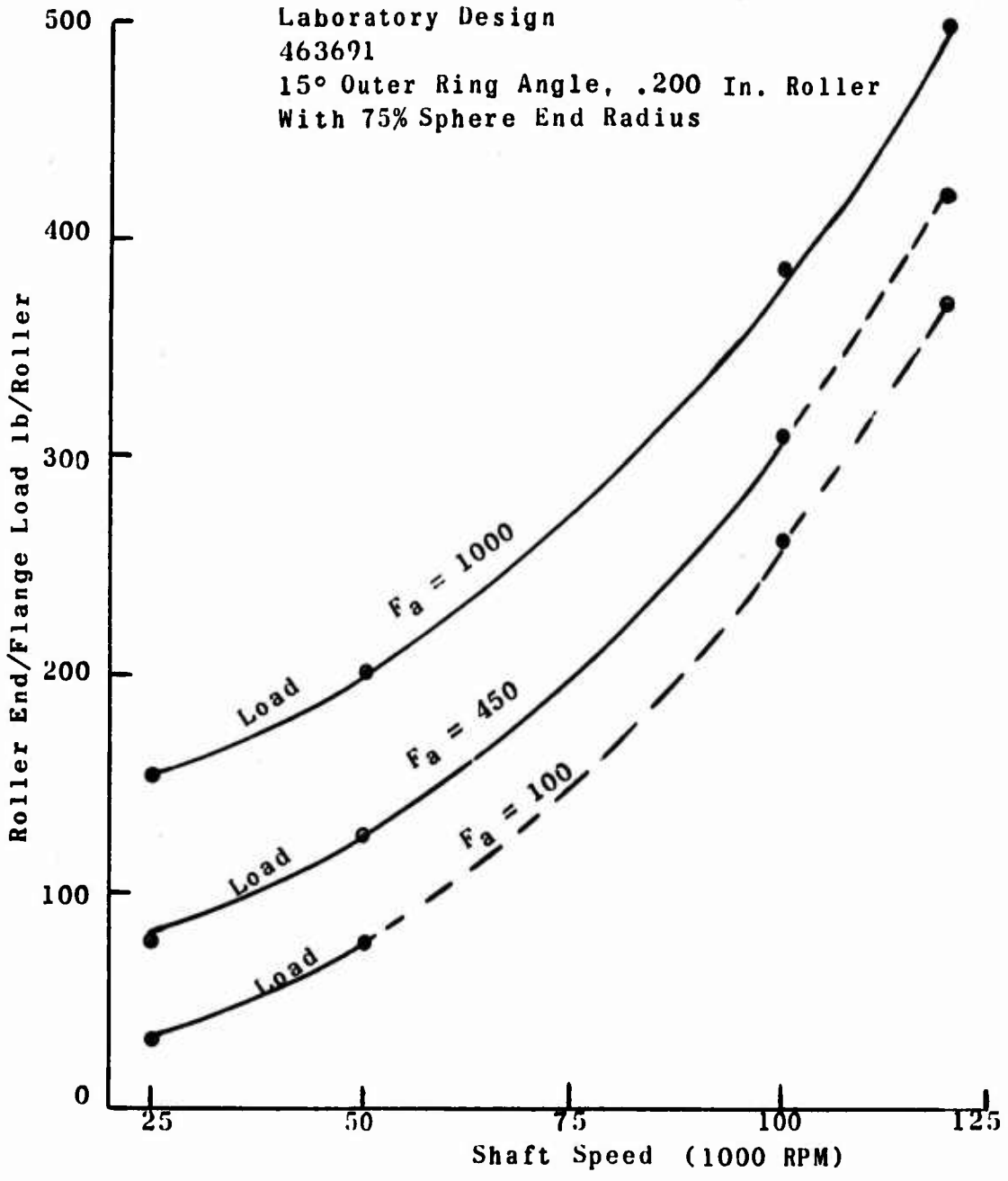

Figure 30. Roller End/Flange Load vs. Shaft Speed.

at the higher speeds. Also, flange load becomes relatively insensitive to external thrust at very high speeds. For example, at 100,000 rpm a more than doubling of the external thrust from 450 lb to 1000 lb only increases the flange force from 31 lb to 38 lb.

The flange contact stresses are a function of the flange load and the contact geometry. The principal geometrical variable is the roller sphere end radius. Figure 31 shows the maximum Hertzian contact stresses for a 15° bearing, under 450 lb thrust, for various roller end radii. Before any design point can be selected from Figure 31, a criterion for contact failure must be determined.

SKF has studied sliding contacts extensively as they apply to thrust-loaded cylindrical roller bearings, tapered roller bearings, and research configurations consisting of one ball sliding against a similar ball. In all these cases, smearing failure is the limiting factor.

In conventional catalogue tapered roller bearing operation, the flange is relatively lightly loaded and stress levels rarely exceed 20,000 psi. However, overload tests have shown that stresses considerably above this level can be sustained at moderate speeds and under copious lubrication.

Extensive two-ball smearing failure data[1] are summarized in Figure 32. The smearing limit/stresses decrease with increasing contact sliding speed. The small tapered roller bearings being analyzed have roller end sliding speeds of up to 120 ft/sec at 100,000 rpm. A wide extrapolation of the failure data in Figure 32 to 120 ft/sec suggests that a contact stress below 350,000 psi would not precipitate a smearing failure. However, the test data were obtained under room temperature conditions and with a copious supply of lubricant flowing directly to the contact. Further studies showed that the smearing limit is approximately proportional to the square root of the lubricant viscosity in the contact area. Assuming an inner ring flange operating temperature of 300°F, the MIL-L-23699 fluid has diminished in viscosity

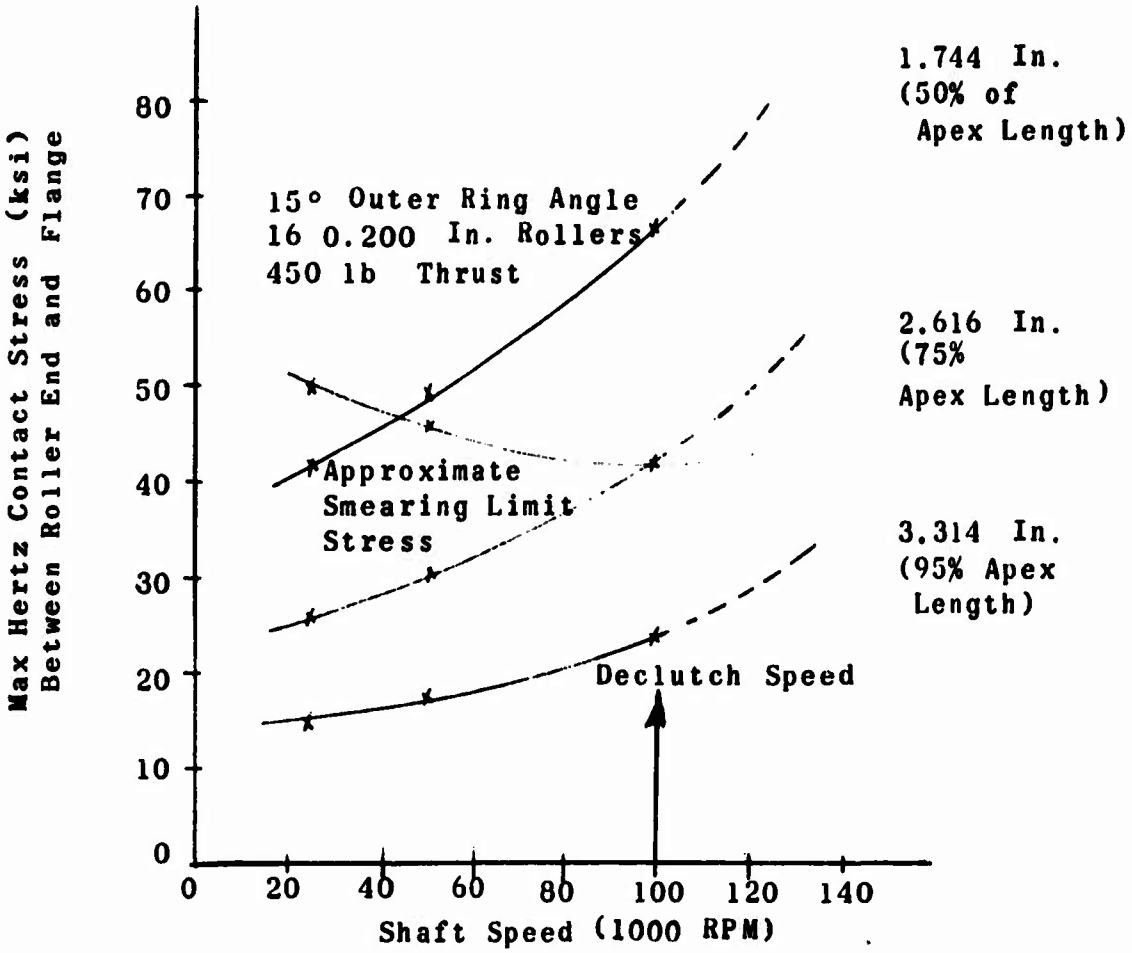

Figure 31. Roller End Contact Stress as a Function of Bearing Speed and Roller End Radius.

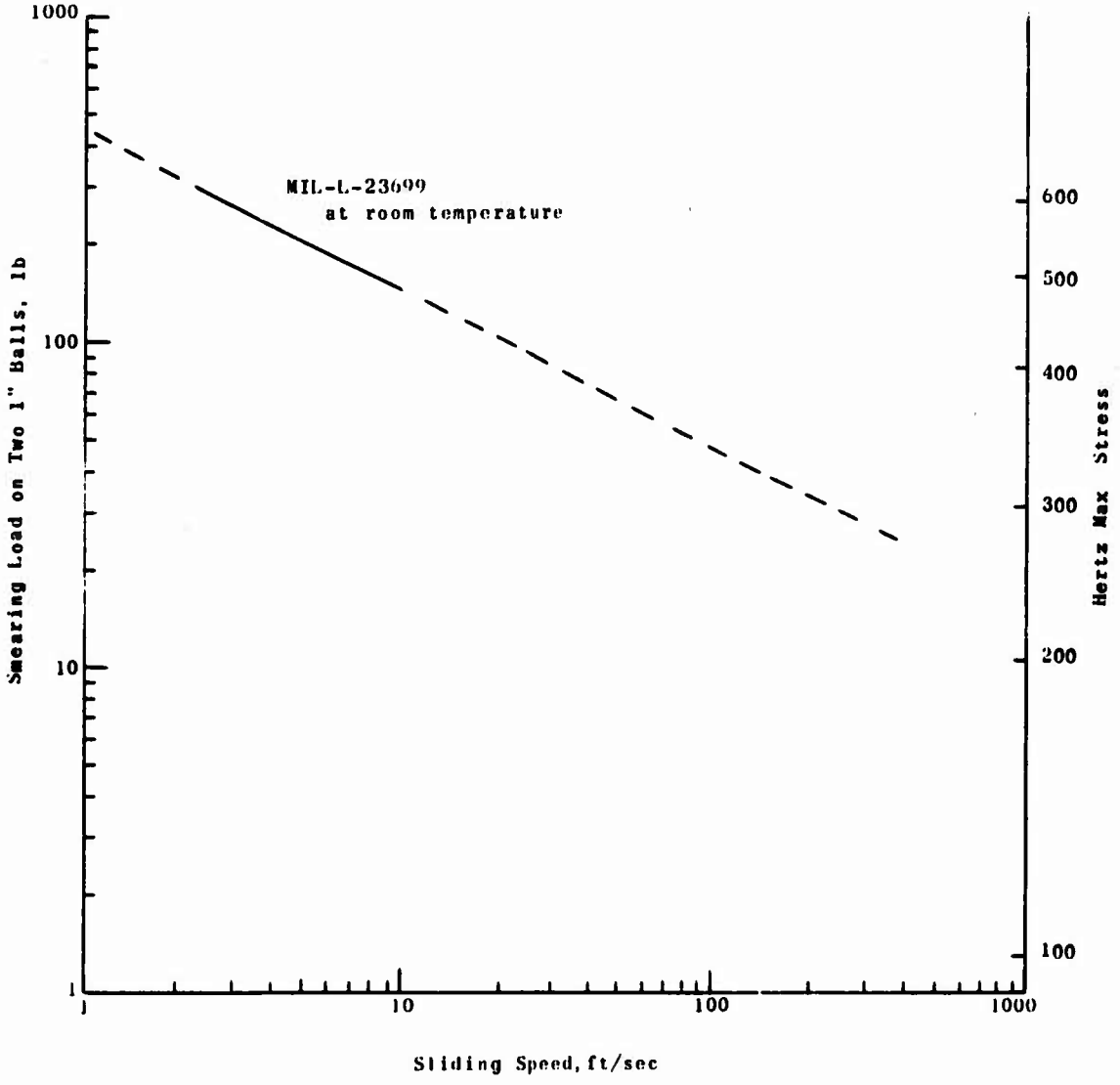

Figure 32. Smearing Limit Stresses for Roller End/Flange Contacts.

sixteen-fold from 40 cs at room temperature to 2.5 cs. A smearing limit of 85,000 psi would thus be anticipated, and a further reduction factor of about 2 allows for the scantiness of the oil supply. The final consequence is a predicted maximum safe smearing limit stress of 42,000 psi. This limit is superimposed on the plot in Figure 31. The smearing limit stresses achieved by this long extrapolative route are approximately double the known conservative commerical practice, and so a decision was made to permit attainment of stresses of up to 42,000 psi at the extreme limits of the target performance envelope of the test bearing.

Roller end radius, as a fraction of the geometric apex length of the bearing, defines the shape of the roller end contact spot. When the radius is 100% of apex, there is line contact with the flange across the entire roller end. The slightest amount of roller skew causes highly undesirable edge loading. Design practice in commercial bearings is to make the radius 85 to 95% of apex to accommodate some skew, and to make the contact spot an ellipse. It is important that the ellipse minor axis does not exceed the available flange height even under the highest roller end loading. Computed axis dimensions reveal that contact ellipse will remain with the flange annulus for all contact conditions spanned in Figure 31.

Roller end radius in this design is thus restricted only by the smearing limit stress. Consequently, the greatest amount of roller skew can be tolerated without edge loading by selecting the smallest end radius consistent with the smearing limits. From Figure 31, this radius is 2.616 in. (75% of apex). Elastohydrodynamic film formation is also dependent to some extent upon the entrainment space and the shape of the contact ellipse with respect to the rolling velocity vector. Preliminary calculation, in a NASA project[2] has shown that the film formation is fortuitously optimized when the roller end radius is approximately 75% of apex length.

Tapered roller bearings, in normal application where they run at moderate speeds, usually fail by spalling fatigue of the inner ring cone surface. The faster the running speed, the greater the rate of accumulation of stress cycles and the shorter the bearing life as expressed in hours of operation. When a tapered roller bearing is operated at a high enough speed that centrifugal forces on the rollers become significant, the inner ring contact is progressively relieved of its load and consequently the fatigue life increases dramatically.

The computed fatigue life of tapers having various outer ring angles is shown in Figure 33. The fatigue calculations, drawn from Appendix I, are based only on inner and outer ring contacts. Flange fatigue (thus far never experience in an actual bearing) has been neglected. The curve for the 15° outer ring angle bearing illustrates the usual inner ring life loss due to rate of cycling up to a speed of about 25,000 rpm, when under 450 lb thrust. At speeds above 25,000 rpm, the inner ring life improves continuously and would become infinite at the declutch speed due to complete loss of loading.

The contact loading at the outer ring, on the other hand, remains constant at all speeds, and so its life in cycles remains constant except for possibly a small beneficial speed effect. In terms of hours, the outer ring life decreases hyperbolically with speed, as shown by the constructed curve in Figure 33.

The computed bearing life (considering the inner and outer ring contacts simultaneously) is thus inner-ring-dominated at low speeds, reaches a maximum near the declutch speed, and then falls off again at very high speeds due to the outer ring; of course, the life domain above the declutch speed is primarily academic.

The design optimization for fatigue life thus requires the bearing to operate quite close to its declutch speed when under maximum shaft speed and thrust load. The 15° outer ring angle selection satisfies this optimization.

Finally, the question of bearing power consumption manifests itself as a problem of cooling the bearing at high speeds. The computations, detailed in Appendix I, predict the heat generation in several of the candidate

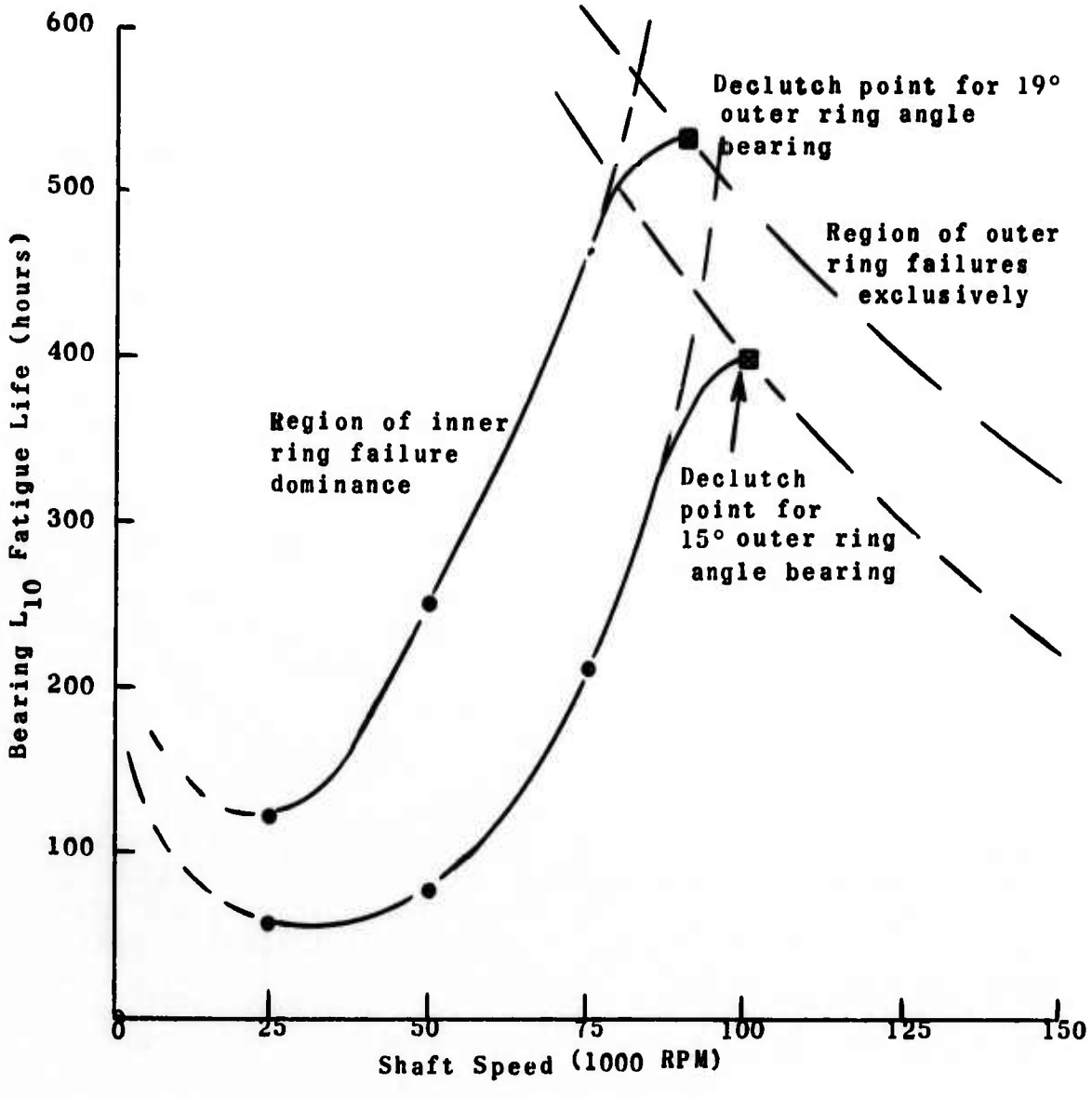

Based Upon Data From Figure 52 of Appendix I.

Figure 33. Qualitative Map of Bearing L_{10} Fatigue Life as a Function of Speed, for Two Bearings of Differing Outer Ring Angle Under 450-Lb Thrust.

designs of high-speed tapered bearings. Figures 44 and 46 show that roller end to flange friction is calculated to be quite minor compared with that of the conical rolling contacts. At low speeds, heat generation is relatively small for all designs, but it rapidly becomes massive as operation approaches a declutch condition. The dramatic increase in frictional heating arises from the assumed isothermal Newtonian fluid assumptions being valid as the inner ring contact unloads and the consequent high rate of slip needed to supply the roller drive. The only clear design criterion that can be extracted from this heat generation calculation is that the declutch condition is detrimental to cool running. Unfortunately, this conflicts with the preceding requirements, and consequently engineering judgment is required.

As the degree of credibility that could be attached to the skidding heat generation values was appreciably less than that ascribed to the parameters in other studies, the 15° outer ring angle bearing was selected as the test specimen configuration.

The entire design selection process described above has been based upon the presence of a predetermined constant magnitude of pure thrust load in the test rig. Such a condition is unlikely to occur in practice, where load is likely to vary with bearing position.

When a shaft is supported on one or more tapered roller bearings which are operating at, or close to, their declutch speeds, the system is inherently low in spring stiffness in the radial direction. Consequently, any small unbalance force in the rotor can lead to large radial displacements and the onset of rotor whirling. The result is that "declutching" is likely to appear at a speed lower than predicted by the assumptions of pure thrust load. The degree of loss of operating range is governed by the entire rotor dynamics situation and is not predictable by the relatively simple analysis performed so far.

The future plans in 2-10 lb/sec gas turbines, however, include 3×10^6 DN speeds. The outer ring flange bearing concept is one method of circumventing operation in the declutch regime since, by design, thrust load and centrifugal forces are carried through the outer ring roller track and

flange, with the inner race roller path contact load remaining constant with speed changes (Figure 23). The theoretical speed capacity of this design concept is limited only by the load-carrying capacity of the bearing components.

B. PHASE II

The testing portions of this program were conducted in two distinct stages. The preliminary test effort utilized a mechanically driven tester, described in Section II, operated at speeds up to 46,000 rpm (1.15 million DN) to identify designs and to complete an initial evaluation of the various experimental designs. These tests were conducted with a single mechanically driven tester, described in Section II, operated at speeds up to 46,000 rpm, 1.15 million DN, to identify critical areas in the conventional tapered roller bearing designs and to complete an initial evaluation of the various experimental designs. These tests were conducted with a single tapered roller bearing test specimen mounted on one end of the shaft with a 7205 size angular contact ball bearing mounted on the other end as a nontest element. Nine tests were run in this manner, under an applied axial load of 459 pounds, equivalent to a c/p = 6.95 and using circulating oil for lubrication. Outer ring temperatures, oil-in, oil-out temperatures, and oil flow rates were recorded for each bearing during the test.

The remaining tests were run using the air turbine drive, also described in Section II, which was designed to have a speed capability of up to 120,000 rpm (5 million DN). In this series, experimental groups of inner ring flanged design bearings and outer ring flanged design bearings were tested in the step-speed mode to establish the maximum speed capability of each design. It was necessary to run these tests with two tapered roller bearings mounted on the test shaft to provide the uniform dynamic response characteristics required at these extreme speeds.

1. Tests of Inner Ring Flanged Bearings

Experimental evaluations were conducted for four distinct versions of tapered roller bearings having a flange on the inner ring. The detailed differences in these designs were discussed in Section III, and the variations can be classified as: (1) commercial; (2) modified commercial, where an aircraft type cage was substituted

for the commerical variety and means of supplying oil directly to the roller end-flange contact was added, (3) aircraft standard where rings of the modified commercial design were finished to aircraft tolerances and an improved roller end flange contact geometry was provided; and (4) an experimental high-speed design which incorporated all of the improvements of (3) in a bearing having smaller diameter rollers to limit centrifugal force. The testing of each of these designs is discussed in the following subsections.

a. Tests of Commerical Bearings

Initial tests were conducted on six bearings of class 4 quality obtained through normal commercial sources to clarify the critical areas of conventional tapered roller bearing design and to provide a solid basis for the evolution of experimental high-speed designs.

Bearings were tested at increasing speeds, applied in a stepwise manner, with temperature stabilization of the system being assured at one level prior to proceeding to the next higher speed level, until some system limitation was reached. (Detailed discussion of test procedures is given in Section IV-B). Lubrication was provided by jetting a petroleum-based oil, Velocite #10, having a viscosity of 20.4 cs at 100°F, into the inboard end of the bearing (the large end of the taper) at a rate of 0.6 to 0.8 gallon per minute. This oil, which was supplied at a temperature of 79°-80°F, was generally sufficient to maintain the outer ring operating temperature between 180° and 200°F in the 30,000 to 40,000 rpm speed range. However, significant scatter was noted, and in one case (bearing number 2) a temperature of 225°F was recorded at a speed of 34,500 rpm.

Four of the six bearings tested during this series failed in some manner. The first two bearings tested seized, after reaching speeds of 18,000 and 36,000 rpm respectively. Damage to the test specimens was limited due to the presence of an overtorque limiting device in the drive, and it was possible to

make the following observations. Evidence of heavy contact, some smearing, and discoloration due to excessive heat generation was noted at the roller end/flange contact area and was the probable cause of the bearing seizure. Roller path smearing and heat discoloration were also found on the inner rings, probably having occurred at bearing seizure; and heavy roller/cross rib contact was evident on the cage, which could also have occurred during the seizure.

The third bearing tested reached a speed of 48,750 rpm (1.2 million DN) before it also seized. This bearing exhibited the same general damage as the previous bearings, but in addition the stamped cage was found to be distorted. Although this could result from seizure, it is probable that it was precipitated from the interaction of cage imbalance and the large centrifugal forces generated at this high speed.

The test of bearing number four was aborted after a test speed of 38,800 rpm was reached, when the scavenging of oil from the test system was interrupted. The increased heat generation due to oil churning and the inability to remove heat from the bearing area resulted in a thermal instability that produced the seizure of the test specimen. Heavy smearing was found on the inner ring roller path and flange contact areas and on the diameter of the roller near the large end.

Bearing number five was tested under a reduced axial load of 100 pounds to observe the behavior of the system under conditions where the declutch phenomenon had been predicted by calculation to occur. An axial vibration of the load plug was observed at a speed of 37,000 rpm where declutch had been predicted. The test was terminated, and the bearing was disassembled and visually examined. No component damage was noted at this time. However, minor evidence of contact was found on the shaft and the housing liner (normal diametral clearance 0.008 inch), indicating that a loss of control of the shaft centerline location had occurred.

The sixth bearing tested was experimentally fitted with a chrome-plated inner ring to provide a hard, wear-resistant contact surface. (Such a plating is not suitable for prolonged service, since it peels off in cycle stressing.) This test specimen operated successfully at full load for 5.4 hours at 36,000-37,000 rpm before the test was stopped to permit the examination of the bearing components. Only moderate signs of wear and surface distress were noted at this point.

Generally, the results of these tests exceeded expectations in that all of these bearings, made only to standard accuracy, exhibited the capability of operating at speeds in excess of 18,000 rpm, and a speed of 48,750 rpm (1.2 million DN) was reached with one specimen. These speeds were substantially in excess of those anticipated and resulted in the establishment of the maximum speed goal of the project at 2.5-3 million DN originally established.

The other results collected from this test series were as anticipated. The roller end/flange contact proved to be difficult to lubricate and cool at these high-speed conditions. The stamped steel cage was shown to distort under the centrifugal forces and, as distorted, would provide inadequate roller guidance. In addition, the theoretically predicted phenomenon of inner ring declutching, i.e., the reduction of the inner ring/roller contact force to zero, was demonstrated to exist in the reduced load test.

One of the areas that had been projected to cause some difficulty in the development of a high-speed tapered roller bearing was the substantial rate of heat generation anticipated. Much of the heat was expected to arise at the sliding contact between the roller ends and the flange, although the cage and churning oil are also significant heat sources. To measure the magnitude of this heat generation the test data collected were analyzed to obtain a comparison of the overall heat generation rate of the tapered roller bearings with that of the angular contact ball bearing located on the other end of

the shaft. These rates were approximated by calculating the amount of heat transferred to the oil by determining oil inlet and outlet temperatures and flowrates. The results are summarized in Table III.

TABLE III. COMPARISON OF HEAT GENERATION RATES OF ANGULAR CONTACT BALL BEARINGS AND COMMERCIAL (GRADE 4) TAPERED ROLLER BEARINGS

Average Heat Removed By Circulating Oil - Btu/Hr*		
Speed Range (rpm)	Ball Bearing	Conventional Tapered Roller Bearing
10,000-20,000	545	3425
20,000-25,000	850	4855
25,000-30,000	1075	7055
30,000-35,000	2800	8200
35,000-40,000	1485	11350
40,000-45,000	2580	10100
45,000-50,000	1175	11200

*Average values for speed values within the speed range referenced.

These data clearly indicate that in these tests the heat generation rate of the tapered roller bearing was 5-10 times greater than that of the angular contact ball bearing. Thus, the original assumption that heat generation could be a problem area was confirmed, and the importance of reducing the heat generated in the bearing and the necessity of providing a method to quickly remove the heat generated, particularly from the flange contact area, was highlighted.

b. Tests of Modified Conventional Bearings

Bearings tested during this series were obtained commercially, as were those used in the previous tests, and then modified for higher speed operation, as described in detail in Section III. The bearings were fitted with a machined, silver-plated steel cage of aircraft design which was land riding, in lieu of roller riding as is the

commercial cage. Six holes were located radially through the inner ring into the undercut at the junction of the flange and roller path to allow oil to be supplied directly to the flange face.

Test conduct was basically identical to that of previous tests. Changes were made in the lubrication supply. MIL-L-23699 lubricating oil, a mixed-ester-based fluid having a viscosity of 28 cs, at 100°F (a standard aircraft engine lubricant) was used as the test lubricant. The lubricant was jetted into the bearing as before, and was also delivered to the inside of the hollow shaft, where it could be pumped by centrifugal action through holes in the shaft and bearing inner ring to the flange surface. During these tests the oil was supplied at a rate of 0.7-0.8 gallon per minute per bearing at a temperature of 100°F, which maintained the bearing outer ring operating temperatures between 170°and 180°F in the 30,000- to 40,000-rpm range and between 200° and 210°F at the maximum speed of 46,000 rpm.

During this series, two bearings were tested to a maximum speed of 46,000 rpm, the maximum speed limitation of the mechanical drive system, with both bearings being suspended for examination prior to failure. The first bearing was operated briefly at a speed of 50,000 rpm, but the characteristics of the test rig prevented such high speed in sustained testing. One bearing, 093101, accumulated 7.75 hours in the 45,000-50,000-rpm range and 0.55 hours at 50,000-51,000 rpm at suspension; while the second bearing, 093102, was suspended after running 21.0 hours at 46,000 rpm. No operating difficulties were encountered with either bearing.

Posttest examination disclosed lighttraces of smearing on the inner ring flanges of both bearings. In addition, 093102 had a narrow band of oil degradation products and moderate polishing on the inner ring flange surface and on large ends of the rollers. The cage pockets of both bearings had indications of moderate to heavy wear and smearing at the small end, where contact was made by

the unground portion of the roller. The pocket cross bars of the cages also indicated contact. That of bearing 093101 exhibited signs of heavy contact, having moderate to heavy smearing on the cross bar surfaces and ridges at both the leading and trailing pocket edges from the flow of the silver plating. The cage pockets from bearing 093102 showed only light to moderate signs of metal flow in the pockets and had some minor indications that roller skew had been experienced. However, these signs were all relatively minor. Both bearings were considered to be in excellent condition at the conclusion of the test.

These results clearly indicated that the successful lubrication of the flange area and the use of an aircraft-quality machined and balanced cage drastically improve the operating characteristics of an inner ring flanged tapered roller bearing running below the declutching regime.

Once again, heat generation rate was calculated for the bearings tested in this series. Table IV contains a comparison of the average values obtained from the conventional bearings and these modified conventional bearings over the range of speeds experienced. The design changes significantly reduced the heat generation rate across the entire range of speeds. (This difference is larger than can be directly noted, since the change to a thicker lubricant and the increased oil flow rate used in this series both tend to increase the amount of heat generated within a bearing.) One can conclude from the dramatic drop in heat generation (a) that a well-lubricated and cooled flanged roller end contact reduces friction forces appreciably, and/or (b) that a roller-riding stamped cage causes or tolerates roller contact and stress conditions, creating high friction, which a machined land-riding, well lubricated and balanced cage minimizes.

TABLE IV. COMPARISON OF BEARING HEAT GENERATION RATES AS A FUNCTION OF SPEED OF MODIFIED TAPERED ROLLER BEARINGS AND STANDARD COMMERCIAL TAPERED ROLLER BEARINGS

Speed Range (RPM)	Average Heat Removed by Circulating Oil - Btu/Hr Conventional Bearings	Modified Conventional Bearings
10,000-20,000	3425	1158
20,000-25,000	4855	2240
25,000-30,000	7055	5240
30,000-35,000	8200	5478
35,000-40,000	11350	4347
40,000-45,000	10100	7378
45,000-50,000	11200	7914

*Bearings were not tested under identical lubrication conditions, and values are thus not directly comparable (see text for details).

During these tests, calculations were being completed to analytically determine the design parameters of an ultrahigh-speed tapered roller bearing. These calculations established that the roller size, primarily diameter, and the roller end/flange contact geometry of this bearing design are not optimum for speeds in the 2 million DN speed range. For that reason, testing of this design variation was terminated.

c. Tests of Aircraft Toleranced, Standard Design Bearings

While the preceding test series was being completed, two bearings were manufactured in accord with the conventional bearing design parameters, but being held to typical aircraft tolerances, which are tighter than those used for the commercial product. A change in roller end sphere radius was incorporated using a nominal value of 75% of the apex distance, in lieu of the 95% conventional value. Only three radial holes from the bore to the flange undercut were used. The details of this design are described in Section III. These bearings were then tested.

Tests were conducted essentially as described previously. The first bearing, 093201, was taken successfully through the step-speed sequence and then operated for 20 hours at 46,000 rpm. Lubrication was provided as in the preceding test, and once again the operating temperature at 46,000 rpm ranged from 200°-210°F. The second bearing was taken through an identical sequence. Then, after approximately 3 hours of operation at 46,000 rpm, it was decided to increase the operating temperature of the bearing to allow an evaluation of possible thermal effects. The temperature of the oil supply was increased to 190°F, which increased the outer ring operating temperature to 250°-260°F. The final 17.2 hours of operation at 46,000 rpm were accumulated at these conditions.

The components of both bearings, 093201 and 093202, were in excellent condition after completion of the test sequence. The flange surfaces of both bearings were in excellent condition, with no indications of smearing. The roller paths on the rings showed some signs of distress, indicating the presence of an edge loading condition at the small ends of the rollers.

The cages of these bearings were also in excellent condition. Some moderate smearing and metal (silver) flow had occurred in the pockets due to roller contact, and some polishing was noted on the land control surfaces. The contacts between the roller small ends and the cage rails produced less significant distress than previously noted, since the roller small end surfaces had been ground. Some indications of roller skew were visible. The pocket trailing corners were worn through the plating to the base metal in bearing 093201. However, in bearing 093202 the skewing appeared to have been more intermittent. Smearing and metal flow were found on the leading side of 9 of the 14 pockets, while only light distress was evident in the remaining 5 pockets.

The general condition of these bearing components was better than that of the modified conventional bearings

previously tested. These results seemed to indicate that a closer toleranced bearing is indeed an advantage, if not a necessity, when the high-speed operation of tapered roller bearings is considered. The tolerance effect is further illustrated by the variations noted in the contacts of the rollers in the cage pockets. This type of variation can only be attributed to small dimensional variations which permitted the rollers to react differently to similar external forces. The control of roller skew is a critical factor in the development of any high-speed line contact bearing.

No effect could be seen from the reduction of the flange oil supply holes from six in the first experimental group to three in this group. However, it was considered that this factor would be more critical at higher speeds.

The reduction in heat generated by these bearings is the second major effect noted from their operation. The roller sphere end radius was ground to 75% of apex radius, decreased from the nominal 95% of the commercial bearing rollers (093100 bearings), and provided a flange/roller end contact more receptive to cooling and to lubricant circulation.

The heat generation rates were again calculated for these bearings, and the data given in Table V is compared to that of the modified conventional bearings. A further significant reduction is noted, indicating that the more open roller end/flange conformity and/or tighter tolerances have a significant effect on heat generated by a bearing. It can also be noted that the trend of heat generation rates for this series is continuous, indicating that no significant variations in thermal operating characeristics were encountered across the operating temperature range encountered.

TABLE V. COMPARISON OF BEARING HEAT GENERATION RATES AS A FUNCTION OF SPEED FOR MODIFIED COMMERCIAL TAPERED ROLLER BEARING DESIGN AND AIRCRAFT TOLERANCED STANDARD DESIGN

Speed Range (rpm)	Average Heat Removed by Circulating Oil - Btu/Hr: Modified Conventional Bearing 093100	Aircraft Toleranced Conventional Brgs. 093200*
10,000-20,000	1158	870
20,000-25,000	2240	883
25,000-30,000	5240	-
30,000-35,000	5478	2142
35,000-40,000	4347	2617
40,000-45,000	7378	3497
45,000-50,000	7914	4273

*Includes 17.2 hours of operation at 250°F outer ring temperature for bearing 093202.

These heat generation figures show considerable reduction in magnitude relative to those of the conventional tapered roller bearings and the 093100 series tested. These 093200 series bearing values are, however, still 1.5 times the values calculated for the 7205 ball bearings (Table III), and about 25% of the values found with the conventional bearings.

d. Tests of Experimental High-Speed Bearings

These bearings were designed after the results of the testing of the first three series of bearings had been evaluated and a computer design analysis had been conducted. These bearings incorporate a reduced roller diameter to reduce centrifugal effects, a 0.200-inch large-end diameter in lieu of the 0.244 inch existing in previous bearings, and a roller sphere end radius of 70% of the apex radius - a further reduction from the 75% used in the previous series. The roller included angle was decreased and the inner ring roller path angle was correspondingly increased to reduce the flange loading. Details of this design are given in Section III.

Initially, three bearings of this design were run to a 46,000-rpm maximum speed in the mechanically driven test machine under conditions identical to those used in the previous group. Subsequently, the air turbine powered rig was developed, and two of these original bearings and two additional bearings were operated at speeds up to 90,100 rpm.

Bearing 093301 was taken through the step-speed sequence and then operated at 46,000 rpm with an outer ring temperature of 200°F for a period of 20 hours. The second test bearing, 093302, ran at 46,000 rpm and 210°F for 5.2 hours after completing the step-speed sequence to establish comparability to bearing 093301. The outer ring temperature was then increased to 250°F by increasing the oil-in temperature to 170°-180°F for the remaining 17.1 hours at 46,000 rpm and 200°F temperature to permit changeover to the higher speed air turbine powered tester. During all of these tests, the oil supply rate was maintained at 0.7-0.8 gallon per minute.

All three bearings were in excellent condition at the conclusion of this phase of the test, showing the best appearance of the designs tested to this point. There were no signs of distress on the inner ring roller paths, and only a light polish on the outer ring roller path. The roller end contact was clearly marked on the midpoint of the flange surface, but no smearing or other distress was evident. No end smearing or outer diameter distress was visible on the rollers. The cage showed moderate to heavy flow of the silver-plated metal on both the pocket leading and trailing cross bars due to roller movements in the pockets, but no smearing or excessive wear of the plating on the bar surfaces.

Subsequent to the development of the air-turbine-powered test rig and the testing of the outer ring flanged design, bearings 093302 and 093303 were remounted as a pair for testing to establish the maximum speed capabilities of the inner ring flanged

design. However, bearing 093303 failed at 52,000 rpm due to the inadvertent failure to supply a sufficient amount of lubricant to the roller end/flange interface. Extreme roller end wear was noted in the contact areas, illustrated in Figures 34 & 35, while extreme smearing and galling of the flange surface were also present. The cage showed moderate to heavy contact at the cross bars and the pocket ends, with some wear on the cage inner diameter. The roller outer diameter and inner ring roller path surfaces were lightly frosted in appearance.

The most direct evidence that a lack of sufficient lubricant being supplied to the roller end/flange interface was the cause of failure was the presence of heat distress on portions of the flange outer diameter. This surface was heat-discolored a deep blue over an approximate 50° arc between the lubricant supply holes. Directly opposite the holes were short 10°-15° arcs where no heat distress had occurred, indicating that these areas received adequate cooling. This pattern is illustrated in Figure 34. It is thus concluded that lubricant was not delivered to the radial holes in sufficient quantities to adequately cool the entire area of the roller end/flange contact zone. The centrifugal force, which delivers the oil from the under-race reservoir, was in this case throwing the oil off the inner ring before it could be transferred to the areas between the holes by the rollers.

This bearing was then replaced with an angular contact ball bearing, and testing of bearing 093302 was continued, reaching a maximum speed of 90,100 rpm (2.25 million DN). Testing was suspended at that point when the pipe supplying oil to the hollow shaft became disconnected and rubbed on the shaft. The resulting extreme vibrations and loss of control of shaft rotation probably masked a declutch mode of operation and caused it to escape observation. This pipe had probably become loosened through the vibrations incurred during normal operation and those excessive vibrations resulting from an inadvertent operation at an estimated 375- to 400-pound load (due to a load system malfunction) in the declutched mode for approximately 0.3 hour at

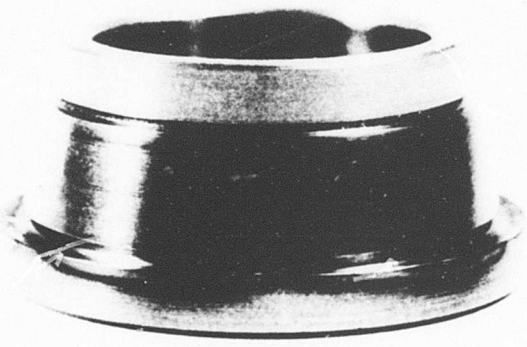

Figure 34. Bearing 093303 Showing (1) Roller End Wear and (2) Heat Pattern on Cone OD.

Roller End - Sixty Magnification

Figure 35. Roller End Wear-Experimental Bearing 093303.

77,000 rpm. This bearing accumulated 6.3 hours in the 70,000- to 80,000-rpm range, 0.5 hour in excess of 80,000 rpm, and 0.1 hour at the 90,100-rpm speed. After disassembly, the bearing was found to be in excellent condition. The roller sphered ends showed only minor glazing and very light smearing, and the inner ring flange was in a similar condition. The load track was clearly defined high on the flange surface, and no surface damage was noted. The roller outer diameter and both roller paths were lightly frosted, and no heat discoloration was found.

Bearings 093304 and 093305 were tested with the direct objective of attaining an extended period of operation in the declutch mode to ascertain, if possible, the effect of declutching. Declutching of the bearings under 460 pounds axial load was attained at about 85,000 rpm, as was theoretically predicted, and the speed was increased to 90,100 rpm and maintained for a period of 1.1 hours. No audible change in noise or vibration level occurred from the speed increase above 85,000 rpm, as would be expected from the occurrence of a shaft critical. Bearing temperatures remained essentially unaffected by this speed increase; the drive end bearing operated in the 240°-250°F range, and the load bearing operated much hotter at 340°-350°F outer ring temperature.

The previous test run in which a reduced load of 375-400 pounds was inadvertently applied resulted in a similar noise and vibration pattern becoming prominent at about 77,000 rpm. This was eliminated and a smooth running condition restored by the increase of load back to the normal 460 pounds. Therefore, it is concluded that since the vibrations were load dependent, the operation was in the declutch mode and not in the region of a shaft critical.

The condition of the bearings after this period of declutched operation was satisfactory. No damage

had occurred to the flange or roller path surfaces. However, evidence of heavy roller contact was found in the cage pockets. Flow of the silver plating was found in the leading edge of the cage pockets from the load end bearing cage (093304) and from the trailing edge of the drive end bearing cage (093305). Signs of roller skew were plainly visible in the 093304 cage wear patterns but were masked by the heavy roller contact in the 093305 bearing. Nonetheless, it was judged that the bearings were satisfactory for subsequent tests. This indicates that even in the declutched condition, a tapered roller bearing is functional, providing that the rotor location is maintained with acceptable accuracy.

The final test of the inner ring flanged bearings was conducted with the previously run bearings 093304 and 093305 being operated continuously at 80,000 rpm (2 million DN), about 5,000 rpm below the previously determined declutch point. A total of 30.5 test hours were accumulated, of which 22.5 hours were at the test speed. Suspension of the test was precipitated by an axial fracture of the inner ring of bearing 093305 shown in Figure 36 at an oil hole, causing an instantaneous seizure of the inner ring and cage through inner ring expansion. The cage and rollers therefore increased rotational speed to match the inner ring, which gave them the centrifugal force component equivalent to an inner ring speed of 200,000 rpm in a normal bearing.

This force displaced all of the rollers radially outward so contact was located high on the flange. The spinning of the rollers on the flange in a fixed position produced a contact situation far exceeding the lubrication capabilities present. The roller ends burned circular patterns in the flange face; and one roller, skewed by the presence of the crack, caught the large end corner on the flange and "walked" out of the bearing. This roller wedged at the outer ring/bearing housing/cage interfaces and locked up the system.

The cause of the inner ring fracture was a crack initiating at one of the radial oil holes

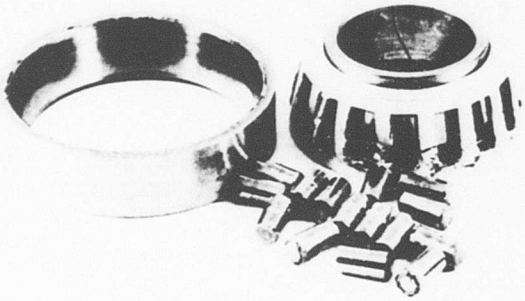

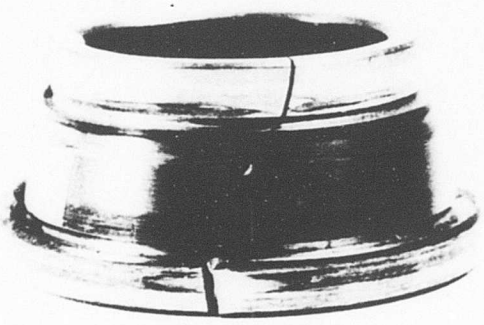

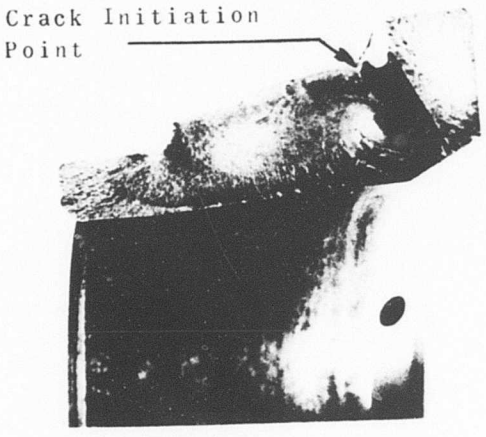

Figure 36. Bearing 093305 Inner Ring Fracture - Experimental Bearings.

used to provide oil to the flange surface. Examination of the fracture indicated that the crack initiated at the edge of the hole in the undercut. The ring section is shown in Figure 37, and the repeated cycling by roller passage of the thin section immediately under the roller path edge most likely precipitated the crack. The crack propagated to the bearing bore, at which point centrifugal force probably was a major contributor to final rupture. Small cracks were also found at two other oil holes in this inner ring which had not progressed to a critical stage. Examination of the eight other inner ring flanged bearings tested in functional or step/speed tests disclosed three other inner rings with similar cracks, including one in one of the commercial bearings. This latter bearing having had the radial holes put in an otherwise finished bearing, leads to the belief that the cracks are not heat-treat related.

The presence of these cracks, none of which had progressed to an operationally disruptive state, also indicates that the formation and/or propagation of the crack is a time-dependent occurrence, in line with a material fatigue related mechanism.

It is not inferred that oil holes in flange undercuts are necessarily failure prone. When bearings with such holes are produced for service, additional care can be taken in design and fabrication to avoid loading hole edges and thus prevent cracking.

The outer ring showed no effect from this sequence of events, except the ID corner where the loose roller wedged. The inner ring flange surfaces show the roller end burn marks high on the flange surfaces, and the roller path shows the axial markings where the rollers spun at the instant of cage/inner ring lockup. The cage shows severe wear in the OD at the land contact surfaces, indicating a short period of rotation in heavy contact with the inner ring, most likely in the moment immediately prior to lockup of the two components.

Heat generation rates for these bearings across the entire speed range were calculated and are compared

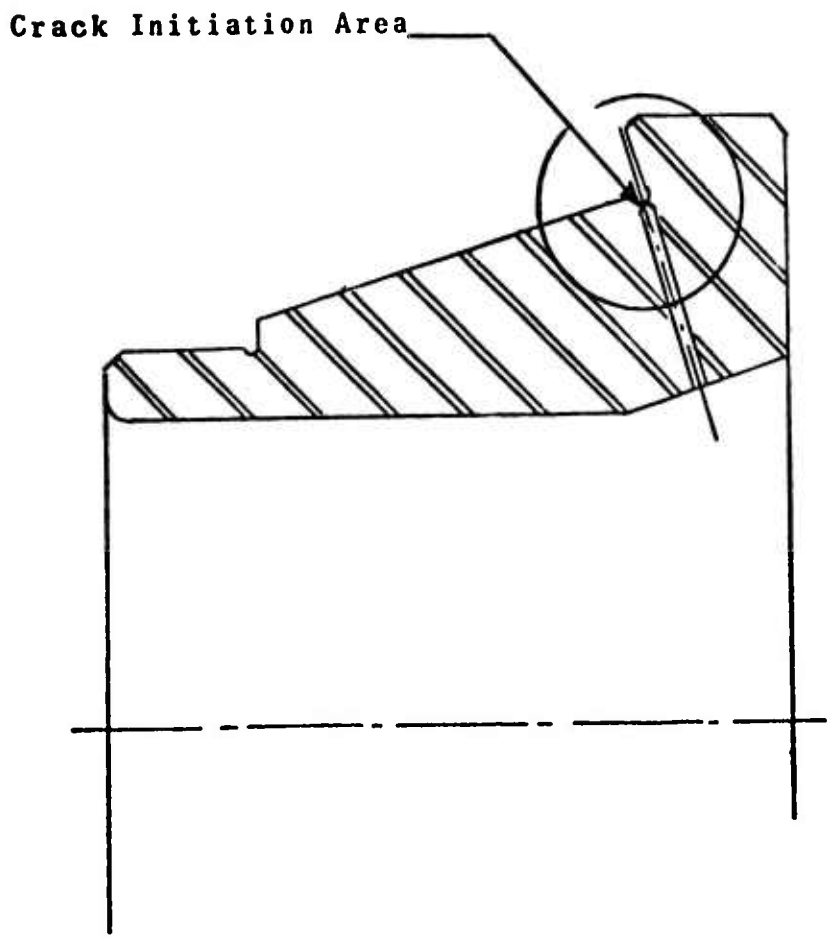

Figure 37. Crack Initiation Area, Inner Ring Flanged Design.

in Table VI with that of the aircraft toleranced standard design, which had the lowest heat generation rate of the inner ring flanged designs. At low speeds, the heat generation rate of the experimental design is much greater than that of the aircraft toleranced standard design. However, this difference seems to decrease as the speed is increased.

TABLE VI. COMPARISON OF BEARING HEAT GENERATION RATES FOR AIRCRAFT TOLERANCED STANDARD DESIGN TAPERED ROLLER BEARINGS AND EXPERIMENTAL DESIGN BEARINGS, MAXIMUM SPEED 90,100 RPM

Speed Range (rpm)	Average Heat Removed by Circulating Oil - Btu/Hr*	
	Aircraft Toleranced Standard Bearings 093200	Experimental Design Bearings 093300
10,000-20,000	870	1836
20,000-30,000	883	2438
30,000-40,000	2300	3678
40,000-50,000	4176	5678
50,000-60,000		5717
60,000-70,000		6560
70,000-80,000		9644
80,000-90,000		9531
90,000-100,000		9914

*Includes 17.2 hours of operation at 250°F outer ring temperatures for bearing 093202 and for bearing 093302.

Figure 38 shows a plot of the heat generation rates as a function of speed for all of the inner ring flanged bearing designs. This figure indicates that the slope of the curve for the experimental design is less steep than that of the standard, even when aircraft tolerances are used. Furthermore, it appears that the rate of change of heat generation with speed is constant for the experimental

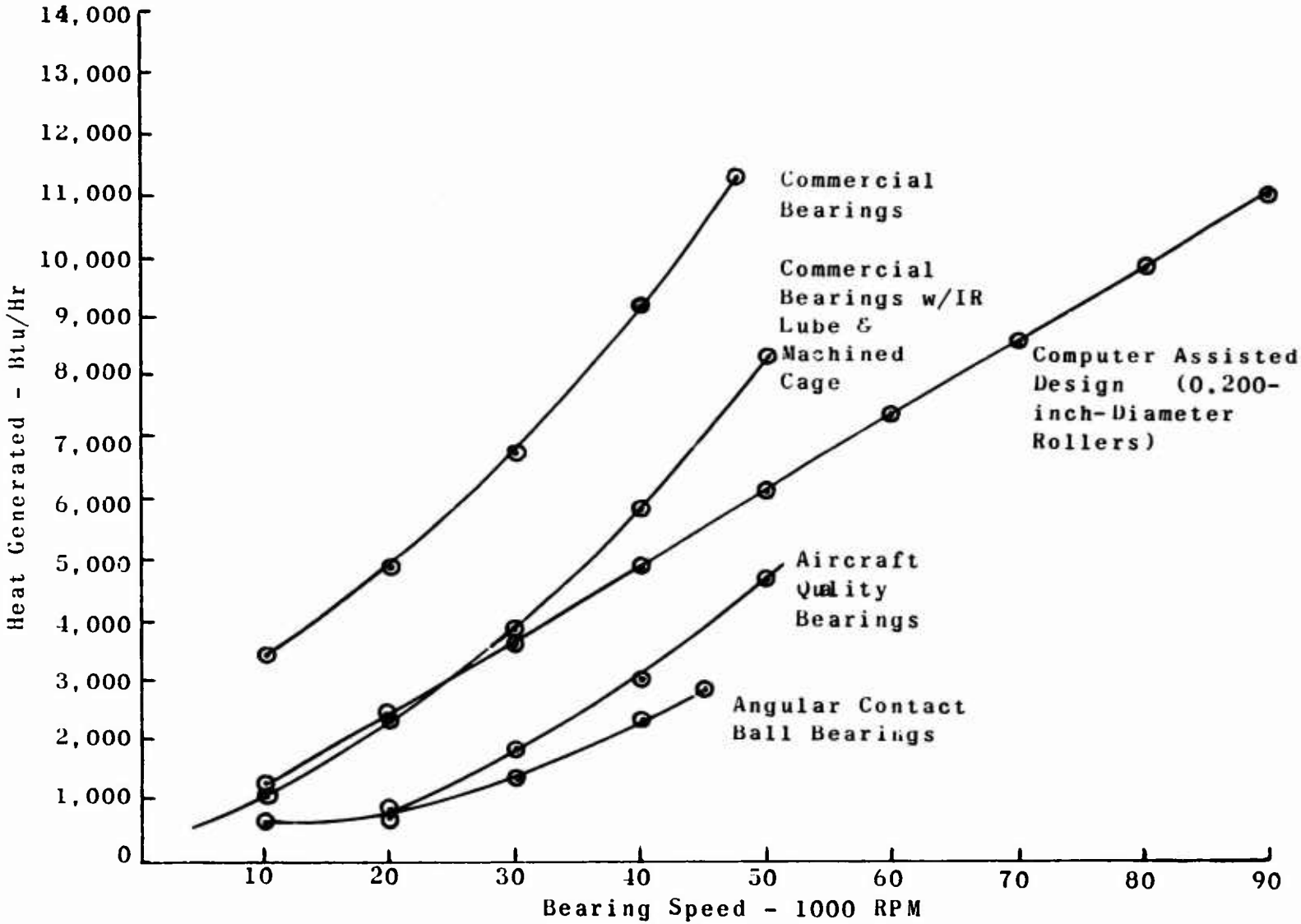

Figure 38. Heat Generation Rates, Inner Ring Flanged Tapered Roller Bearings and Angular Contact Ball Bearings.

design, while it is an increasing function for the standard designs. This being the case, a cross-over of the curves would be expected in the region of 70,000 rpm. Thus, the experimental design is the best inner ring flanged design tested in this program for the highest speeds.

The testing has shown that the power consumption curves (Figure 36) as predicted show an upturn as the declutch condition is approached; it is therefore not surprising that the air turbine had insufficient power to propel the bearings to even higher speeds than the 90,000 rpm which was achieved.

Taking the relatively meager heat generation data to vindicate the computed heat generation curves, one can speculate that the test bearing configuration can be made to perform even more dramatically simply by increasing the thrust load to 1000 pounds. A review of the design parameters, at 1000 pounds thrust, reveals that the flange loads and stresses would increase only slightly. There would be some fatigue life sacrifice, but heat generation, and consequently flange cooling and lubrication problems, could easily have been halved based on the analytical results.

The unusual trade-off of reducing <u>total</u> bearing friction by increasing applied thrust load is novel and highly speculative and needs to be experimentally tested.

In summary, the results of this phase of the program indicate that inner ring flanged tapers are a viable design that can be developed to serve as an aircraft gas turbine main-shaft support bearing.

<u>2. Tests of Outer Ring Flanged Bearings</u>

The tests of this bearing design configuration were also conducted on both the mechanically driven and air turbine powered test rigs. Initial evaluation was completed on three individual bearings at speeds up to 46,000 rpm on the mechanically driven rig. Testing was subsequently attempted

on the air turbine rig using an individual tapered roller bearing operating with an angular contact ball bearing on the other end of the shaft. However, the two bearing designs are sufficiently different that dynamic instabilities were developed at the higher speeds, probably due to differences in radial stiffness values. The remaining three tests were then run using a pair of test bearings on the shaft.

Step-speed testing was initiated on the first bearing in this group using a 460-pound axial load and supplying oil from jets to the outboard side of the bearing (the small end of the taper). Since the flange is located on the outer ring in this instance, the under-race oil supply to the inner ring was discontinued. Testing proceeded up to a speed of 46,000 rpm, at which point constant-speed operation commenced. After 9.1 hours at this speed, and a total running time of 77.15 hours, the bearing seized. The posttest examination disclosed that a spalling failure had occurred and had progressed to the point where all components were excessively spalled, and finally caused the bearing to seize. Damage was too extensive to allow any further comment on the operating characteristics of the bearing.

Testing of bearing 094102 was then conducted in a similar manner. This test was terminated after 1.4 hours of operation at 46,000 rpm, accumulating a total operating time of 33.1 hours. Examination of this bearing showed that spalling existed on both race surfaces near the small end of the taper and some distress was also noted on the rollers in this region. These two early fatigue type failures and the obvious edge loading condition noted in the second bearing indicated the need to reevaluate the bearing design.

A characteristic of the outer ring flanged design is that relatively high contact loads are produced for a given applied loading. Thus, the 460-pound load used in these tests produced much higher roller loading in this design than it had in the inner ring flanged design. Calculations showed that, at 50,000 rpm, an identical contact load to the new flange design would result if the applied load were reduced to 240 pounds. Since the main goal of this project is to obtain operational speed limitations of the bearing designs, this load reduction was effected to reduce the occurrence of fatigue failure. At the same time, the roller path angle of the inner ring was increased by 0°1' to reduce the angular error at the small end and thus eliminate the load bias that had existed.

Figure 39 illustrates the effect on theoretical inner ring life of the load change. This curve indicates that the life obtained under this loading at 10,000 rpm is increased relative to that of the original load. However, it must be noted that these life calculations are, at best, approximations. The fatigue life of the flange contact is not considered, and this creates difficulties in interpretation with high-speed tapered roller bearings. This is particularly illustrated by the life curve of the inner ring flanged bearing, which unrealistically tends to go to infinity as the load shifts from the inner race contact to the flange. Thus, actual life comparisons between designs can be made only after a significant amount of testing has been completed, allowing the establishment of realistic fatigue criteria.

A third bearing test was then conducted using the new load and altered internal geometry. This bearing, 094103, accumulated a total life of 70 hours, including 20 hours at 46,000 rpm, without failing. Posttest examination disclosed that the bearing was in excellent condition and that the load bias had been eliminated (see Figure 40).

Testing was then initiated using the air turbine rig with bearing 094104. This bearing failed at a speed of 60,000 rpm when an oil jet became mislocated and did not supply an adequate amount of lubrication to the flange/roller end contact area. Some evidence of dynamic instability was also noted during this run, which could have produced the mislocation of the jet, due to the difference in radial stiffness of the two bearings used on the shaft. Subsequent tests were conducted using pairs of outer ring flanged tapered roller bearings. The lives accumulated by all these bearings during testing are given in Table VII.

Bearing 094103 was the only specimen which went through the test series without suffering a failure. This bearing also reached the highest speed achieved during this program, 95,000 rpm, in conjunction with bearing 094106. At the conclusion of this run, which was deliberately terminated after 2.1 hours at speed to allow the examination of the bearings, both bearings showed the effects of severe heat generation on the oil-out side of the bearing (the large end of the taper), through heat discoloration in the flange area and on the large ends of the cages. Additionally, small spalls

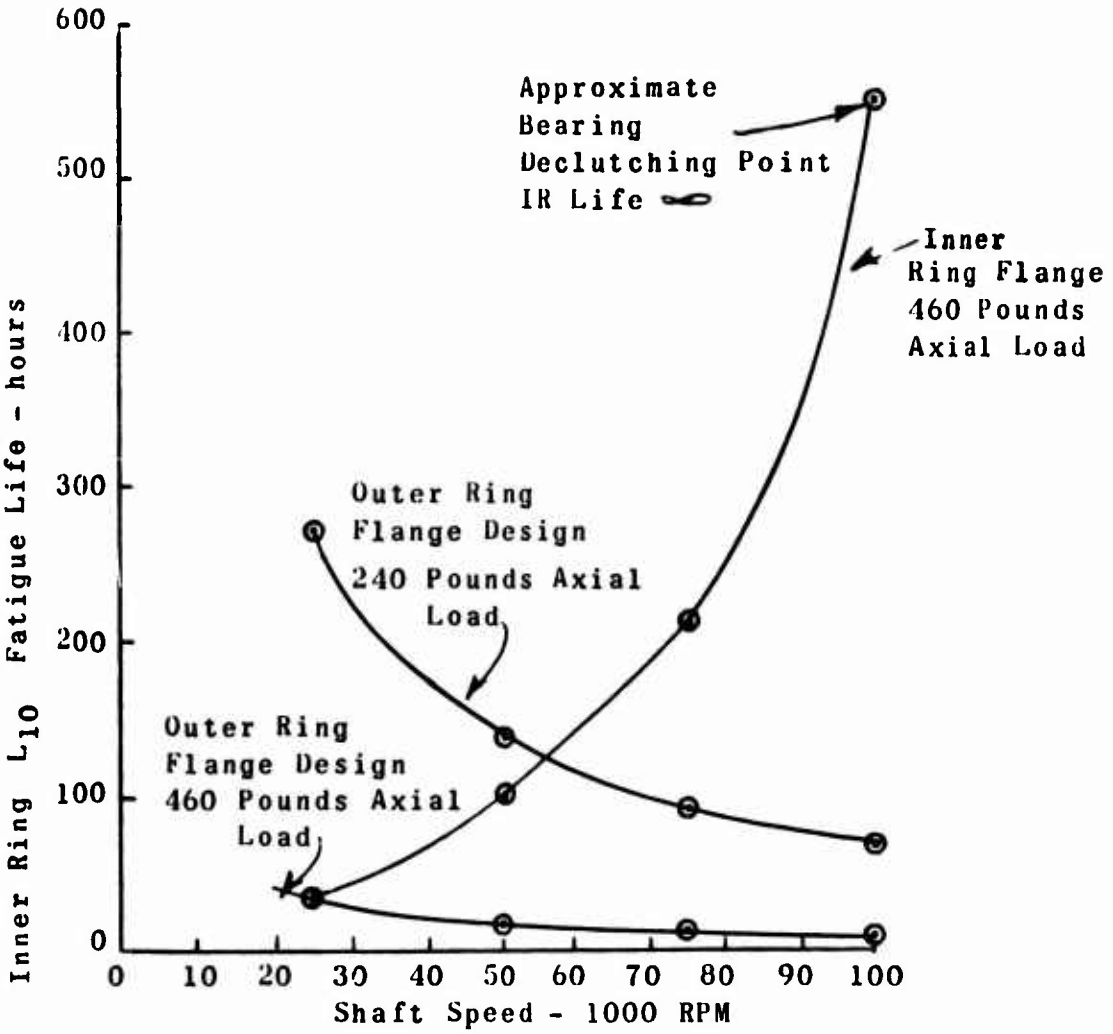

Figure 39. Theoretical Inner Ring L_{10} Fatigue Life vs Shaft Speed.

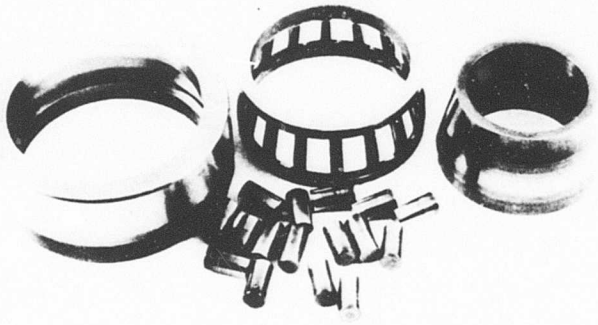

Test Bearing No. 094103

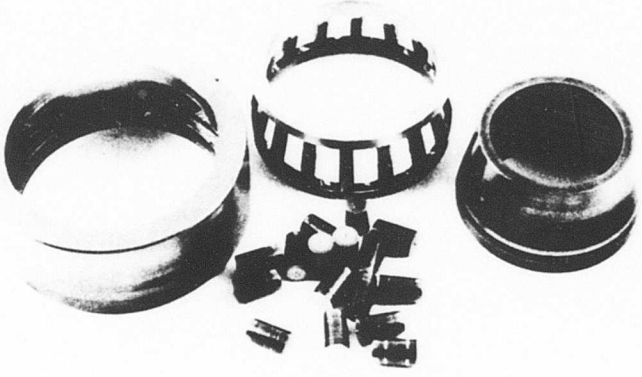

Test Bearing No. 094105

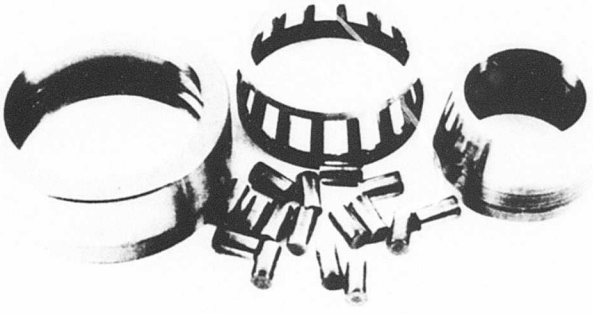

Test Bearing No. 094106

Figure 40. Post Test Conditions of Sample Bearings-
Outer Ring Flanged Design.

TABLE VII. SPEED/TIME TABULATIONS FOR OUTER RING FLANGED BEARINGS 094101 TO 094109

Speed Range (RPM)	Time at Speed Bearing Number 094101	094102	094103	094104	094105	094106	094107	094107A	094108	094109
0-10,000	12.35	12.50	21.30	1.75	7.60	5.40	1.70	1.1	6.0	6.0
10,000-20,000	20.60	5.50	18.00	0.45	2.50	1.20	0.50	0.3	1.0	1.0
20,000-30,000	10.15	4.00	13.00	0.92	1.80	1.70	1.10	0.4		
30,000-40,000	22.70	9.20	7.00	0.75	1.80	3.90	1.10	1.0	1.4	1.4
40,000-50,000	11.35	1.9	29.70	1.20	4.60	2.00	0.30	0.7	0.6	0.6
50,000-60,000			1.20	0.10	2.10	3.30	1.60	0.9	4.1	4.1
60,000-70,000			6.35		4.35	3.60	1.10	0.5		
70,000-80,000			4.40		4.10	3.00	2.10	0.6		
80,000-90,000			8.60		8.20	8.90	8.30	0.2		
90,000-100,000			2.10			2.30		0.2		
TOTAL	77.15	33.10	112.15	5.17*	37.05	35.30	17.80	5.90	13.10	13.10

*INCLUDES 1.87 AT 100-LB AXIAL LOAD.

were evident on two rollers from bearing 094106, while surface distress appeared on most of the remaining rollers. Other than this, the physical damage to the bearings was limited to light smearing on the flanges and silver flow found in the pockets of the cage caused by heavy roller contact. The roller end/flange contact was located in the middle third of the flange in bearing 094103 and on the flange half near the undercut in bearing 094106. These combined factors indicate the viability of this design as a candidate bearing for operation in a high-speed environment.

The major operational problem noted during these tests is the lubrication of the flange/roller end contacts. Heat discoloration was noted in this area on most of the bearings tested, while roller end wear, up to 0.013 inch, and heavy smearing were noted on bearings 094103, 094107A*, and 094108. The wear in bearing 094108 was so severe that the increased looseness in the bearing resulted in the loss of centerline control of the shaft and the suspension of testing on this and the paired bearing 094109.

The lubrication of this flange area must be improved to make this a practical bearing system. Two competing theories now exist as to why difficulties were encountered during this program. The first possibility is that, not enough cool

*After minor spalling of the rollers forced the discontinuance of the test on bearing 094107, the rollers were replaced and the resulting assembly was denoted as 094107A.

lubricant is reaching this area, since the oil is supplied at the small end of the bearing and must pass over the hot components before reaching the flanges. This hot oil would then have limited heat absorption capacity and would offer only a reduced amount of lubrication. The other theory indicates that oil is trapped in a pool in the flange corner and the fresh cooler oil passes over the top of this pool and out of the bearing without cooling this area. The trapped oil would then become quite hot and cease to lubricate the flange adequately. Future testing should determine the reason for this problem and establish a practical solution.

Table VIII and Figure 41 compare the heat generation rates for the outer ring flanged bearing and the best inner ring flanged design, the "experimental" group. At identical applied loads, the heat generation rate of this bearing design would be expected to be greater than that of the inner ring flanged bearing due to the increased contact loads. The data obtained, however, were not sufficient to bear this out. At identical contact loads (50,000 rpm), the heat generation rate of the outer ring bearing appeared to be generally less and continued to be less with outer ring contact loads, which increase with increase in speed (Table IX).

TABLE VIII. RELATIVE HEAT GENERATION RATES OF INNER RING FLANGED DESIGN BEARINGS AND OUTER RING FLANGED DESIGN BEARINGS

	Average Heat Removed by Circulating Oil Btu/Hr	
Speed Range (rpm)	Inner Ring Flanged Design at 460-lb Load	Outer Ring Flanged Design Bearings at 240-lb Load
10,000-20,000	1836	1866
20,000-30,000	2438	2983
30,000-40,000	3678	2886
40,000-50,000	5678	3780
50,000-60,000	5717	6707
60,000-70,000	6560	6327
70,000-80,000	9044	7782
80,000-90,000	9531	8744
90,000-100,000	9914	11748

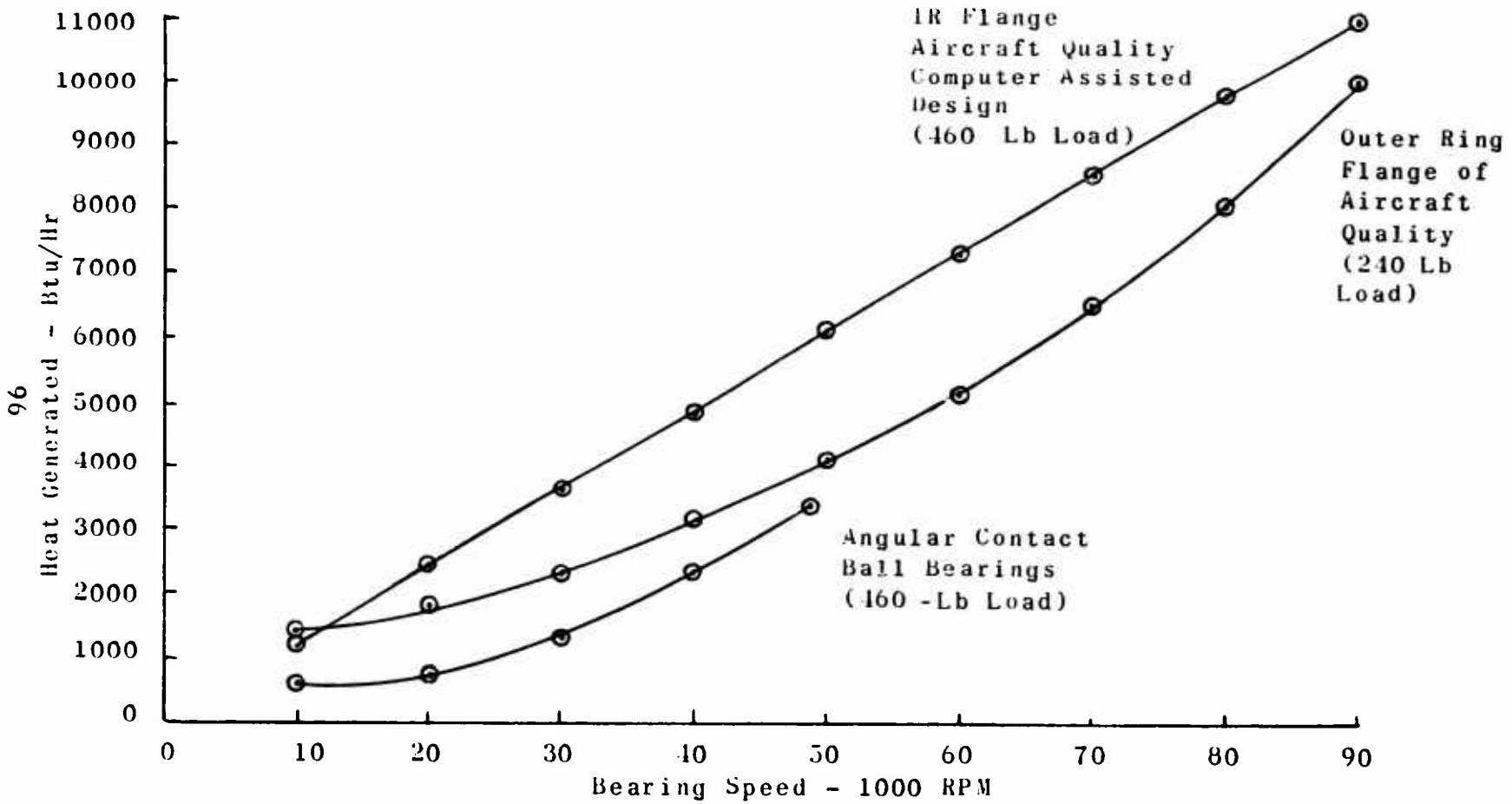

Figure 41. Heat Generation Rates Inner Ring and Outer Ring Flanged Tapered Roller Bearings and Angular Contact Ball Bearings.

Further tests are needed to establish more definitely the heat generation characteristics of these two designs.

The results of this program indicate that both the experimentally designed inner ring flanged tapered roller bearing and the novel outer ring flanged tapered roller bearing are candidates for gas turbine shaft support systems. This program did not clearly demonstrate the superiority of one design over the other. The outer ring flanged bearing attained the highest speed (under reduced applied load) and appears to be capable of yet higher speeds with only minor development. The inner ring flanged bearing also demonstrated a significant speed capability (2.13 million DN) and a vastly superior load-carrying capacity, and it will lend itself more easily to production in quantity. However, additional speed capabilities seem to be available in this instance only by the development of a bearing/rotor configuration to adequately solve the problems associated with the declutching phenomenon.

TABLE IX. CONTACT LOAD COMPARISON OF INNER RING FLANGED AND OUTER RING FLANGED BEARINGS UNDER CONSTANT EXTERNAL APPLIED LOAD AND INCREASING SPEED

Bearing Element	Contact Force at Speed		
	50,000 rpm	75,000 rpm	100,000 rpm
A. Inner Ring Flanged Bearings-463691 Design (093300 Series)			
IR Roller Path	78 lb	12.1 lb	-
OR Roller Path	108	108	108
Flange Load	12	21	30
Centrifugal Load	30.5	68.4	121
B. Outer Ring Flanged Bearings-L-42032 Design (094100 Series)			
IR Roller Path	74.4	74.4	74.4
OR Roller Path	103	140	190
Flange Load	12.1	21.8	35.4
Centrifugal Load	30.2	68.4	121

VI. CONCLUSIONS

1. Two tapered roller bearing designs have been developed which have demonstrated speed capability in the 2.13 to 2.4 million DN range. The results of this program have established the feasibility of the tapered roller bearing for use in ultra high-speed applications such as aircraft gas turbine engines.

2. The novel outer ring flanged tapered roller bearing design developed under this program is capable of (at least short term) operation to 2.4 million DN. Additional speed capability appears to be available with minor design improvements, but the load-carrying capacity of this design is limited.

3. The inner ring flanged design has demonstrated a speed capability up to 2.13 million DN operation, and has a load-carrying capacity which is significantly greater than that of the outer ring flanged design.

The speed capability is circumscribed by the occurrence of declutching and a significant amount of bearing/rotor configuration development work will be required in order to surpass the current performance limitation.

4. There is no evidence of superiority of either the inner or outer ring flange design. Continued development of both designs appears warranted. Any selection between them must be made on a case-by-case basis, for the requirements of the application.

5. The critical considerations of high-speed tapered roller bearing design are (1) the roller end/flange interface where the heat generation rate must be balanced by sufficient cooling capability for the required thrust load carrying capacity, (2) the effect of centrifugal force on roller path and flange load, and (3) the limiting factors of declutching on the inner ring flanged design.

VII. RECOMMENDATIONS

1. The development effort to date has adequately shown that tapered roller bearings of inner or outer ring flanged design have potential for gas turbine applications. The program has indicated that both designs currently have limitations: the occurrence of declutching in the inner ring flanged bearing, the limited load-carrying ability, and increased difficulty in lubricating and cooling the flange of the outer ring flanged design. None of these limitations appear to be insurmountable; therefore, it is recommended that development effort be applied to both configurations for the purpose of obtaining a bearing which will meet the requirements of future aircraft gas turbine engines.

2. The conditions foreseen for the application of this bearing include temperatures in excess of 350°F (General Electric Corporation - Table II). M-50 tool steel is normally used for main-shaft bearings at these temperatures because of its resistance to loss of hardness and high load-carrying ability under extended periods of high temperature. For the use of the Army, additionally, a resistance to ballistic impact is considered to be a requisite material attribute for bearings and is normally better in carburized steels. Similar resistance to crack propagation can be obtained in M-50 steel by using a heat treatment which yields a hard layer in the contact areas and a relatively soft core. It is recommended, therefore, that the development of a skin hardening technique to be applied to M-50 material be undertaken. The successful result will preserve the extended life and temperature resistance benefits currently available from through hardened M-50 and add the resistance to shock loading from ballistic impact commonly available from case hardened parts.

LITERATURE CITED

1. Cocks, M., et al., FINAL SUMMARY REPORT ON PROJECTS I TO IV OF A BASIC STUDY OF THE SLIDING CONTACTS IN ROLLING BEARINGS, SKF Industries, Inc.; SKF AL69P003, U.S. Department of the Navy, Naval Air Systems Command, Washington, D.C., 1969, DDC AD 848 433L.

2. Crecelius, William, DYNAMIC AND THERMAL ANALYSIS OF HIGH SPEED TAPERED ROLLER BEARINGS UNDER COMBINED LOADING, SKF Industries, Inc.; SKF AL73P010, NASA CR-121207, NASA Lewis Research Center, Cleveland, Ohio, June 1973.

3. Lundberg, G., ELASTISCHE BERÜHRUNG ZWEIER HALBRÄUME, Forschung auf dem Gebiete des Ingenieurwesens 10, 5, Berline; September/October, 1939.

4. Harris, T., AN ANALYTICAL METHOD TO PREDICT SKIDDING IN HIGH SPEED ROLLER BEARINGS, ASLE Transactions, 9, 1966, pp. 229-441.

5. Dowson, D. and Higginson, G., THEORY OF ROLLER BEARING LUBRICATION AND DEFORMATION, Proceedings of the Institution of Mechanical Engineers, 177, 1963, pp. 58-69.

6. Harris, T., PREDICTING THE PERFORMANCE OF ROLLING BEARINGS IN EXCEPTIONAL APPLICATIONS, Lubrication Engineering, March 1969, pp. 25-133.

7. ASME, Pressure-Viscosity Report, Vol. II, 1953.

APPENDIX I
ANALYTICAL EVALUATION OF PERFORMANCE OF 25 MM BORE THRUST LOADED, TAPERED ROLLER BEARING

1. PURPOSE

The purpose of the analytical effort required under U. S. Army Contract DAAJ02-70-C-0047 was to evaluate the high-speed (1×10^6 to 3×10^6 DN) performance of a thrust-loaded, conventional-design, tapered roller bearing. The results of this study were necessary as input for establishing design parameters for the first group of prototype bearings to be manufactured and tested under this program.

2. SUMMARY

2.1 Tapered Bearing Analysis

To perform the analysis, SKF Computer Program AE69Y002, "Analysis of Dynamic Performanc Characteristics of Tapered Roller Bearings", was used to determine the effects of various bearing apex angles and roller diameters on frictional heat generation; rolling surface fatigue life; roller end flange loading and roller end/flange contact, frictional heat generation. Table X presents the bearing design characteristics and Table XI presents the bearing operating conditions investigated in the parametric study.

2.2 Ball Bearing Analysis

In addition to the tapered roller bearing study, Computer Program AE69Y004, "Analysis of Dynamic Performance Characteristics of Thrust Loaded Angular Contact Ball Bearings", was used to establish the performance characteristics of a thrust-loaded, angular-contact ball bearing having radial boundary dimensions identical to those of the tapered bearing under study, and subjected to the same operating conditions. The ball bearing design characteristics are listed in Table XII. Since angular contact ball bearings are nearly universally employed under the high-speed, thrust-load, operating conditions of gas

TABLE X. TAPERED ROLLER BEARING DESIGN CHARACTERISTICS AND VARIATIONS	
BORE	0.9843 in.
O.D.	2.0472 in.
WIDTH	0.7010 in.
APEX ANGLE	10° 13° 16° 19° and 22°
LARGE END ROLLER DIAMETER	0.200 and 0.244 in.
ROLLER EFFECTIVE LENGTH	
a. INNER RACEWAY	0.3037 in.
b. OUTER RACEWAY	0.3418 in.
NUMBER OF ROLLERS	16 with 0.200 large end diameter 14 with 0.244 large end diameter

TABLE XI. OPERATING PARAMETERS	
THRUST LOAD	460 and 960 pounds
SHAFT SPEED	25,000 50,000 75,000 100,000 RPM
LUBRICANT	MIL L 23699 at 275°F

TABLE XII. BALL BEARING DESIGN CHARACTERISTICS	
BORE	0.9843 in.
O.D.	2.0472 in.
WIDTH	0.5906 in.
FREE CONTACT ANGLE	22°
BALL DIAMETER	0.3125 in.
NUMBER OF BALLS	12
MATERIAL	AISI 52100

turbine main-shaft applications, it was necessary to compare ball bearing predicted performance with that of the tapered roller bearing to determine the feasibility of using the latter. Hence, where it is applicable, ball bearing data is included in the graphs and tables developed for this study.

3. CONCLUSIONS

3.1 An inner ring flanged tapered roller bearing design was selected to be evaluated by actual testing, in accordance with the contract objectives. This bearing has a 13° 21' 40" apex angle and a roller with a 0.200-in. large-end diameter (LED). The complete bearing design is represented in Figure 42. This bearing design selection was made by weighting, most heavily, those design characteristics which would minimize the roller end/flange load and the friction heat generation at the roller end/flange contacts. It is currently considered that roller end/flange contact overloading and heat generation are the most probable sources of failure for high-speed operation.

3.2 Analytical evidence suggests that a conventional-design, inner-ring-flanged, tapered roller bearing should not be employed for operation at high speeds, under light to moderate axial loading.

3.3 Bearings with large roller diameters and bearing apex angles will produce the following trends, as compared with bearings having small roller diameters and apex angles:

1. Higher L_{10} lives.
2. Higher sliding heat generation.
3. Higher flange loads.
4. Higher, roller end/flange, frictional heat generation. These trends can be examined in Figure 42 through 46.

3.4 Bearing fatigue L_{10} life tends to increase as the bearing shaft speed increases, because as shaft speed increases, load at the inner ring tends to shift to the flange as opposed to the roller path.

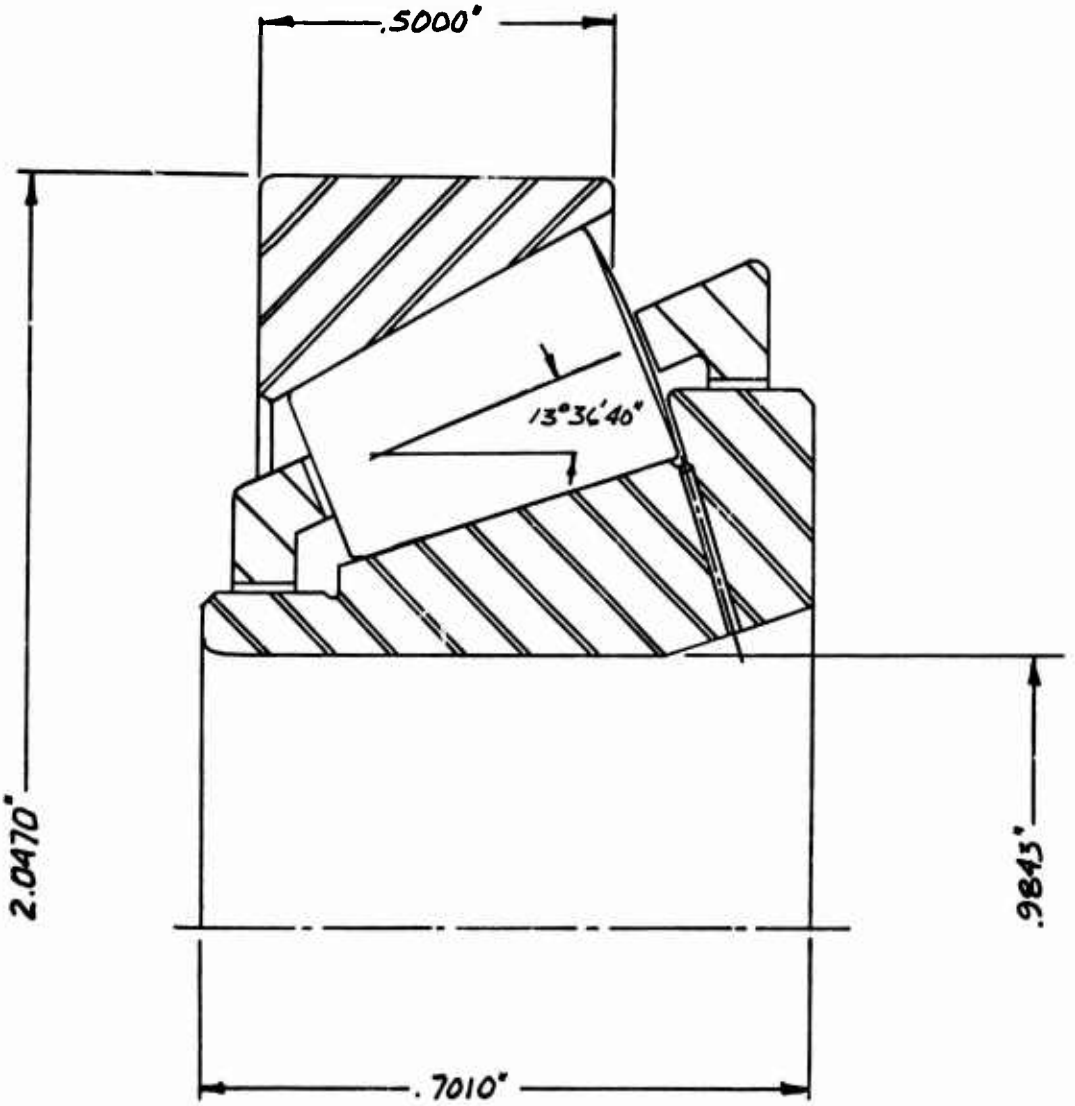

BEARING DESIGN CHARACTERISTICS

INNER RING

1. INNER RACEWAY HALF ANGLE 11°43'20"
2. INNER RACEWAY SURFACE ROUGHNESS 5 MICROINCHES A.A.
3. FLANGE HALF ANGLE
4. FLANGE SURFACE ROUGHNESS 5 MICROINCHES

OUTER RING

1. OUTER RACEWAY HALF ANGLE 15°00'00"
2. OUTER RACEWAY SURFACE ROUGHNESS 5 MICROINCHES A.A.

ROLLER

1. INCLUDED ANGLE
2. SURFACE ROUGHNESS 5 MICROINCHES A.A.
3. CROWN RADIUS 200 INCHES.
4. NUMBER OF ROLLERS 16

Figure 42. Test Bearing Design.

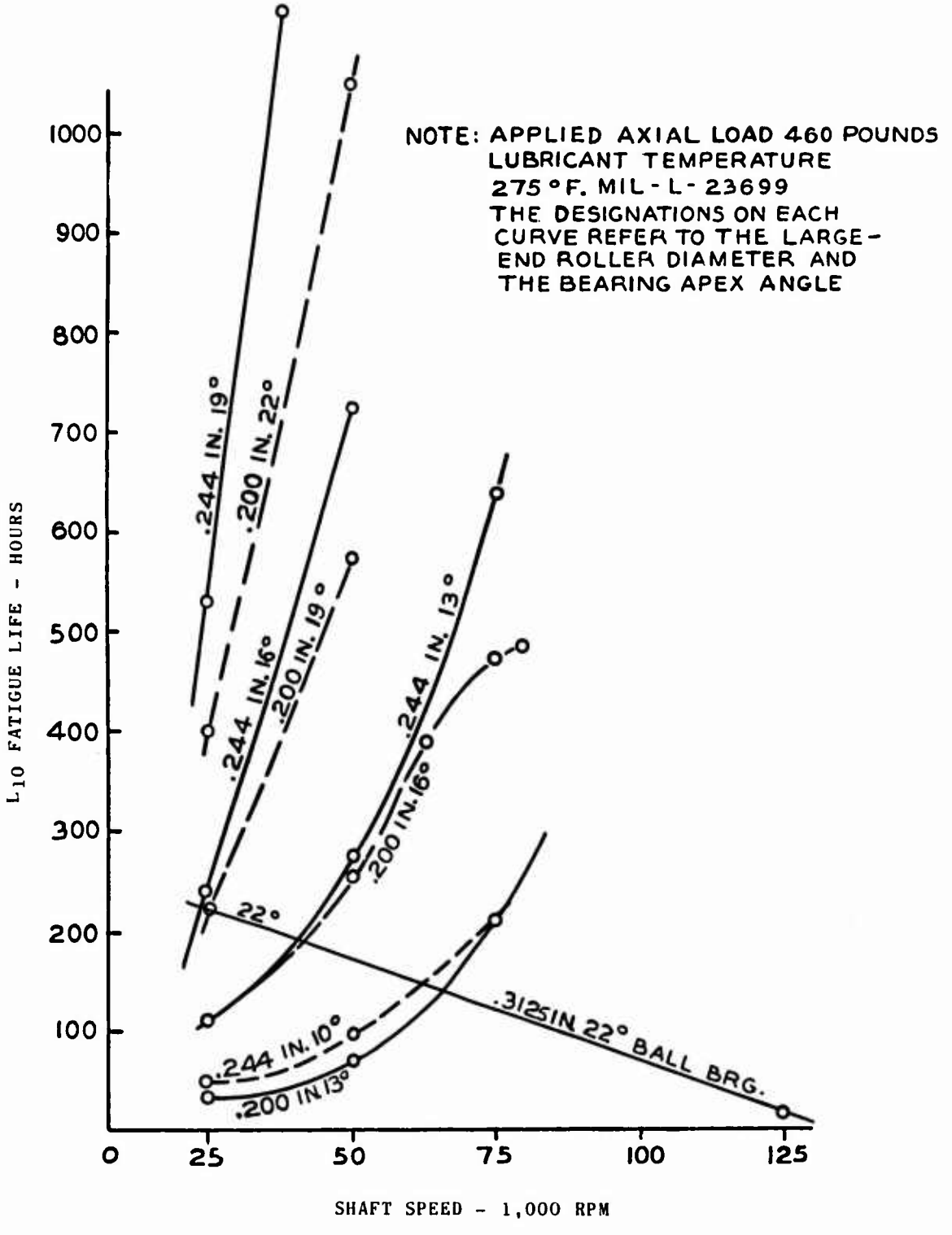

Figure 43. L_{10} Fatigue Life Versus Shaft Speed.

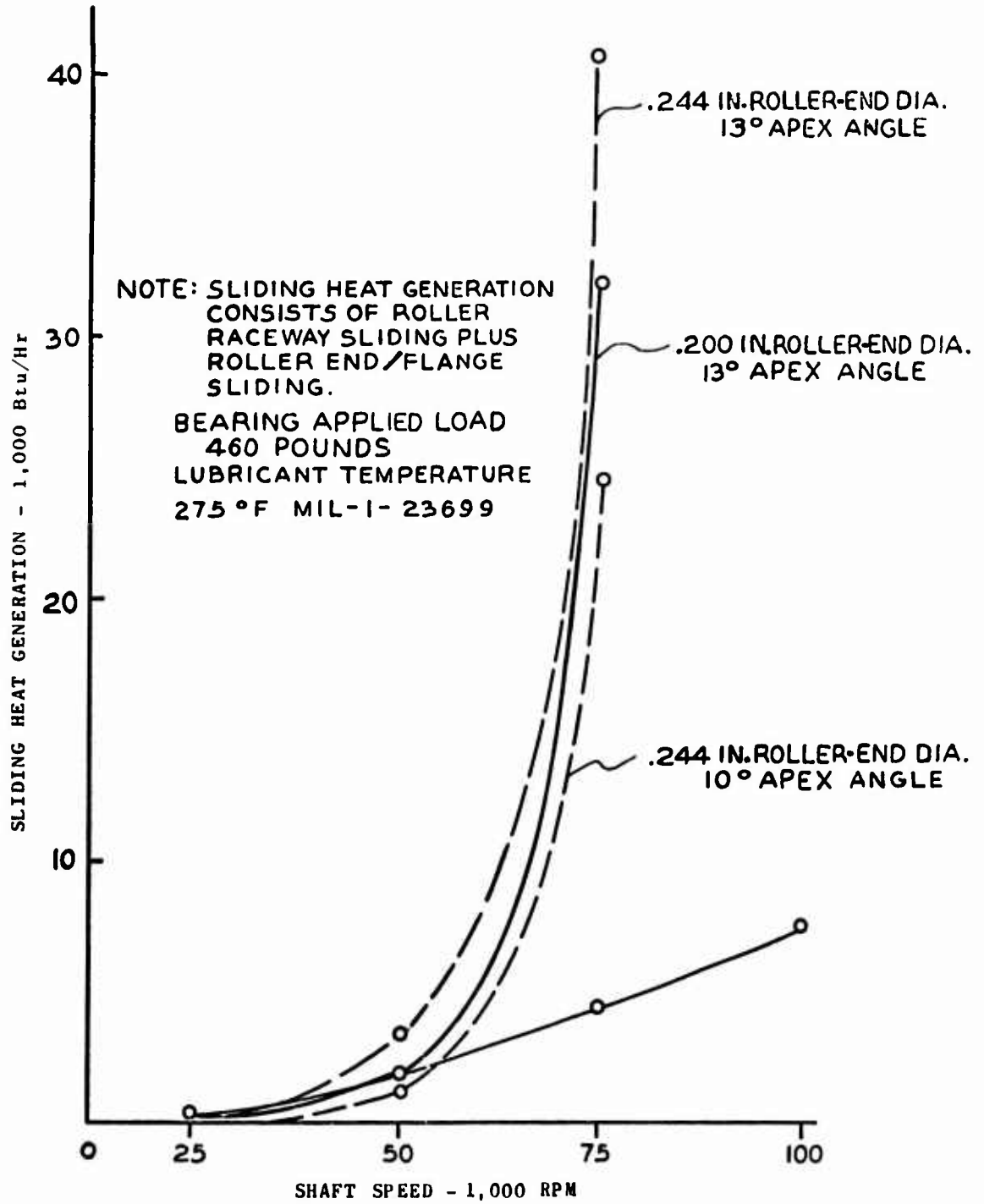

Figure 44. Sliding Heat Generation Versus Shaft Speed.

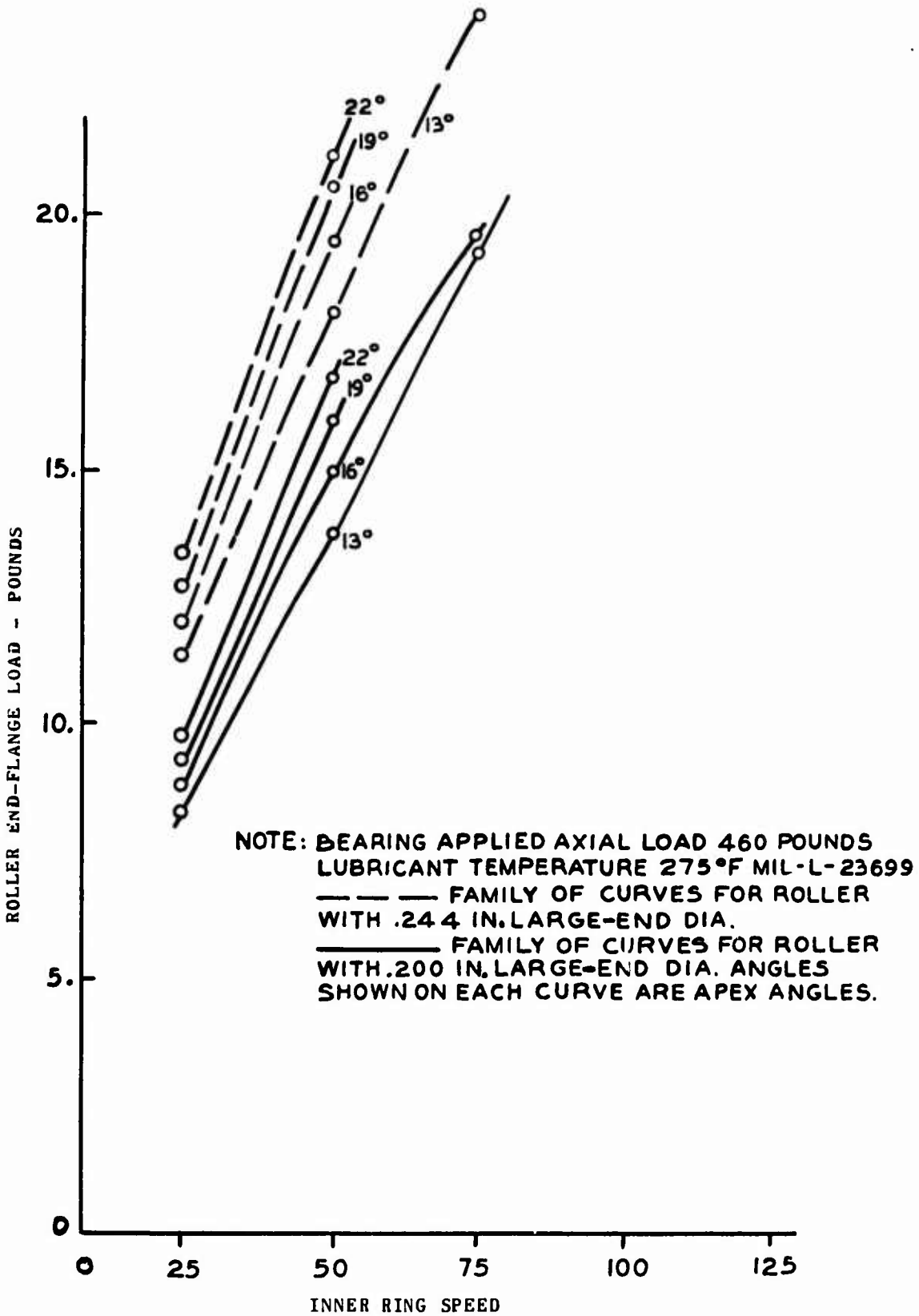

Figure 45. Roller End/Flange Load Versus Shaft Speed.

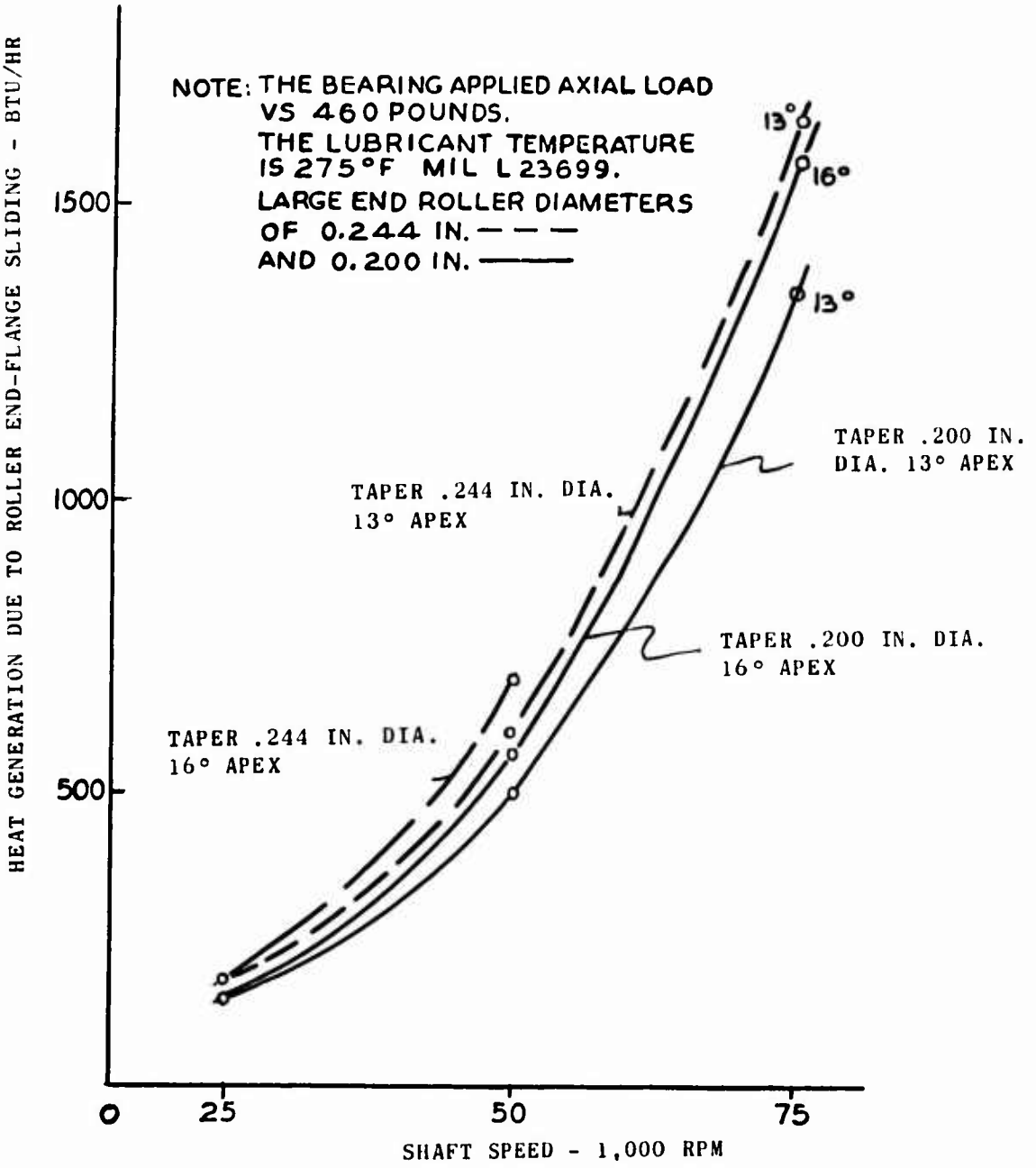

Figure 46. Roller End Flange Heat Generation Versus Shaft Speed.

Since bearing L_{10} life tends to be inner raceway limited at slow speeds, overall L_{10} life tends to increase.

3.5 A set of completely definitive design criteria for high-speed operation was not established, since no analytical model consisting of limiting, functional, parametric values has been established for the roller end/flange contact.

4. DISCUSSION OF RESULTS

4.1 Test Bearing Design Selection

Selection of an optimum tapered bearing design for initial testing was the purpose of the work performed. For this study the bearing design was limited to an inner ring, integral flange configuration. Data presented in Table XIII were used in the design selection. The bearing design presented in Figure 42 was selected. Selection of this design was not straightforward, since design characteristics which tend to increase bearing life, such as high apex angle and large roller diameter, have the tendency to reduce bearing high-speed operating capability. The larger the roller diameter and apex angle, the more rapid the shift of the inner ring load from the roller path to the flange, with increasing shaft speed. Thus, the bearing tends to declutch at relatively slow shaft speeds. Declutching is defined as the tendency for the inner ring normal load to approach zero under the effect of high cage speed and roller centrifugal force. Also, sliding heat generation, flange heat generation, and flange load tend to increase with high apex angles and large roller diameters.

In the design selection process, those design characteristics which tend to minimize sliding heat, flange heat, and flange load were weighted most heavily. As mentioned previously, roller end/flange contact appears to be the factor which limits the bearings' ability to operate satisfactorily at high speeds. Consideration was also given to the fact that design characteristics creating higher operating speed capabilities

TABLE XIII. DESIGN SELECTION DATA

Bearing Operating Conditions		Bearing Design Parameters		Bearing Operating Parameters			
Axial Load (lb)	Shaft Speed (rpm)	Roller Large End. Dia. (rpm)	Apex Angle (deg)	Sliding Heat (Btu/hr)	Load Life (hr)	Flange Heat (Btu/hr)	Flange Load (lb)
460.	50000.	.244	10.	1800.	69.	518.	16.
460.	50000.	.244	13.	3995.	273.	605.	18.
460.	50000.	.200	13.	2787.	93.	501.	14.
460.	50000.	.200	16.	4957.	253.	570.	15.
460.	50000.	.200	19.	7504.	568.	658.	16.
		*.3125	22.	1988.	186.		
460.	75000.	.244	10.	25946.	209.	1317.	23.
460.	75000.	.244	13.	42321.	638.	1647.	24.
460.	75000.	.200	13.	33439.	212.	1350.	19.
460.	75000.	.200	16.	43100.	471.	1575.	20.
460.	75000.	.200	19.	N.S.	N.S.	N.S.	N.S.
		*.3125	22.	4611.	142.		
960.	75000.	.244	10.	383.	3.	1630.	35.
960.	75000.	.244	13.	1904.	13.	1868.	40.
960.	75000.	.200	13.	939.	4.	1542.	30.
960.	75000.	.200	16.	4601.	12.	1736.	34.
960	75000.	.200	19.	8645.	28.	1933.	37.
		*.3125	22.	13964.	21.		
960	100000.	.244	10.	7563.	7.	3016.	48.
960	100000.	.244	13.	41466.	25.	3786.	53.
960	100000.	.200	13.	16406.	4.	3021.	42.
960	100000.	.200	16.	50484.	19.	3660.	45.
960	100000.	.200	19.	77186.	38.	4287.	47.
		*.3125	22.	39548.	14.		

* Refers to Ball Bearing Data.

would also be weighted more heavily than raceway life considerations. The result is a low-contact-angle, small-diameter roller design, which is shown by Figure 42. The roller diameter selected appeared to be a practical minimum from both manufacturing and raceway life standpoints.

A roller crown radius of 200 inches was selected as a design criterion, based primarily on manufacturing considerations. Analysis yielded ideal crown radii of 190 inches and 50 inches for the applied axial loads of 460 and 960 pounds respectively.

Table XIII represents a brief summary of the parametric study. Represented in this table are five tapered bearing designs, one ball bearing design, four sets of operating conditions, and the four sets of operating characteristics previously mentioned. Table XIII reveals that if it is necessary to choose a bearing design to operate under the full spectrum of load and speed conditions presented, a ball bearing is the logical choice. This conclusion can be reached by examining the L_{10} life and sliding heat generation estimates. Realizing that performance of the roller end/flange contact may be the limiting factor in a tapered roller bearing's ability to operate at high speed, the choice of the ball bearing appears best.

4.2 Conventional Tapered Roller Bearing Operating Characteristics

Figure 43 presents the effect of roller diameter and apex angle on bearing L_{10} life. Figure 44 shows the effect of roller diameter and apex angle on bearing sliding, frictional, heat generation at high operating speeds. Figures 45 and 46 indicate the effects of roller diameter and apex angle on roller end/flange loading and roller end/flange heat generation respectively. The large increase in heat generation occurring between 50,000 and 75,000 rpm shaft speed indicates the bearing's tendency to declutch, skid, and thus generate frictional heat.

4.3 High-Speed Tapered Roller Bearing Load Distribution Analysis

The prime reason for the conventional bearing's predicted poor performance at high speed can be seen from the simplified two-dimensional free-body diagram of Figure 47 . The bearing angles referenced in Figure 47 are defined in Figure 48 . It can be determined from Figure 47 that the magnitude of the outer ring normal load tends to remain constant with increasing speed. It is further evident that outer ring normal load is a function of only the applied axial load, since the number of rollers and the outer ring contact angle remain constant, notwithstanding increasing speed. The result is that with increasing speed, centrifugal force increases, and it can be accommodated only by a reduction in the inner raceway roller load and an increase in the roller end/flange load.

In the majority of high-speed applications, the shaft is the rotating member of the assembly and the housing the stationary member. Traction at the inner ring roller path is thus largely responsible for driving the cage and roller assembly. As the inner ring roller path load decreases, traction decreases, and skidding and the accompnaying heat generation at the inner raceway roller path contact increase.

Figures 42 and 45 reveal that for bearing designs having higher apex angles and larger roller diameters, there is an absence of data points at shaft speeds greater than 50,000 rpm. This lack of data occurs because at shaft speeds between 50,000 and 75,000 rpm, the bearing mathematically becomes unstable as the inner ring roller path unloads, and a mathematical solution was not reached. The mathematical instability appears to be indicative of functional instability.

Table XIII indicates that significantly less roller raceway sliding heat generation occurs at 960 pounds load than at 460 pounds. This difference is indicative of the higher inner raceway traction forces which result at higher applied loads.

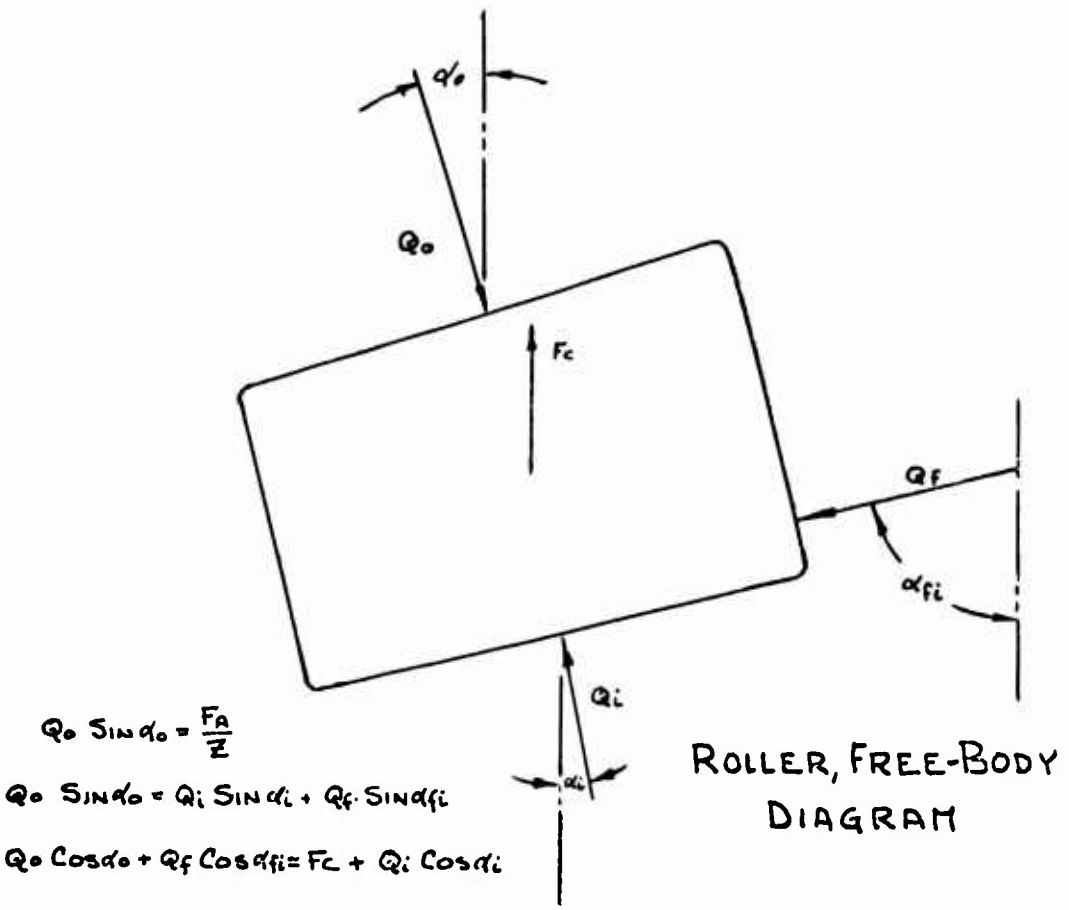

Q_o Roller, Outer Ring Normal Load
Q_i Roller, Inner Ring Normal Load
Q_f Roller, Inner Ring Flange Normal Load
F_c Roller, Centrifugal Force
Outer Ring Half Angle
Inner Ring Half Angle
Inner Ring Flange Half Angle
Applied Axial Load
Number of Rollers Per Bearing

Note: With Increasing Cage Orbital Speed, The Magnitude of

a. F_c Increases
b. Q_o Remains Constant
c. Q_f Increases
d. Q_i Decreases
e. , and Remain Constant

Figure 47. Inner Ring Flange, Bearing Roller Free-Body Diagram and Equilibrium Equations.

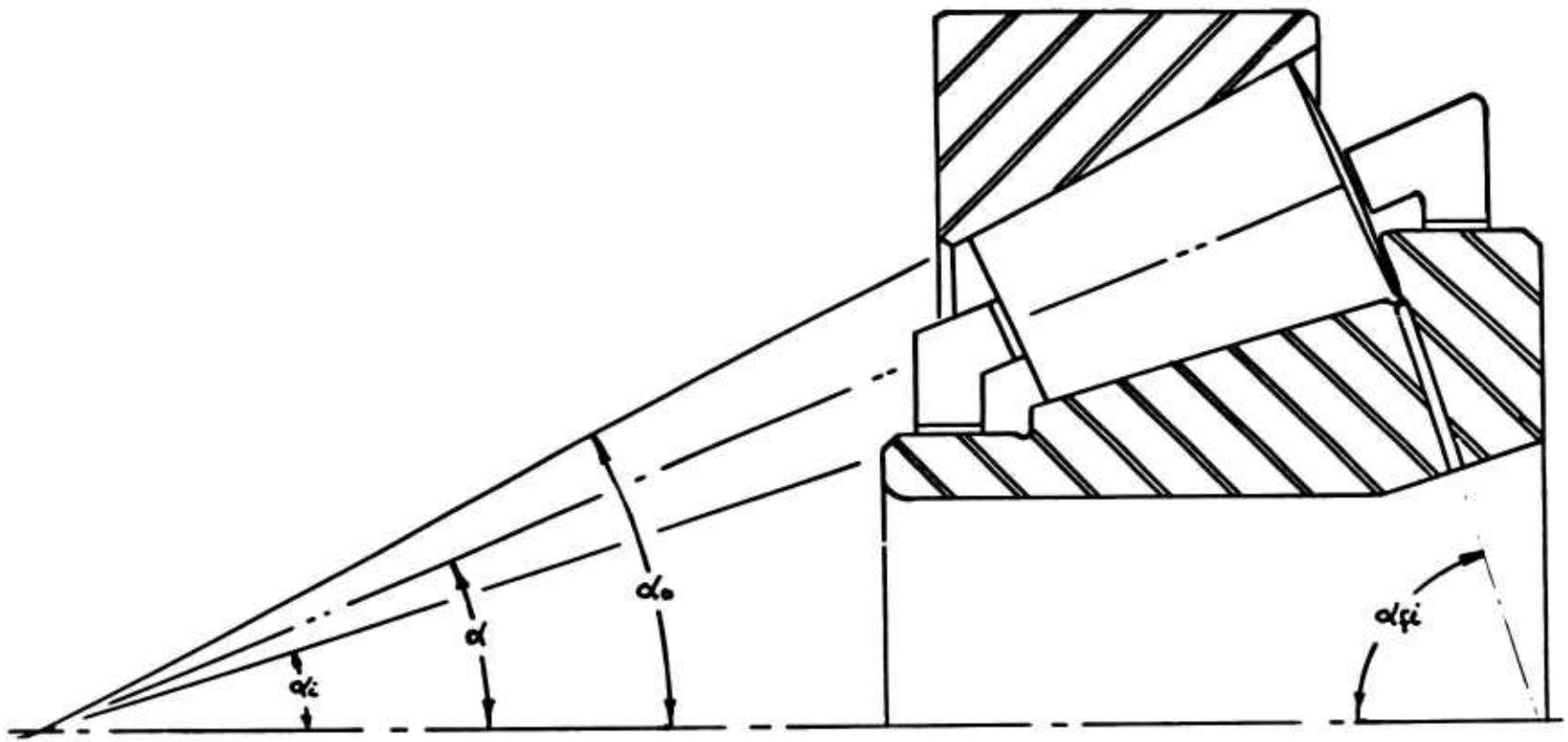

Bearing Angle Designations

α_i Inner Ring Half Angle

α Outer Ring Half Angle

α_{fi} Inner Ring Flange Half Angle

α_o Bearing Half Apex Angle

Figure 48. Bearing Angle Designations.

5. METHOD OF ANALYSIS

5.1 Analytical Methods of AE69Y002

Appendix II contains the operations manual for SKF AE69Y002. Section 1 of this manual describes the analyses employed in AE69Y002, and thus the major methods of this study.

5.2 Optimum Roller Crowning

The determination of the roller crown radius was made with the use of the Lundberg equation presented in Ref. (3). This equation accounts for the roller raceway contact geometry and the applied roller load to yield the crown radius which will provide a roller load distribution which is uniform over the entire length of the roller.

5.3 Friction Heat Generation at the Roller End/Flange Contact

The roller end/flange contact, friction, heat generation is estimated in AE69Y002 with the following equation:

$$H = C*Z*\mu*Q_f*V_f$$

where H = flange frictional heat

C = mechanical to thermal energy conversion constant

Z = number of rollers

Q_f = roller end/flange normal load

V_f = sliding velocity of the roller end/flange contact

μ = coefficient of friction

For this analysis, the coefficient of friction at the roller end/flange contact was estimated to be 0.02.

6. RECOMMENDATIONS FOR FURTHER STUDY

The analysis completed to date suggest three directions for future study.

6.1 Sliding Surface Failure Model

Lundberg-Palmgren fatigue life theory and recent work on lubrication and material effects provide the means by which the rolling contact surfaces can be analytically modeled. Rolling surface design and performance characteristics can be determined and compared against established norms. This is not the case with the sliding surface which exists at the roller end/flange contact. Currently an analytical model does not exist, which, with flange load, speed, and lubrication conditions as input will provide failure mode and time to failure as output. Need for this type of model has presented itself in this high-speed bearing investigation.

6.2 Outer Ring Flanged Bearing

Study of the inner ring flanged bearing's two-dimensional free-body-diagram, Figure 48 has revealed that under pure axial loading and increasingly high shaft speed, the outer ring normal load remains constant, the inner ring normal load decreases, the flange load increases, and the bearing tends to declutch.

The free-body diagram of an outer-ring-flanged bearing is presented along with the applicable equilibrium equations in Figure 49 . This figure reveals that with increasing speed, the inner ring normal load remains constant and the outer ring roller path shares the centrifugal force loading with the outer ring flange. The tendency toward inner raceway skidding is substantially reduced. This bearing configuration should be considered for future study.

6.3 Combined Axial and Radial Loads at High Speed

Declutching, which is characteristic of the axially loaded bearing, tends to be eliminated with the addition of a radial load to the bearing. This suggests that the conventional inner ring flanged tapered roller bearing might best be applied under high-speed combined radial-axial load conditions. Under such conditions the performance of a tapered roller bearing may surpass the performance of the ball bearing. This appears to be a promising area for analytical investigation.

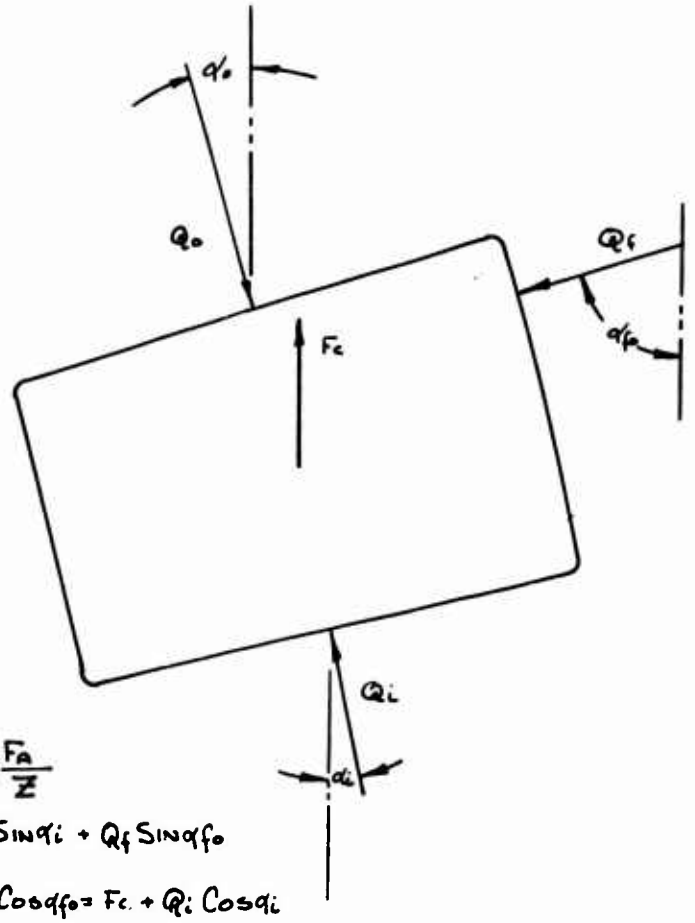

$$Q_i \sin\alpha_i = \frac{F_A}{Z}$$

$$Q_o \sin\alpha_o = Q_i \sin\alpha_i + Q_f \sin\alpha_{fo}$$

$$Q_o \cos\alpha_o + Q_f \cos\alpha_{fo} = F_c + Q_i \cos\alpha_i$$

$Q_o \equiv$ Roller, Outer Ring Normal Load
$Q_i \equiv$ Roller, Inner Ring Normal Load
$Q_f \equiv$ Roller, Outer Ring Flange Normal Load
$F_c \equiv$ Roller, Centrifugal Force

$\alpha_o \equiv$ Outer Ring Half Angle
$\alpha_i \equiv$ Inner Ring Half Angle
$\alpha_{fo} \equiv$ Outer Ring Flange Half Angle

$F_A \equiv$ Applied Axial Load
$Z \equiv$ Number of Rollers Per Bearing

Note: With Increasing Cage Orbital Speed, the Magnitude of

a. F_c increases
b. Q_o increases
c. Q_f increases
d. Q_i Remains Constant
e. α_o, α_i & α_{fo} Remain Constant

Figure 49. Outer Ring Flanged Bearing, Roller Free-Body Diagram and Equilibrium Equations.

APPENDIX II
SKF COMPUTER PROGRAM AE69Y002
ANALYSIS OF DYNAMIC PERFORMANCE CHARACTERISTICS OF TAPERED ROLLER BEARINGS UNDER RADIAL, AXIAL AND MOMENT LOADING

A. DESCRIPTION OF ANALYSIS

1. General

This program is designed to calculate the endurance and speed characteristics of tapered roller bearings subjected to combined radial, thrust, moment and/or misalignment loading. Bearings having any type of roller and/or raceway crowning may be evaluated. To arrive at a solution to the speed problem, it is necessary to determine distribution of applied loading among the rollers and also distribution of loading along the profile of each roller-to-raceway contact. Hence, sufficient information is developed to permit an estimation of raceway and bearing fatigue lives. The general analytical methods are detailed in Ref. (4,5).

2. Special Features

1. Lubrication and Friction Forces

To determine the traction forces between rollers and raceways, elastohydrodynamic (EHD) lubrication analysis is used. Isothermal, Newtonian lubricant characteristics are assumed. The data of Dowson (4) are used to establish lubricant film thicknesses. Traction forces are calculated assuming a linear sliding velocity gradient in the roller-to-raceway contacts. Account is taken of the amount of lubricant in the bearing cavity and the drag on the orbiting rollers affected thereby. Drag of inner or outer land riding cages on the roller set is also considered.

Lubricant pressure-viscosity data are input to each problem according to the assumed lubricant emergence temperature.

2. Roller Crowning

In arriving at a load distribution solution, any type of roller and/or raceway crowning may be

evaluated. Actual 100% reliability is calculated in accordance with Ref. (6).

B. PROGRAM INPUT

1. General

Program input consists of six types of data; i.e., dimensional, operation, control, steel, lubrication and incremental. Figure 50 shows sample input format. All input units are inches, pounds, degrees or rpm unless otherwise specified.

2. Dimensional Data

1. Number of rollers per bearing row.
2. Number of bearing rows.
3. Roller large-end diameter.
4. Total roller length; i.e., end-to-end, inches.
5. Inner raceway maximum effective length; see Figure 51.
6. Outer raceway maximum effective length; see Figure 51.
7. Inner raceway equivalent crown radius ($R=1/(1/R_R+1/Ri)$).
8. Outer raceway equivalent crown radius ($R=1/(1/R_R+1/Ro)$).
9. Number of axial laminae into which each contact is segregated; if left blank or 0, the program inserts 10. Maximum is 30; sec.
10. Cup half angle; see Figure 53.
11. Roller included angle; see Figure 51.
12. Flange half angle; see Figure 53.
13. Roller end sphere radius; see Figure 51.
14. Perpendicular distance from either raceway to point on flange at which roller end-to-flange contact occurs, inches

SKF COMPUTER PROGRAM AE69Y002 INPUT DATA
ANALYSIS OF DYNAMIC CHARACTERISTICS OF TAPERED ROLLER BEARINGS UNDER RADIAL AXIAL AND MOMENT LOADING

CARD NO.1

TITLE CARD	73 R	74 P	75 L	76 S	78 DC	79 D

CARD NO.2

10 O.ROLLERS/ROW	20 NO. ROWS	30 ROLLER LARGE END DIAMETER	40 ROLLER LENGTH END-TO-END	50 INNER RACEWAY MAX. EFF. LENGTH	60 OUTER RACEWAY MAX. EFF. LENGTH	70 INNER RACEWAY CROWN RADIUS	80 OUTER RACEWAY CROWN RADIUS

CARD NO.3

10 O. OF LAMINAE	20 CUP HALF ANGLE °	30 ROLLER INCLUDED ANGLE - °	40 FLANGE HALF ANGLE, °	50 ROLLER END SPHERE RADIUS	60 ROLLER-FLANGE CON. HT. ABOVE RACEWAY	70 OUTER + HSG. X-SECTION AREA	80 ROLLER ID/OD (LARGE END)

CARD NO.4

10 -INNER RING, IN.4	20 I-OUTER RING, IN.4	30 I-HOUSING, IN.4	40 I-SHAFT, IN.4	50 R-INNER RING, IN.	60 R-OUTER RING, IN.	70 R-HOUSING, IN.	80 R-SHAFT, IN.

CARD NO.5

10 -INNER RING, PSI	20 E-OUTER RING, PSI	30 E-HOUSING, PSI	40 E-SHAFT, PSI	50 μ-INNER RING	60 μ-OUTER RING	70 μ-HOUSING	80 μ-SHAFT

CARD NO.6

10 CLER COMPLEMENT ORIENTATION	20 INNER RACEWAY SURFACE FIN.-μ IN.	30 OUTER RACEWAY SURFACE FIN. μ IN.	40 ROLLER SURFACE FINISH IN.	50 ROLLER-FLANGE FRICTION COEFF	60 SPAN BETWEEN ROLL SMALL ENDS-2 ROW	70 TYPE OF 2-ROW MOUNTING

.) R=1 FOR LAST OR ONLY DATA SET, R=0 OTHERWISE (b) P=0 NORMAL MODE, P=1 DEBUG MODE (C) L=1 FOR 1ST. OR ONLY DATA SET, L=0 FOR SUBSEQUENT DATA SETS IF LUBRICANT DATA CARDS ARE OMMITED (d) S=1 FOR 1ST. OR ONLY DATA SET, S=0 FOR SUBSEQUENT DATA SETS IF STEEL DATA CARDS ARE OMITTED. (e) DC=00 MEANS INDEPENDENT DATA SET, DC=01 MEANS DATA ARE PART OF DUTY CYCLE; IN WHICH CASE SET DC=-1 FOR LAST DATA SET TO ESTIMATE OVERALL FATIGUE LIFE (f) D=0 NORMAL MODE, D=1 TO READ ROLLER DIAMETER VARIATION DATA (g) IF "NO. OF LAMINAE" IS LEFT BLANK OR 0., PROGRAM INSERTS 20 (h) IF CARD 5 IS BLANK, PROGRAM INSERTS E=29600000 AND μ=0.25 (i) "ROLLER COMPLEMENT ORIENTATION" = 0. SETS ROLLER AT 0° AZIMUTH, =1. SETS ROLLER AT HALF PITCH ANGLE FROM 0° (j) SETTING CROWN RADIUS TO 0. YIELDS INFINITE RADIUS; I.E, NO CROWN; SET = -1 TO READ VARIABLE CROWN DROP (K) SET ITEM 7, CARD 6 =1. FOR BACK-TO-BACK MOUNTING; = -1. FOR FACE-TO-FACE MOUNTING.

Figure 50. Sample Input Data Format.

CARD NO.7

VOL. FRACTION LUBE IN BEARING SPACE	LAND DIAMETER	CAGE-LAND RUBBING AREA	CAGE-LAND CLEARANCE	CAGE TYPE

IF L=1 IN CARD 1, CARDS 8-12 ARE REQUIRED; IF L=0, THEY ARE OMITTED

CARD NO. 8

DESCRIPTION OF LUBRICANT

CARD NO. 9

LOWER TEMPERATURE LIMIT °F	UPPER TEMPERATURE LIMIT °F

CARD NO. 10

$\eta_o(T_i)$, CP	$\eta(T_i, P_2)$, CP	$\eta(T_i, P_3)$, CP	$\eta(T_i, P_4)$, CP	$\eta(T_i, P_5)$, CP	$\eta(T_i, P_6)$, CP	$\eta(T_i, P_7)$, CP

CARD NO. 11

$\eta_o(T_u)$, CP	$\eta(T_u, P_2)$, CP	$\eta(T_u, P_3)$, CP	$\eta(T_u, P_4)$, CP	$\eta(T_u, P_5)$, CP	$\eta(T_u, P_6)$, CP	$\eta(T_u, P_7)$, CP

CARD NO. 12

P_1, psi	P_2, psi	P_3, psi	P_4, psi	P_5, psi	P_6, psi	P_7, psi

IF S=1 IN CARD 1, CARD 13 IS REQUIRED; IF S=0, IT IS OMITTED

CARD NO. 13

TYPE OF INNER RING (CONE) STEEL	LIFE IMPROVEMENT FACTOR	TYPE OF OUTER RING (CUP) STEEL	LIFE IMPROVEMENT FACTOR

Figure 50. Continued.

IF "INNER RACEWAY CROWN RADIUS" = -1., CARDS 14(i) ARE REQUIRED; OTHERWISE THEY ARE OMITTED. CARDS 14(i) SPECIFY CROWN DROP ON RADIUS FOR EACH AXIAL LOCATION ALONG THE EFFECTIVE LENGTH OF ROLLER-RACEWAY CONTACT $1 \leq m \leq 25$

CARD NO. 14 (i)

10	20	30	40	50	60	70	8
$CD_{i,1}$	$CD_{i,2}$			$CD_{i,m}$			

IF "OUTER RACEWAY CROWN RADIUS" = -1. CARDS 15(i) ARE REQUIRED OTHERWISE THEY ARE OMITTED. CARDS 15(i) SPECIFY CROWN DROP ON RADIUS FOR EACH AXIAL LOCATION ALONG THE EFFECTIVE LENGTH OF ROLLER-RACEWAY CONTACT $1 \leq m \leq 25$

CARD NO. 15 (i)

10	20	30	40	50	60	70	8
$CD_{o,1}$	$CD_{o,2}$			$CD_{o,m}$			

IF D = 1, CARDS 16(i) ARE REQUIRED; IF D = 0, THEY ARE OMITTED. CARDS 16(i) SPECIFY DEVIATION OF ROLLER LARGE END O.D. FROM NOMINAL DIMENSION AT EACH AZIMUTHAL LOCATION $4 \leq Z \leq 80$

CARD NO. 16 (i)

10	20	30	40	50	60	70	8
ΔD_1	ΔD_2			$\Delta D_{Z/2+1}$			

CARD NO. 17

10	20	30	40	50	60	70	8
BEARING END PLAY	2-POINT OUT-OF-ROUNDNESS	3-POINT OUT-OF-ROUNDNESS	SHAFT SPEED RPM	OUTER RING SPEED RPM	RADIAL LOAD, LB.	AXIAL LOAD, LB.	MOMENT LOAD IN.-LB.

CARD NO. 18

10	20	30	40	50	60	70	8
END PLAY INCREMENT	2-PT. O-O-R INCREMENT	3-PT. O-O-R INCREMENT	SHAFT SPEED INCREMENT, RPM	OUTER RING SPEED INCREMENT, RPM	RADIAL LOAD, LB. INCREMENT, LB.	AXIAL LOAD INCREMENT, LB.	MOMENT LOAD INCREMENT, IN.-LB

CARD NO. 19

10	20	30	40	50
MISALIGNMENT, MINUTES	MISALIGNMENT INCREMENT, MIN.	LUBRICANT TEMPERATURE, °F	TEMPERATURE INCREMENT, °F	EHD CALCULATION SUPPRESS SIGNAL

CARD NO. 20

2	4	6	8	10	12	14	16	18
NP_e	NOR	NS_i	NS_o	NF_r	NF_a	NM_o	NM_i	NT

NP_e = NO. ENDPLAY INCREMENTS (01-99); NOR = NO. O-O-R INCREMENTS (01-99);
NS_i - NO. SHAFT SPEED INCREMENTS (01-99); NS_o = NO. OUTER RING SPEED INC. (01-99);
NF_a = NO. AXIAL LOAD INC. (01-99); NM_o = NO. MOMENT LOAD INC. (01-99)
NM_i = NO. MISALIGNMENT INC. (01-99); NT = NO. TEMPERATURE INC. (01-99);
SET ITEM 5, CARD 19 = 1. TO PERFORM EHD CALCULATIONS; OTHERWISE LEAVE BLANK (0)

Figure 50. Continued.

IF DC = -1, CARD 21 IS REQUIRED; OTHERWISE IT IS OMITTED. CARD 21 SPECIFIES TIME FRACTIONAL DURATION FOR EACH OPERATING CONDITION FOR WHICH DC WAS EQUAL TO 01 OR -1.
IT IS NECESSARY THAT $\sum_{m=1}^{m=n} a_m = 1.000$ AND $1 \leq m \leq 20$

CARD NO. 21

1–4	5–8	9–12	13–16	17–20	21–24	25–28	29–32	33–36	37–40	41–44	45–48	49–52	53–56	57–60	61–64	65–68	69–72	73–76	77–80
a_1	a_2	a_3									a_m								

Figure 50. Continued.

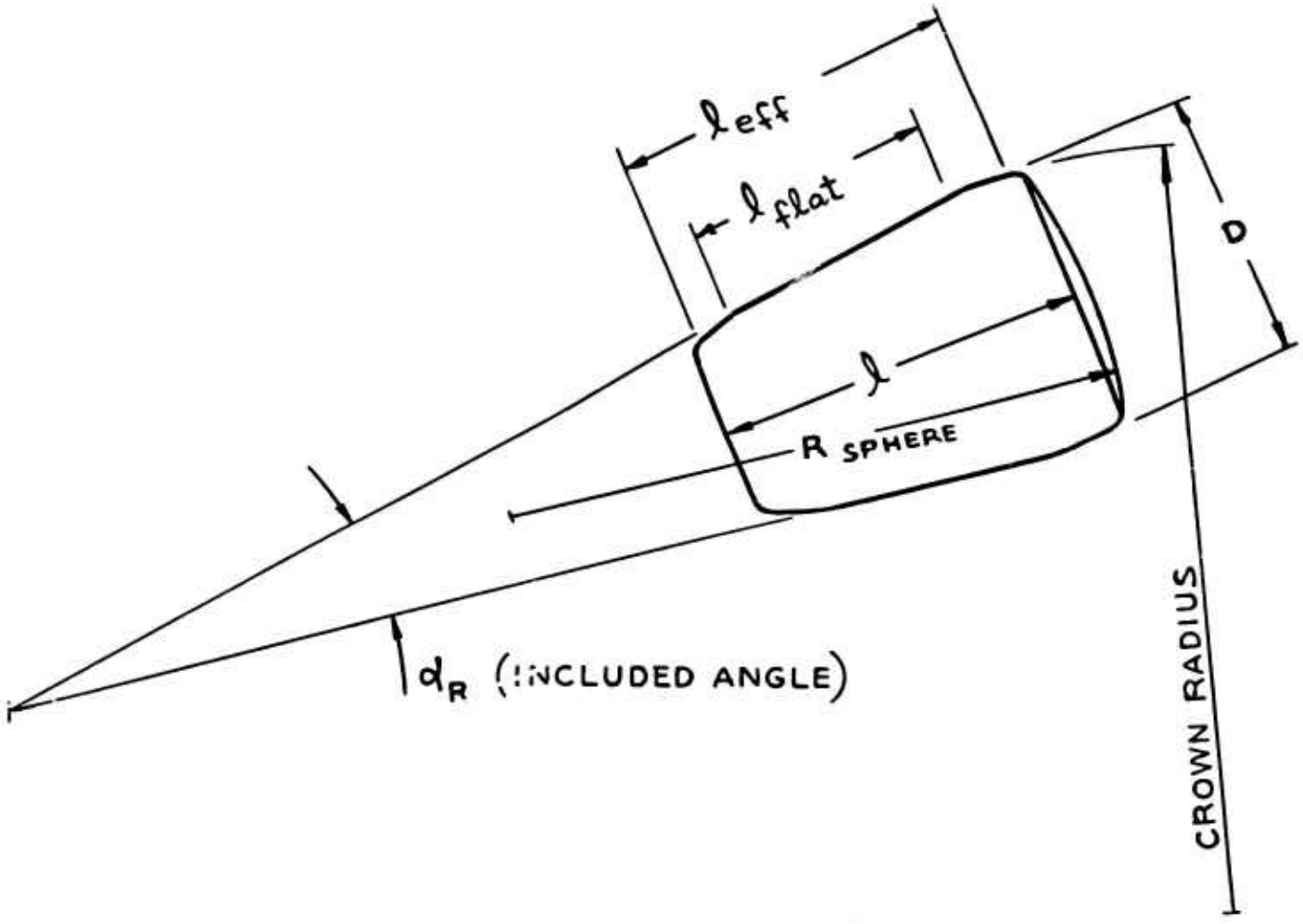

Figure 51. Tapered Roller Geometry.

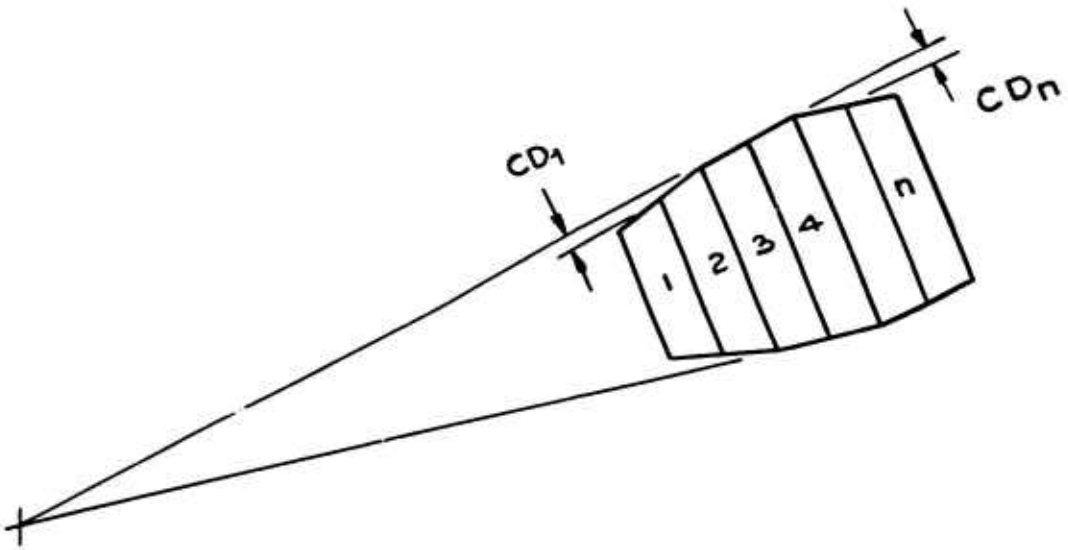

Figure 52. Laminated Roller Structure (Assumed)
Showing Crown Drop vs. Length.

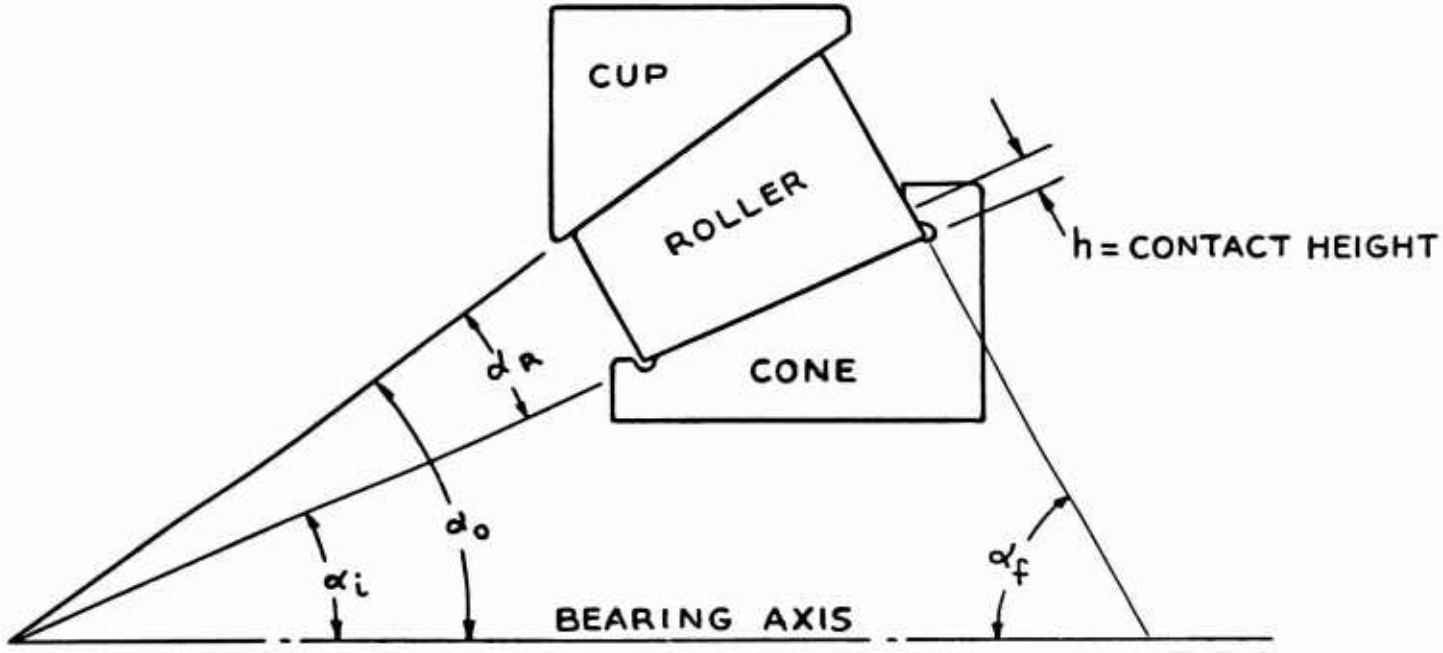

Figure 53. Tapered Roller Bearing Geometry.

15. Cross-sectional area of the outer ring and housing as a unit, inches^2. If the outer ring has a close fit in the housing, use A=Ao+EoAh/Eh; otherwise, use A=Ao.

16. Roller ID/OD or hollowness ratio (large end) for pin type cage bearings.

17. Inner and outer ring, housing and shaft stiffness criteria for bending (assuming a strap-type outer ring support as shown by Figure 54.

    a. Moments of inertia of cross sections, inches^4.

    b. Radii to the ring neutral axes in bending, inches.

    c. Moduli of elasticity, psi.

    d. Poisson's ratio.

    e. If all moduli of elasticity and Poisson's ratios are set equal to zero or left blank, the program inserts E = 29.6 million and Poisson's ratio = 0.25 for all elements.

18. Inner and outer raceway and roller rms surface finishes, microinches.

19. Roller end-to-flange friction coefficient.

20. Span between roller small ends (for two-row bearing).

21. Volumetric decimal fraction of the bearing cavity occupied by the lubricant; i.e., 0.15.

22. Cage land diameter.

23. Abutting contact (rubbing) area between the cage rails and the inner or outer ring land, inches^2.

24. Clearance between the cage rails and the inner or outer ring land (on a radius).

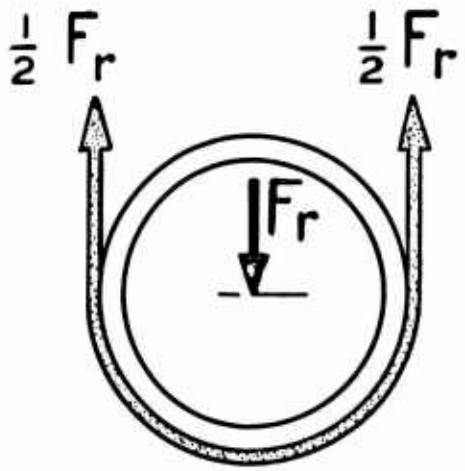

Figure 54. Strap-Type Support of Bearing Outer Ring.

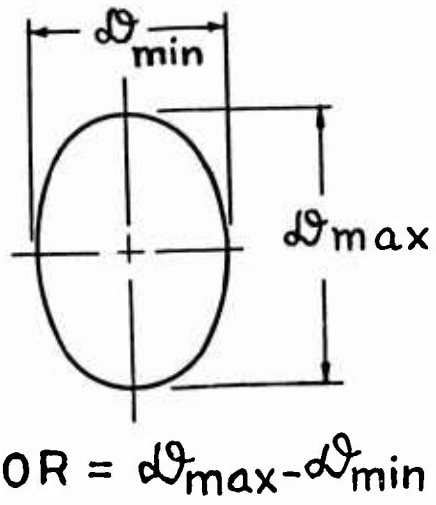

Figure 55. Two-Point Out-of-Roundness.

3. Lubrication Data

1. Lubricant description; e.g., MIL-L-7808 DIESTER.

2. Lower and upper temperature limits at which lubricant viscosity versus pressure data are assessed, °F.

3. Seven viscosity-pressure points at each temperature limit; e.g.,

T = 100°F; T = 425°F
= 11., 50., 300., 900., 3000., 8000., 25000., cp
= .7, 2., 5., 9., 15., 21., 30. cp
P = 0., 20,000., 40,000., 60,000., 80,000., 100,000., 200,000. psi

ASME data per Ref. (7) may be used.

4. Steel Data

1. Type of inner ring (cone) steel.

2. Steel life improvement factor for inner ring (use 1 for AISI52100).

3. Type of outer ring (cup) steel.

4. Steel life improvement factor for outer ring (use 1 for AISI52100).

5. Optional Operation

These data are read only on signal as detailed in sections 9.1 and 9.2.

1. Inner roller-to-raceway crown drop as a function of roller azimuth.

2. Outer roller-to-raceway crown drop as a function of roller azimuth.

3. Deviation of roller large end OD from nominal dimension specified in 2.3 as a function of roller azimuth.

6. Operational Data

1. Bearing end play.

2. Two-point out-of-round outer raceway.

   In card 17, item 2 is the outer raceway out-of-roundness of a constant cross-section outer ring. Out-of-roundness is the difference between the major and minor axes of the outer raceway. See Figure 55 .

   In the above situation, the outer raceway input two-point out-of-roundness or resultant two-point out-of-roundness is oriented with the major axis aligned in the direction of applied radial load. To phase shift, the major axis 90°, card 17, item 2 must be specified as a negative quantity.

3. Three-point out-of-round outer raceway

   On card 17, three-point out-of-roundness is the difference between the maximum and minimum radii of the outer raceway. See Figure 56 . A negative value causes a phase shift of 60°.

4. Shaft speed, rpm.

5. Outer ring speed, rpm.

6. Applied radial and axial loads.

7. Applied moment load, inch-pounds.

8. Misalignment, minutes.

9. Lubricant emergence temperature, °F.

7. Incremental Data

1. End-play increment.

2. Two-point out-of-round increment.

3. Three-point out-of-round increment.

4. Shaft speed increment.

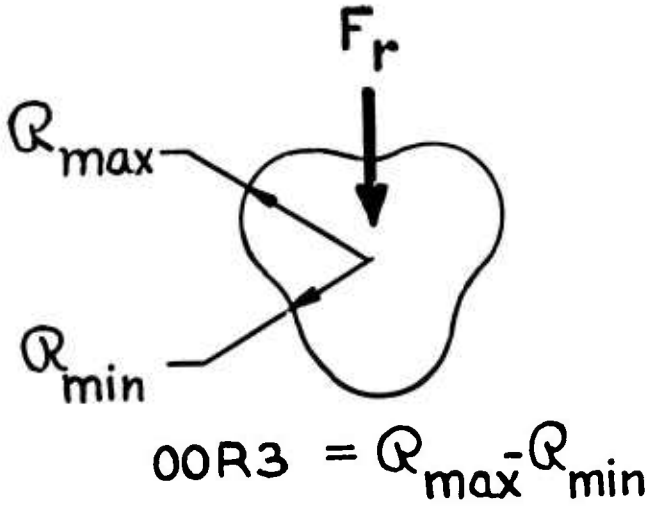

Figure 56. Three-Point Outer Ring Out-of-Roundness.

5. Outer ring speed increment.

6. Radial load increment.

7. Axial load increment.

8. Moment load increment.

9. Mialignment increment, minutes.

10. Temperature increment.

11. Number of end-play increments (01-99).

12. Number of out-of-round increments (01-99).

13. Number of shaft-speed increments (01-99).

14. Number of outer-ring-speed increments (01-99).

15. Number of radial-load increments (01-99).

16. Number of axial-load increments (01-99).

17. Number of moment-load increments (01-99).

18. Number of misalignment increments (01-99).

19. Number of temperature increments (01-99).

20. Decimal time fraction, e.g., .25, over which each operational condition exists. Up to and including 20 duty cycle conditions may be considered. The total of the time fractions must equal 1. A separate set of operational input is required corresponding to a time fraction; i.e., incremental data may not be used.

8. Parameter Increment Data

1. General

The program is capable of performing a parametric study with a single input data set. Increments (or decrements) may be applied to the following parameters: end play, two-point out-of-roundness or interference, three-point out-of-roundness, shaft speed, outer ring speed, radial load, axial load, moment load, misalignment and lubricant temperature.

Each data set must contain an increment set. Setting the number of increments to 01 affects program operation upon only the non-incremented parameter. The maximum number of increments which can be specified for any single parameter is 99.

2. Example of Incrementation

To investigate one operational condition per data set requires that card 20 contain 0101010101010101 in colums 1 to 18 inclusive.

As an example of incremental operation, assume that it is desired to investigate the following speed and load conditions for a given bearing:

10,000, 15,000, 20,000 rpm

50 200 lb

In card 17, shaft speed is set at 10,000 and radial load at 50. In card 18, shaft speed increment is set at 5000 and radial load increment at 150. In card 20, NSI is set to 03 and NFR to 02. Upon program execution, the following conditions will be run:

Condition	Speed	Load
1	10,000	50
2	10,000	200
3	15,000	50
4	15,000	200
5	20,000	50
6	20,000	200

Care must be exercised in allocating the number of increments in card 20, as it is theoretically possible to generate $(9)^{99}$ sets of output data set.

9. Program Control Data

1. Title Card Data

The "Title" card must contain a 1 in column 1 to effect a change of page with each new data set.

a. Column 73, card 1 is an input data read signal. For a single data set or for the last data, column 73 must contain a number 1 or greater, or else the program searches for new data after the problem has been completed. Otherwise, to read new data, column 73 is zero or blank.

b. For normal production operation, column 74, card 1 is zero or blank. Should a problem abort, it may be rerun in the debug mode by placing a 1 in column 74. Intermediate data developed thereby may be sent to SKF for failure investigation.

c. Column 75, card 1 is a lubricant data input signal. This signal must be 1 for the first or only data set. For succeeding data sets it may be set to zero or left blank, thereby retaining the lubricant data from the previous data set. When this is done, data set cards 8-12 inclusive may be omitted.

d. Column 76, card 1 must contain 1 for the first or only data set to read the steel data of card 13. On succeeding data sets, this column may be set to zero or left blank, thereby retaining the steel data from the previous data set.

e. Columns 77 and 78, card 1 permit calculation of bearing fatigue life according to a duty cycle which is specified by card 21 of the final data set. If duty cycle fatigue life calculations are required, columns 77 and 78 must contain 01 for each data set except the last, for which these columns must contain -1. To bypass duty cycle calculations, columns 77 and 78 may be set to 00 or left blank.

f. To evaluate roller diameter variation within the roller set, column 79, card 1 is set to 1. Cards 16 (= 1,2...) are then required. These cards specify roller diameter deviation (from the mean) at each roller location. If column 79 is zero or blank, cards 16 are omitted.

2. Roller and Raceway Crowning

Setting either or both items 7 and 8, card 2, i.e., crown radius equal to -1, permits the evaluation of any type of roller and/or raceway crowning. Such a signal requires cards 14 and/or 15 (= 1,2...) to be read in sequence. These cards specify total crown drop, i.e., roller and raceway, as a function of laminum axial location. Using a positive value of roller crown radius in card 2, items 7 and 8 causes the program to calculate crown drop.

3. EHD Calculations

Set item 5, card 19 equal to 1 to perform roller speed and friction calculations using EHD lubrication theory. Otherwise, leave blank or 0 to omit calculations.

4. Roller Complement Orientation

Set item 1, card 6 to 0 to place the first roller at 0° azimuth, i.e., directly under the radial load. Set item 1, card 6 to 1 to set the first roller at 1/2 pitch angle from 0°.

5. Type of Two-Row Bearing Mounting

Set item 7, card 6 to 1 for a back-to-back mounting for a two-row bearing. Set to 0 for a face-to-face mounting.

6. Cage Type

Set item 5, card 7 to -1 for an outer ring land riding cage, 0 for a roller riding cage, and 1 for an inner ring land riding cage.

C. PROGRAM OUTPUT

1. General

Input data are printed out for each run, including parametric alterations owing to incrementation. Lubricant temperature limits and viscosity-pressure data corresponding to these limits do not appear as output; however, lubricant viscosity in cp corresponding to atmospheric pressure and assumed lubricant temperature does appear. Data are organized according to roller azimuthal location for inner ring, outer ring and the bearing as a whole.

2. Bearing Performance Data

1. L_{10} fatigue life.
2. Radial load.
3. Axial load.
4. Cage speed, rpm.
5. Cage speed slip, percent.
6. Rolling motion heat generation, Btu/hour.
7. Sliding motion heat generation, Btu/hour.
8. Heat generation due to sliding between roller ends and inner ring flange.

3. Inner and Outer Ring Roller-Raceway Data Versus Azimuthal Location

1. Roller-to-raceway load.
2. Roller-to-raceway effective contact length.
3. Coefficient of friction between roller and raceway.
4. Ring radial deflections. Positive ring deflections are directed outside the base circle; negative ring deflections are directed inside the base circle.

5. Roller-to-raceway minimum lubricant film thickness, microinches.

6. Ratios of minimum lubricant film thickness to rms composite surface roughness. Film thickness and Lambda values equal to 0 indicate either (1) film thickness is of the order of roller-raceway clearance or (2) the calculation has been bypassed owing to program failure in the TRB8 subroutine.

7. Maximum Hertz stress as a function of axial location along the roller, psi. Stress is located at the center of each laminum.

8. Raceway L_{10} fatigue life.

4. Roller Data Versus Azimuth

1. Angle of inclination of true rolling axis, minutes.

2. Speed about the roller axis.

3. Load between roller end and ring flange.

4. Gyroscopic moment, inch-pounds.

5. Skewing moment, inch-pounds.

6. Cage web - roller load.

5. Bearing Data

1. Change in diametral clearance caused by sliding friction heat generation.

2. Radial deflection; i.e., the shift of the inner ring center toward the outer ring center.

3. Axial deflection; i.e., the axial shift of the inner ring toward the outer ring.

4. Misalignment; i.e., the tilt of the inner ring with respect to the outer ring.

5. Actual fatigue life, hours.

6. AFBMA fatigue life, hours.

7. Fatigue life according to Timken method.

8. Estimated no-failure life, hours.

9. Effective axial end play.

10. Total estimated frictional heat generation, Btu/hour.

6. Program Failure Data

1. "30 ITERATIONS ON CENTRIFUGAL FORCE FAIL TO YIELD A SOLUTION"; program prints out all data before proceeding to next problem. All EHD data, i.e., speeds, film thickness, film thickness-to-surface roughness ratio, skidding heat generation, cage web loads, etc., are final values; however, they may not be valid.

2. "SINGULAR MATRIX IN SIMEQ ROUTINE-BEARING LOAD DISTRIBUTION SUBROUTINE"; program proceeds to the next problem after printing out input data and the error message.

3. "30 ITERATIONS IN BEARING LOAD DISTRIBUTION SUBROUTINE FAIL TO YIELD A SOLUTION"; program proceeds to the next problem after printing out input data and the error message.

4. "30 ITERATIONS FAIL TO YIELD SOLUTION IN Q(M, K, J) CALCULATION"; program proceeds to the next problem after printing out input data and error message.

5. "SINGULAR MATRIX IN SIMEQ SUBROUTINE-SPEED SUBROUTINE"; program prints out load distribution life and deflection data. Speed data permits to simple rolling only.

6. "15 ITERACTIONS IN SPEED SUBROUTINE FAIL TO YIELD A SOLUTION"; program prints out load distribution bearing life and ring data before proceeding to next problem. Roller and cage speeds data are final values; however, they are not valid.

APPENDIX III
TEST DESCRIPTION AND BEARING ANALYSIS

PHASE II - INITIAL INNER RING DESIGN FEASIBILITY TESTS

A. Commercial Bearing Baseline Tests

Run Number 1 - Timken 07097 inner ring/07204 outer ring bearing achieved 18,000 rpm in 12 speed steps with 0.45-0.50 gpm flow of Velocite #10 oil. In returning to test after an overnight shutdown, the bearing seized at 12,100 rpm. Disassembly showed severe burning of the roller large ends and inner ring flange surfaces. Failure of the lubricant to penetrate this critical area in sufficient quantity is the cause of failure. The stamped cage was found to be permanently distorted. Test load was 450 pounds.

Run Number 2 - Timken 07097 inner ring/07204 outer ring bearing achieved 36,000 rpm in 22 speed steps after 4.15 hours total running time. Time at speed was .05 hour. Lubricant was Velocite #10 at 0.45-0.50 gallon/minute.

The bearing seized due to internal thermal buildup as in Run Number 1. The rollers were found to be severely burned with smearing and galling on the OD and on the large end. The inner-race roller path was also found to have severe smearing from the system inertial effects after seizure. The flange was severely burned and showed extensive galling and smearing. The crossbars of the stamped cage showed metal flow for the length of the roller as well as discoloration from excessive heat. The outer ring roller path showed severe heat discoloration and smearing. Test load was 450 pounds.

Run Number 3 - Timken 07097 inner ring/07204 outer ring. The oil flow was increased to approximately 0.705 gallon/minute to the test bearing. The maximum speed attained was 48,750 rpm. This was achieved in the second of two test runs. The first achieved 15,400 rpm after 7.4 hours in 26 speed steps. A maximum temperature of 207°F was measured. Time at speed was 0.2 hour. The second test achieved 18,750 rpm in an additional 4.2 hours and 21 speed steps. As that speed was reached, the temperature increased sharply (80°F to 305°F, outer ring) and the bearing was shut down manually.

Disassembly showed the severe heat discoloration found on the previous roller path surfaces, the inner ring flange and the rollers. Cage distress similar to that previously found was noted. No seizure occurred and only minimal smearing was found. Test load was 450 pounds.

Run Number 4 - Tyson 07100 inner ring/07204 inner ring. This bearing achieved 38,800 rpm in the second of two test runs. The first test was manually shut down after 0.1 hour at 25,200 rpm and 17 speed steps and 5.2 hours total elapsed time. The bearing seized during the second test run after 0.1 hour at 38,800 rpm. Failure was determined to be due to loss of clearance because of heat generated by oil churning after an oil scavenging system failure permitted the bearing cavity to fill with oil. The condition of the bearings was as described in Run Number 1 and 2. Test load was 450 pounds axially applied.

Run Number 5 - Timken 07097 inner ring/07204 outer ring. This test was conducted to confirm the existence of a declutching (roller lift-off) phenomenon. The axial load was adjusted to 101 pounds, for which declutching was calculated to occur at about 35,000 rpm. The bearing was run in at 134 pounds for 2.8 hours at 7000 rpm, and the load was then reduced to 101 pounds and the speed increased in steps. The tapered roller bearing declutched at about 37,500 rpm, as evidenced by the axial movement against the applied load by the outer-ring-containing load plug. The loss of axial location of the shaft permitted it to rub against an internal portion of the oil jet system. The system was manually shut down. No damage to the tapered roller bearing or its accompanying ball bearing was found.

Run Number 6 - Tyson 07100 inner ring/07204 outer ring. test bearing was chromized on the inner ring roller path and flange surface and the rollers to provide improved wear surfaces. The test load was 450 pounds. The oil flow was gradually increased to about 0.756 gallon/minute during the test. The bearing was run for a total of 8.6 hours, of which 5.4 hours were at speeds in the 35,000 to 37,000 rpm range. At disassembly, no bearing damage was found. Operating temperature was 203°-208°F (outer ring).

B. First Experimental Bearing Configurations

The following descriptions are of tests conducted on the

mechanically driven test rig. The power source was a 50-horsepower variable-speed DC motor driving through an 8:1 ratio gearbox speed increaser. Many of the bearings described below were subjected to subsequent increased speed tests in the air turbine test rig.

1. The first design variation was tested in contract **Phase** II, and consisted of bearings having commercial races (of Class 4 quality) of carburizing steel, modified by the addition of six oil delivery holes from the bore to the flange undercut for improved flange lubricant, and the provision of a new small end land for cage control. The cage was a machined, silver-plated cage of 4340 steel (Figure 4). The lubricant used was MIL-L-23699, an aircraft type mixed-ester lubricant. The applied axial load was 260 pounds.

Bearing 093101

This bearing reached a maximum speed of 50,500 rpm. A total of 41.75 hours of operation at all speeds was compiled.

In order to increase the speed capability of the test rig beyond the 50,000 rpm rated maximum of the gearbox, a jackshaft was inserted in the drive system, to be belt driven from the gearbox. The test rig was assembled as in Figure 2 . The oil was delivered to the test bearing from the liner on the inboard side, and to the roller end/flange contact area from an under-race oil supply delivered from the center of the shaft through radial holes in the shaft and bearing inner ring to the desired location.

Oil leakage to the belt of the jack shaft with resulting belt slippage, oil scavenging problems from the jack shaft and shaft resonant vibration problems in the jack shaft indicated that an excessive development time was required to achieve satisfactory operations. This element was therefore abandoned. A maximum test speed of 50,500 rpm was reached with the gearbox in direct drive to the test unit. A critical frequency was encountered at 48,000 to 50,000 rpm on the gearbox output shaft, which forced a manual shutdown of the test after 0.45 hours at maximum speed.

The bearing test was discontinued at this point, having

accumulated 41.75 total hours running time of which 8.3 hours were in excess of 45,000 rpm.

The bearing showed no traces of operational difficulty or distress. Very light traces of smearing were found on the inner ring flange. The cage pockets showed moderate to heavy wear and smearing in the pocket small end, where contacted by the roller unground small end.

Bearing 093102

A maximum operational speed of 46,000 rpm (1.15×10^6 DN) was picked as the maximum attainable with the direct drive with the gearbox. This was dictated by the gearbox output shaft vibration critical found in the preceding test run. This bearing reached the target speed and operated successfully for 21.0 hours at that speed. The oil flow was held constant at 0.79 gallon/minute. The outer ring temperature leveled off in the 195°-200°F range. After completion of the test, disassembly of the bearing showed moderate smearing on the inner ring flange surface and on the roller large ends and a narrow band of oil degradation products. The cage pockets showed moderate to heavy wear and smearing on the pocket small end, where contacted by the roller unground small end.

The Group 2 bearings were of 52100 steel, with three (instead of six) bore-to-flange-undercut holes for flange lubrication and with the rollers ground on the small end to reduce the cage pocket distress. The roller small end corner radius was also reduced to maximize the roller end surface. The cage was ground on all surfaces to improve balance, dimensional control, and surface finish before silver plating. In other respects, these bearings are similar to those of Group 1 (Figure 5). MIL-L-23699 oil was the lubricant. The test load was 160 pounds, axially applied as in the Group 1 bearings.

Bearing 093201

This bearing completed 21.0 hours at 46,000 rpm without operational problems. The flange showed very light smearing. The rollers showed some light frosting on the OD caused by the grinding shoes used in the

grinding operation conducted on the roller small end. This frosting "printed out" on the inner ring roller path during the test run and produced a polished contact area on the outer ring roller path. There is a narrow band of roller edge loading distress on the small end of the roller path. However, the outer ring roller path (free state) angle is smaller than the combined inner ring and roller included angle (by 0° 0' 47.8"), so it is indicated that the edge contact should be on the roller large end. Calculations indicate that the mounted inner ring roller path angle was sufficiently changed by the interference fit on the bore (by 0° 1" 29" at a maximum fit of 0.00026 inch tight) to cause the roller pinch at the small end.

The 093201 cage shows moderate to heavy smearing and wear in the pocket small end, with the silver plating worn through at the pocket trailing corner due to roller skewing. Moderate to heavy smearing and wear are evident on the crossbar at the pocket trailing side and on the large pocket end diagonally from the small end wear spot. Some cage contact with the inner ring land surface is evident in the cage ID, but apparently not enough to cause cage unbalance or to affect performance.

Bearing 093202

This bearing completed 5.3 hours at 46,000 rpm at an outer ring temperature of 210°F. The oil flow rate was then adjusted from 0.79 gallon/minute of 100°F oil to 0.72 gallon/minute of 190°F oil to produce an outer ring temperature of 250°F. The bearing completed 17.2 hours at this speed with no operational difficulties.

Some very light smearing was found on the inner ring flange surface, and with light traces of roller corner contact due to roller skewing. As in bearing 093201, the frosted appearance of the roller OD, caused by the grinding shoes used during roller end grinding, "printed out" on the inner race roller path and produced a polished contact area on the outer ring roller path. At the conclusion of the 250°F operation, oil degradation products were found on all cage surfaces, with wear patterns showing a roller skewing more severe than found

in bearing 093201. Heavy smearing was found on the pocket small end and cage on the pocket trailing cross-bar. The skewing appears to have been intermittent, with roller movement causing moderate to heavy smearing and material flow on the pocket leading edges in 9 of the 14 pockets, with light distress showing in the remaining 5 pockets.

3. The design of the Group 3 bearings was derived from the analytical work conducted in Phase 1 of this program. Due to the complex interplay of the various parameters of the tapered roller bearing, the design is a combination of computer calculation, engineering judgement and manufacturing capability. All comparisons following are made to the bearing designs previously tested. The design of the Group 3 bearings incorporated rollers of reduced diameter, to minimize the roller centrifugal force and hence the flange force, and a roller included angle reduced from that of the preceding bearings, which also tends to reduce the flange load. The inner ring angle was increased, allowing the two roller path angles to approach each other and thereby give an additional reduction of the inner ring flange load. The rings were fabricated from 52100 steel and have six radial holes from the bore to the flange undercut for flange lubrication. The cage is 4340 steel, ground all over and silver plated, as in Group 2.

The lubricant was MIL-L-23699, and the load was 460 pounds, as in Groups 1 and 2 previously discussed.

Bearing 093301

This bearing completed 20.0 hours at 46,000 rpm with no operational difficulties. The outer ring temperature was measured at 200°-250°F with 0.76 gallon/minute of 100°F oil supplied to the bearing. The bearing showed no signs of distress in the inner ring roller path, and the outer ring roller path showed only a light polish. No smearing was found on the inner ring flange, with the roller end contact zone clearly showing at the midpoint of the flange.

The cage showed light to moderate wear in the pocket small end, with the roller large-end contact showing

at the pocket end mid point. All cage pockets showed moderate to heavy flow of the silver-plate metal on both the pocket leading and trailing crossbars due to roller movements in the pockets.

Bearing 093302

This bearing was tested in the procedure used for bearing 093202, in that it was tested for 5.2 hours at 46,000 rpm with a measured outer ring temperature of 205°-210°F. The parity with 093301 thus established, the oil temperature was increased to 175°F with a constant quantity oil flow (0.77 gallon/minute) and an additional 17.1 hours accumulated at the 46,000 rpm target speed and 250°F outer ring temperature. The inner ring showed no distress after the test, and the outer ring roller path showed only the light polish found in 093301. The flange was in a similarly excellent condition, with no smearing evident and only a polished track at the flange midpoint to indicate the roller large end contact. The cage appearance and condition were as found in bearing 093301.

Bearing 093303

This bearing operated at 46,000 rpm for 9.6 hours with no operational distress. The total elapsed time of test was 33.4 hours. Lubricant was supplied at 100°F temperature at the rate of 0.73 gallon/minute. The test was terminated prematurely due to a failure in the mechanical drive system. Upon shutdown, a check of the bearing thermocouple also revealed a malfunction in the temperature indicator.

The condition of the bearing upon disassembly was excellent. No visible signs of smearing were found on the roller ends or the flange surface, and the cage showed only light to moderate wear in the contact area. The roller path showed no signs of distress, with the outer ring showing only a light polished track.

C. Second Experimental Bearing Configuration

The following bearings were tested in the mechanically driven test rig. The power source and drive system were the same as

those used in the first experimental bearing configurations (inner ring flanged bearings). A number of bearings were built having the flange located on the outer ring instead of on the inner ring as the conventionally configured bearings discussed above. The ring material was 52100 steel, as were the rollers. The roller path angles were designed to use the rollers of the Group 3 bearings (093300 series, bearing number 463691) described above. The outer-ring-flanged design does not have the load-carrying capacity of the inner-ring-flanged design; and after two bearings were run at 460 pounds axial load, the load was adjusted to 240 pounds axial, which yielded a pounds/roller loading (at 50,000 rpm) which approximately equaled that of the inner-flanged design under 460 pounds axial loading.

Bearing 094101

Bearing 094101 failed catastrophically at 40,000 rpm while the speed was being increased to 46,000 rpm after an interruption of the testing. The inner ring of this bearing contained a large spalled area primarily concentrated around one-half circumference and toward the small end. This pattern correlates with a band of roller edge loading noted in this area during a preliminary inspection. In addition, the outer ring was highly polished and flaked, a number of rollers were flaked and displayed end damage as a result of skidding contact with the flange, and two cage crossbars were broken. None of these latter components displayed any damage prior to this inspection, and the major damage noted was a result of the bearing locking up during the final stages of failure.

Bearing 094102

Testing of bearing 094102 was discontinued after 33.1 hours total running time when visual examination disclosed the presence of a burnished area on the cone at the small end of the rollers, even though extra measures had been used to minimize extraneous effects. Continued testing of this specimen would have resulted in the continued progression of the failure to the extent noted in bearing 094101.

Bearing 094103

Analysis of the test components of bearings 094101 and 094102 after the tests were completed indicated that contributory

factors to the distress noted could be found in the concentricity of the bearing bore to roller path and in possible very slight angular mismatch of the rollers and roller paths. These parts were reground to improve the inaccuracy. The bore-to-roller path concentricity levels and the test shaft bearing seat runout were re-specified to 0.000080 inch maximum. The angle of the inner ring roller path was increased by 0°1' (free state) to move any roller-end bias which may exist toward the roller large-diameter end. The components were then selected to minimize any remaining angular error. The test arbor bearing seat-to-seat eccentricity has been held to 0.00015 inch over the arbor length to minimize this factor.

The test load was 240 pounds axial. The bearing 094103 successfully completed 20 hours at 46,000 rpm. The detailed examination of the parts showed the inner ring to have circumferential lines on the roller path, with the contact area clearly defined around the entire circumference. There is evidence of load bias on the large end of the rollers but not to the point where edge loading occurred. The cup roller path area is in good to excellent condition, with some very small dirt brinells evident. The overall visual appearance is that of a finely ground surface.

The flange (outer ring) surface shows a clear roller end contact area, midway between the raceway undercut and the flange ID. Very light smearing and some minor polishing are evident.

The rollers reflect the conditions of the surfaces with which they were in contact, having circumferential lines to match the cone surface, with a multiplicity of additional, much lighter, circumferential markings found under magnification.

The condition of the cage is good, with clearly defined areas of roller/crossbar contact and with some flowing of the silver plating evident. Roller end contact with the cage side rails shows moderate wear and some smearing.

D. Maximum Speed Capability Tests

The following bearings were tested, on an air-powered turbine unit used to obtain bearing speeds in excess of 50,000 rpm (1,250,000 DN), to the outer-ring-flanged bearing maximum

design speed of 100,000 rpm (2,500,000 DN). The unit is powered by a 750-cfm compressor with a 150-psi delivery capability at 70°F. The test assembly schematic is shown in Figure 2.

Bearing 094104

This bearing achieved a speed of 54,800 rpm, at which point it was shut down because of shaft vibration and rubbing of the shaft on the labyrinth seal.

The bearing showed, upon disassembly, that the roller large end had pits which were attributed to a galling action occurring between the roller end and the outer ring flange. Inadequate lubrication is the base cause. Time at speed was 0.1 hour; total test time was 3.30 hours. Oil flow was 0.56 gallon/minute of MIL-L-23699 oil.

Bearings 094103 and 094105

It was suspected during the previous test run that the concept of the single test bearing run in combination with a single, angular contact ball bearing as the other shaft support was not a satisfactory combination at the elevated speeds in which shaft critical vibration points become of importance because of the differences in spring rates of the tapered roller bearing (stiff) and the ball bearing (soft). The "softer" ball bearing allows the shaft to whip and to rub on the labyrinth from a radial motion allowed when the balls move into the deepest portion of the ball race, losing radial location. After a 1.2-hour test with one outer-ring-flanged tapered bearing (094103) and one ball bearing which was forced to be suspended due to shaft whip, the ball bearing was replaced by bearing number 094105, another outer-ring-flanged tapered roller bearing, thus providing uniform stiffness in both bearing supports. Before the tests proceeded, the shaft assembly was balanced and the balance corrected to 0.001 ounce-inch, an air heater was installed in the air lines to correct an icing problem at the air turbine nozzles, and the deadweight/lever system used to apply the axial load changed to a spring-loaded, direct-acting system to give a faster response to shaft vibrations encountered in the critical speed ranges.

The foregoing steps permitted the bearing pair to achieve the test rig maximum speed, for the loads and torque imposed (due to available nozzle area), of 87,000 rpm and to hold speeds in excess of 80,000 rpm for 8.2 hours, when the test was considered complete and discontinued. Total elapsed time of this test was 23.85 hours (bearing 094103 had previously run in the mechanically powered portion of the program and had accumulated 70.2 hours prior to this test). The oil flow was 0.26 gallon/minute to the load end bearing (094103) and 0.10 gallon/minute to the drive end bearing. The outer ring temperatures were 340°F for 094103 and 255°F for the 094105 bearing. The difference is due to the exhaust air (160°F) from the air turbine cooling the drive end of the test rig.

Also the lubricant supply system contains differences in the method of delivery to the bearings which were of no consequence at low speeds but which proved to be of some importance at high speed. Both bearings were jet lubricated from the outboard side only. The appearance and condition of both bearings indicate that the oil quantity supplied was adequate for lubrication purposes. However, heat discoloration was visible on the oil-out (inboard) side of the bearings, indicating that the quantity or placement of the oil was not satisfactory to provide proper cooling of the bearings.

Basically, however, the bearings were in good condition at the conclusion of the testing. The inboard (oil-out) side of both bearings showed tempering and oil decomposition products on exposed surfaces, with the temper color indicating probable temperatures of 450°F. The roller large end and flange contact surface also showed this effect. The area of roller end contact is clearly visible on the flange surface, with the principal line of contact being located in the approximate center of the flange height. Although some very light surface distress is evident on the flange and roller end, the general condition of these surfaces is considered to be very good. The outer ring roller paths are in excellent condition, while the inner ring roller path shows the circumferential lines previously reported with some heat discoloration and lubricant decomposition products present. The circumferential lines are more evident on 094105 inner ring, where moderate to heavy roller circumferential lines have "printed out". Some roller small end pinch is also evident on this inner ring, although this condition is not extreme.

The silver plating on the cage has reacted to the operating temperature by presenting a black appearance on the inboard (oil-out) side after test, but it is in generally excellent condition. Heavy roller contact is noted on the cage cross-bars. The contact patterns indicates that the roller small end was driving the 094103 bearing cage and that the roller large end was driving the 094105 bearing cage.

The cage land control surfaces are in excellent condition, with no sign of wear or plate removal. The discoloration, normal to silver exposed to heat, can be chipped off to reveal silver underneath.

Bearings 094106 and 094107

Two bearings of the outer ring flanged design, 094106 and 094107, were tested under a 240-pound axial load at speeds in excess of 80,000 rpm for 8.3 hours. The maximum speed attained during this test was 87,500 rpm, with outer ring temperatures of 240°F being recorded for both bearings at the maximum speed. The physical condition of the bearing components at the conclusion of the test was judged to be quite good. The lubricant supply system had been modified prior to the initiation of these tests to jet oil to the bearings from the inboard side as well as from the outboard side as conducted in previous tests. The additional jets succeeded in reducing the OR temperature but did not penetrate the bearing to cool the roller end/flange interface. As before, heat discoloration was evident at the outboard side (large end) of the rollers, the cage, and the roller path surfaces. Only minor glazing was found on the flange surface and roller sphered ends, and the roller paths were in excellent condition with only the usual circumferential lines on the inner ring roller path. The cage showed moderate to heavy smearing and wear in the pockets. One roller showed a small flake at the conclusion of testing. The oil flow was 0.31 gallon/minute to the load end tapered bearings and 0.155 to the drive end bearing.

Bearings 093302 and 093303

The inner ring flanged design bearings 093302 and 093303 were operated under a 460-pound thrust load, resulting in a force distribution which approximates that seen by the outer ring flange design at the lighter load. Bearing 093302

accumulated 6.3 hours in the 70,000- to 80,000-rpm range, 0.5 hour in excess of 80,000 rpm, and 0.1 hour at 90,100 rpm. The test was terminated at 90,100 rpm due to the action of a shaft critical which severed the under-race oil lines. The bearing was found to be in excellent condition after disassembly. The roller sphered ends showed only minor glazing and smearing with the inner ring flange in a similar condition. The load track was clearly defined on the flange, high on the flange surface. The roller OD and roller paths were all lightly frosted. No heat discoloration was found.

Testing of bearing 093303 had previously been discontinued at 52,000 rpm, due to a premature failure caused by insufficient lubrication delivered by the under-race cooling system to the roller end/flange interface. Extreme roller end wear and severe flange smearing and galling were found. The cage showed moderate to heavy contact at the crossbars and pocket ends, with some bearing wear on the cage ID. The roller OD and the roller path surface were lightly frosted in appearance.

Lubricant flow, delivered from both outboard oil jet positions and by the under-race oil distribution system previously used, totaled 0.30 gallon/minute to the load end bearing (093302) and 0.215 gallon/minute to the 093303 bearing before its failure. (It was replaced with a ball bearing for the 90,100-rpm test.) No difficulty was encountered in going through the shaft criticals with the mixed mounting, as was previously noted. This was attributed to the spring-actuated loading system in use.

Bearings 094105 and 094106

The previous test conducted with outer-ring-flanged bearings had incorporated an inboard oil jet, directed at the bearing closed side and primarily intended to cool the bearing. For this test, the axial location of the oil delivery fixture (shaft liner) was adjusted and the oil delivery holes re-aimed to allow the bearing envelope to be penetrated by the oil jet. A new high-air-volume nozzle box was mounted on the turbine wheel to provide more speed to the assembly by permitting a higher rate of airflow to the wheel than the previous nozzle box.

A maximum speed of 56,000 rpm under 240 pounds axial load was achieved, at which point shutdown was forced by sounds of

bearing distress. The drive end bearing, 094105, was found to be failed, with the roller ends badly smeared, and about 0.0136 inch worn from the roller length. The outer ring flange was similary smeared, with extreme galling and some metal flow being evident. Signs of extreme heat buildup and resulting discoloration of both races and the rollers were evident. Damage to the roller paths was otherwise confined to some minor debris brinnelling and narrow areas of burnishing, probably from roller skew during the failure operation mode.

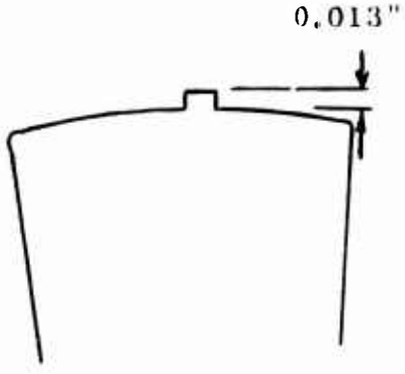

Bearing 094106 was in good condition at the conclusion of this test and is acceptable for further use.

The oil flow was 0.40 gpm for bearing 094106 and 0.27 gpm for bearing 094105. Outer ring temperature during the test was 240°F for bearing 094106 and 230°F for bearing 094105. Great clouds of oil mist were generated in this test by the suction created at the labyrinth seal by the extremely high velocity of the air from the turbine wheel. The oil flow directed to the drive end bearing, 094105, was probably disrupted, and a significant portion of it dissipated in this manner.

Bearings 094107A and 094106

Bearing 094107A was composed of the rings and cage of bearing 094107 and the rollers from bearing 094102, made available due to the occurrence of roller path distress in that bearing.

For this test, the high-volume nozzle box was used and a more efficient oil scavenging system was devised utilizing one scavenge pump inboard and one outboard of each bearing. The axial holes in the face of the outer ring flange were enlarged to 1/16 inch diameter to provide a freer oil flow through the bearing. The applied axial load was 240 pounds.

For mechanical reasons, the test was conducted in two portions. In the initial phase, stable operation at 84,000 rpm was achieved and maintained. Speeds in excess of 90,000 rpm were

also achieved, but stable operation was not; extreme shaft vibration occurred each time this was attempted. A momentary speed excursion to 101,000 rpm was made. However, the shaft vibration was immediate and severe, with rubbing occurring in the labyrinth seal. The test was shut down for repairs to the shaft and seal. The bearings were found to be in satisfactory condition.

During this test, clouds of oil mist continued to be generated. A shield intended to smoothly direct the turbine exhaust air away from the labyrinth area was designed and built and installed when the above-described shaft repairs were completed.

Failure of bearing 094107A occurred at 86,000 rpm upon test resumption, with failure being signaled by extreme shaft vibration at that speed.

Posttest examination indicated that the roller large ends were badly worn and smeared in bearing 094107A, with accompanying smearing and galling of the outer ring flange surface. The roller end/flange contact during the failure period is considered to be the source of the force disturbances which caused the shaft vibrations.

Since this was the second bearing in as many tests to fail with the severe roller end distress, a review of the lubrication system was made. It was found that the cage windage effect and the newly installed improved scavenge system combined to deprive the bearing of its lubricant supply on the open side. The bearing open-side lubrication jets are intended to inject oil into the bearing flange area.

The excessive quantities of oil mist generated with the new high-air-volume turbine nozzle box were eliminated by the use of the vortex shield which was intended to smoothly direct the turbine exhaust air away from the test head.

The oil flow was 0.54 gpm for the 094106 bearing with an OR temperature of 250°F, and 0.45 gpm and 288°F for the 094107A bearing at failure.

Bearings 094106 and 094103

The oil scavenging system was returned to the former system whereby one pump scavenged both inboard and outboard of each bearing. The vortex shield was also installed. A stiffer spring was used for the load application system to increase the rate of response of the load system to shaft vibrations.

Speeds in excess of 90,000 rpm were maintained for 2.1 hours with 1.2 hours of this time being in excess of 95,000 rpm.

Both bearings operated with no audible distress at the 90,000-rpm speed, however, the 094106 bearing (load end bearing) changed its characteristic noise and pitch very drastically between 94,000 and 95,000 rpm. It was initially thought that a shaft vibration point had been encountered, except that the speed drop usually accompanying this occurrence was absent. Repeated speed excursions between 90,000 and 95,000 rpm failed to show any speed or bearing temperature effect, and the test was allowed to proceed. No additional speed was attainable, however, and the test was suspended after 1.2 hours for bearing examination.

Bearing 094103 had incipient flaking failures on four rollers on the large-end OD, with some glazing and minor smearing present on the roller sphered end. The roller large end and the small end were both a deep blue color from heat distress, while the roller midsection was a dark yellow. This indicates the presence of some lubrication in the roller path (but an insufficient amount) and a marginal lubrication condition in the flange/roller area. The outer ring flange was similarly blue, with some glazing and some minor smearing evident. The roller paths on both the outer and the inner rings were dark yellow due to excessive heat. The inner ring was heat discolored at the roller path edges to match the rollers. No flaking or other physical distress of this type was noted on the roller path. The cage showed heavy contact in the pockets, with metal (silver) flow being found at the pocket leading edge at the roller large-end contact and at the trailing edge on the pocket small end, indicating that a tendency toward roller skew existed.

Bearing 094106 was similar to 094103 in posttest condition. The roller OD showed many incipient flakes at the large end, with some minor smearing on the sphered end. The outer and

inner ring roller paths showed heat discoloration at the large-diameter contacts. No other physical damage was evident. The outer ring flange showed some smearing, with "fish scale" marks caused by roller skew. The flange area was also a dark blue color. The cage showed heavy metal flow in the trailing edge of the pockets, normally extending the entire pocket length. Some of this type of contact is also evident on the pocket leading edge at the roller large-end contact. Roller skew is evidenced by this contact pattern plus heavy contact marks by the roller small end at the pocket trailing edge.

The oil flow was 0.75 gpm to the 094106 bearing at the test rig load end, and an OR temperature of 305°F was recorded at maximum speed. Bearing 094103 received 0.64 gpm, and the OR temperature was measured at 345°F.

Bearings 094108 and 094109

The vortex spoiler employed in the previous test to minimize the oil mist generation was removed for this test. No other mechanical changes were made. The test was conducted using outer ring flanged bearings 094108 and 094109 and was aborted at 52,600 rpm due to extreme vibration and noise. Disassembly of the test rig established that the load end lock nut had loosened, allowing the axial separation of the bearings and, thus, loss of radial control of the shaft. The shaft excursions encountered led to damage of varying degrees on both bearings, the shaft seats, the labyrinth bore, and the drive turbine.

Approximately 13 hours of running time was accumulated before the test was terminated.

Both bearings suffered severe damage. Bearing 094108, mounted on the load end of the shaft, had extensive smearing on the flange surface, while the contacting roller ends had been abraded in the contact region. Bearing 094109 showed evidence of severe localized temperature buildup on the roller paths and roller OD surfaces, and some plastic deformation of these surfaces was also noted.

The oil flow as 0.39 gallon/minute to the load end bearing (094108) and 0.55 gallon/minute to the drive end (094109) bearing. Bearing temperature was 210°F for 094108 and 285°F for 094109 at test termination.

Bearings 093304 and 094305 - Declutch Test

This test was used to establish that speed at which declutching of the inner-ring-flanged design tapered roller bearings will occur under the test conditions and to determine the operating characteristics under that condition.

The declutching speed of the inner-ring-flanged bearing was established as being approximately 85,000 rpm at the test loads applied. Two inner-ring-flanged bearings, 093304 and 093305, were tested successfully at speeds up to 85,000 rpm using the previously developed functional test procedures. After operation to this point was satisfactorily established, the speed was increased to 90,100 rpm and maintained for a period of 1.1 hours. As the speed was increased above 85,000, the operation of the tester became rough and noisy and vibration of the load plug could be observed. Throughout the test series, the temperature of the load end bearing, 093304, was maintained at 345°F, while the drive end bearing, 093305, operated significantly cooler, at 240°F. After completion of the test, the bearings were visually examined. The inner ring roller path surfaces of both bearings were in excellent condition, while some polishing was noted on the outer half of the flange faces. The outer ring roller paths displayed signs of heat distress, with a light brown color resulting from a combination of roller contact heat and oil degradation products. The cage pockets of the load end bearing, 093304, showed heavy wear and smearing in the small end of the pockets, indicating that the cage-roller contact pattern had varied from its normal large-end position, probably during the period of declutched operation. The same effect, however, was not as noticeable in the drive end bearing. It is not possible to tell that both bearings had operated in the declutched mode. It is likely that individual bearing characteristics affect the point of initiation of declutching; also, a paired mounting arrangement may load one bearing more heavily as the other declutches.

Both bearings were deemed to be in acceptable condition after the test, and no unacceptable damage was attributable to declutched operation.

Oil flows of 0.72 gallon/minute to the load end bearing

(093304) and 0.35 gallon/minute to the drive end bearing (093305) were maintained. The operating temperature differences were noted.

Bearings 093304 and 093305 - Extended Test

Bearings 093304 and 093305 were reassembled in the tester and the 100-hour extended test was initiated. The speed selected for this run was 80,000 rpm (2 million DN), about 5,000 rpm less than the declutch point previously established. After 13.1 hours, a cross-rib of the cage in the drive end bearing 093305 broke. No damage was found to have occurred to the other parts of the bearing, the cage failure apparently having occurred, or the cross-rib dislodged, at shut-down. Therefore the cage was replaced and testing reinitiated.

A total of 30.5 test hours was accumulated, of which 22.5 hours were at the test speed. Suspension of the test was precipitated by an axial fracture of the 093305 bearing inner ring at an oil hole, causing an instantaneous seizure of the inner ring and cage through inner ring expansion. The inner ring flange surfaces show the roller end burn marks high on the flange surfaces, and the roller path shows the axial markings where the rollers spun at the instant of cage/inner ring lockup. The cage shows severe wear in the ID at the land contact surfaces, indicating a short period of rotation in heavy contact with the inner ring, most likely in the moments immediately prior to lockup of the two components.

The outer ring temperature of this bearing was in the 240°-250°F range throughout the test. The load end bearing operated in the 340°-350°F range. It showed the effects of this heat in terms of discoloration of the ring, cage, and rollers, but showed no distress such as smearing.

Oil flows of 0.55 gallon/minute to bearing 093304 and 0.53 gallon/minute for the drive end bearing 093305 were maintained.